Miniaturized Printed Antennas for RF Energy Harvesting Applications

BY

AHMAD ABU ELHASSAN SALIH IBRAHIM

A Thesis Presented to the

DEANSHIP OF GRADUATE STUDIES

KING FAHD UNIVERSITY OF PETROLEUM & MINERALS

DHAHRAN, SAUDI ARABIA

In Partial Fulfillment of the
Requirements for the Degree of

MASTER OF SCIENCE

In
ELECTRICAL ENGINEERING

DECEMBER 2015

KING FAHD UNIVERSITY OF PETROLEUM & MINERALS

DHAHRAN- 31261, SAUDI ARABIA

DEANSHIP OF GRADUATE STUDIES

This thesis, written by **AHMAD ABU ELHASSAN SALIH IBRAHIM** under the direction his thesis advisor and approved by his thesis committee, has been presented and accepted by the Dean of Graduate Studies, in partial fulfillment of the requirements for the degree of **MASTER OF SCIENCE IN ELECTRICAL ENGINEERING.**
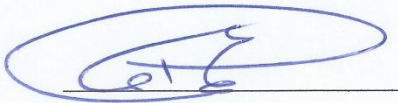
Dr. Ali Ahmad Al-Shaikhi
Department Chairman

Dr. Salam A. Zummo
Dean of Graduate Studies

_24/12/15_
Date
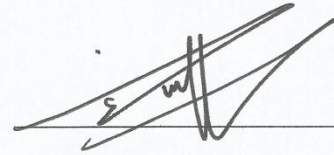
Dr. Mohammad S. Sharawi
(Advisor)

H. Masoudi 21/12/2015

Dr. Husain M. Masoudi
(Member)

H. A. Rag
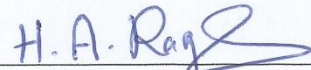
Dr. Hassan Ali Ragheb
(Member)

II

Dedicated to

my Parents and Family for their support

ACKNOWLEDGMENTS

This thesis cannot be done without the help and guidance of my professors, colleagues and friends. Thank you all for your help and support.

Special thanks for my thesis advisor Dr. Mohammad S. Sharawi for introducing me to the microwave field with his precious suggestions, encouragement, patience and his unlimited support. While working under his supervision, he passed to us his motivated research approach, time management and focusing on the goal criteria.

Many thanks to Prof. Hassan A. Ragheb and Prof. Husain M. Masoudi for their valuable comments, discussions and suggestions which open my mind to many new aspects in my research.

I want to thank Mr. Sagar Dhar and Dr. Rifaqat Hussain for passing to me their rich experience in fabrication, measurements and experimental process. I also want to thank our AMSDL research group members for helping encouraging me through the difficult times.

Finally I am really thankful to my friends in KFUPM for their support encouragement and their valuable advices.

TABLE OF CONTENTS

LIST OF TABLES

LIST OF FIGURES

xiii

LIST OF ABBREVIATIONS

RF : Radio Frequency

DC : Direct Current

AC : Alternating Current

MLA : Meander Line Antenna

GSM : Global System for Mobile Communications

UMTS : Universal Mobile Telecommunications System

WLAN : Wireless Local Area Network

DGS : Defected Ground Structure

WSN : Wireless Sensors Networks

ISM : Industrial, Scientific and Medical

ESA : Electrically Small Antenna

AIA : Active Integrated Antenna

RFID : Radio Frequency IDentification

GPS : Global Positioning System

PIFA : Planar Inverted-F Antenna

DBS : Deep Brain Stimulation

FG-CPW	:	Finite Ground Coplanar Waveguide
CCRC	:	Compact CPW Resonant Cell
CPW	:	Coplanar Waveguide
DCP	:	Dual Circularly Polarized
LHCP	:	Left Hand Circular Polarization
RHCP	:	Right Hand Circular Polarization
CRLH	:	Composite Right/Left Hand
UWB	:	Ultra Wide Band
MICS	:	Medical Implant Communications Service
MIMO	:	Multiple Input and Multiple Output
HSDPA	:	High Speed Downlink Packet Access
WCDMA	:	Code Division Multiple Access
WiMAX	:	Worldwide Interoperability for Microwave Access
EBG	:	Electromagnetic Band Gap
SAR	:	Specific Absorption Rate
TLMTM	:	Transmission Line Mushroom Like Metamaterial
HFSS	:	High Frequency Structural Simulator

SMA   :   Sub-Miniature Version A

LoS   :   Line of Sight

FSPL   :   Free Space Path Loss

ABSTRACT

Full Name   : Ahmad Abu Elhassan Salih Ibrahim

Thesis Title   : Miniaturized Printed Antennas for RF Energy Harvesting Applications

Major Field   : Electrical Engineering

Date of Degree : December, 2015

Wireless sensors have been used in several daily life applications such as in medical applications, oil and gas exploration, control systems, among many more. One of the big obstacles in using wireless sensors is how to energize them because using batteries in most cases will not be the optimal way due to many factors like the large number of sensors, their high cost and also the inaccessibility of the sensors in some remote locations. One solution is to harvest ambient radio frequency (RF) energy that is being radiated from wireless systems which exist everywhere or to have dedicated wireless sources covering specific geographic location. An RF energy harvesting system consists of an antenna to capture RF waves and a rectifier to convert RF waves to DC power. In this work, two miniaturized dual-band printed antennas are designed to be integrated with small wireless sensors to energize them using RF harvested energy.

A dual band electrically small meander line antenna (MLA) is designed to cover the most known wireless cellular standards such as GSM 900, GSM 1800 and UMTS. The antenna resonates at 915 and 1900 MHz with wide bandwidth at the higher band. The dual band property is achieved by using two different radiators, each of them is responsible for covering one band and a $\lambda/4$ transformer is used to match the antenna at 915 MHz. The MLA is tested for RF energy harvesting operation, then compared with a reference dipole

antenna that comes with the Powercast P2110-EVAL-01 kit used to evaluate the amount of energy captured. The reference dipole antenna was able to receive the signal up to 5 meters away from the transmitter while the dual band MLA was able to receive the signal up to 3 meters, noting that the dipole antenna size is 4 times larger than the proposed MLA.

A highly miniaturized dual-band patch antenna is designed to cover two WLAN frequency bands at 2.45 and 5.2 GHz. A 74% miniaturization ratio is achieved by using a shorting post and a novel defected ground structure (DGS). The resultant miniaturization ratio is the highest reported thus far in literature for dual-band patch antennas. Two rectifiers are designed to test the patch antenna RF energy harvesting abilities. An Output DC voltage of 0.9 and 0.4 V is measured across 156 and 185 Ω load at 12 and 5 dBm input power at 2.43 and 5.2 GHz, respectively. A 25% and 26.5% conversion efficiency is achieved when the rectifier input power is 12 and 5 dBm at 2.43 and 5.2 GHz, respectively.

ملخص الرسالة

الاسم الكامل: أحمد أبو الحسن صالح ابراهيم

عنوان الرسالة: هوائيات مطبوعه صغيره لتطبيقات حصاد الطاقه من الترددات الراديويه

التخصص: الهندسه الكهربائيه

تاريخ الدرجة العلمية: ديسمبر, 2015

الحساسات اللاسلكيه تستخدم في العديد من تطبيقات حياتنا اليومية مثل التطبيقات الطبيه, النفطيه, استكشافات الغاز, انظمة التحكم و كثير من التطبيقات الاخرى. واحده من المشاكل في استخدام الحساسات اللاسلكيه هي كيفية تزويدها بالطاقه لان استعمال البطاريات في اغلب الحالات هي ليست الطريقه المثلى لعدة عوامل مثل العدد الكبير للحساسات اللاسلكيه, التكلفه العاليه و عدم إمكانية الوصول في بعض المناطق النائية. احد الحلول المطروحه هو حصاد الطاقه من الترددات الراديويه التي تشع من الانظمه اللاسلكيه الموجوده في كل مكان أو استخدام مصدر طاقه مخصص لاسلكي لتغطية منطقه جغرافيه محدده. نظام حصاد الطاقه من الترددات الراديويه يتكون من هوائي لالتقاط موجات الترددات الراديويه و مقوم لتحويل موجات الترددات الراديويه لتيار مباشر يمكن الاستفاده منه. في هذا العمل, تم تصميم هوائيين صغيرين مطبوعين ثنائيات النطاق ليدمجا مع الحساسات اللاسلكيه الصغيره لتزويدهم بالطاقه عن طريق حصاد الطاقه من الترددات الراديويه.

تم تصميم هوائي مموج الخط ثنائي النطاق صغير كهربائيا لتغطية معظم الأنظمه الخليويه اللاسلكيه المعروفه مثل GSM 900, GSM 1800 و UMTS. الهوائي يعمل على الترددين 915 و 1900 ميقاهيرتز. تم تحقيق خاصية ثنائية النطاق عن طريق استخدام مشعين مختلفين كل واحد منهما مسؤول عن نطاق واحد و تم استخدام خط نقل له ربع طول موجي لمطابقة مقاومة الهوائي عند 915 ميقاهيرتز. تم اختبار الهوائي المقترح لعملية حصاد الطاقه من الترددات الراديويه و من ثم تمت مقارنته مع هوائي مرجعي ثنائي القطبيه الذي هو جزء من معدات Powercast P2110-EVAL-01 و هي تستخدم لقياس مقدار الطاقه المجمعه. الهوائي المرجعي ثنائي القطبيه قادر على استقبال

الاشاره حتى مسافة 5 امتار من المرسل بينما الهوائي المقترح ذو الخط المموج قادر قادر على استقبال الاشاره حتى مسافة 3 امتار مع العلم أن حجم الهوائي ثنائي القطبيه يوازي اربعة اضعاف حجم الهوائي المقترح.

تم تصميم هوائي patch ثنائي النطاق ذو معامل تصغير عالي لتغطية ترددين WLAN عند 2.45 و 5.2 جيجاهيرتز. تم تحقيق معامل تصغير مقداره 74% عن طريق استخدام ثقب لتوصيل الهوائي مع الأرضي و أيضا تم حفر شكل على طبقة الأرضي (DGS). نسبة التصغير المتحصل عليها هي الأعلى حتى الان بالنسبه لهوائيات patch ثنائية النطاق. تم تصميم مقومي الموجه عند 2.43 و 5.2 جيجاهيرتز لاختبار امكانيات الهوائي المقترح في حصاد الطاقه من الترددات الراديويه. تم قياس جهد بمقدار0.9 و 0.4 V خلال مقاومه مقدارها 156 و 185 Ω عندما كانت القدره عند مدخل المقوم12 و 5 dBm عند 2.43 و5.2 جيجاهيرتز بالترتيب. تم حساب كفاءة تحويل مقدارها 25% و 26.5% عندما كانت القدره عند مدخل المقوم 12 و 5 dBm عند 2.43 و5.2 جيجاهيرتز بالترتيب.

CHAPTER 1

INTRODUCTION

The tremendous advances in research and science raised the need for monitoring physical phenomena which led to the development of Wireless Sensors Networks (WSNs). A wireless sensor networks usually consist of thousands of sensor nodes where each of them sends and receives information via a link with a central station [1]. These large numbers of sensors use limited power batteries for energy. Such batteries have many disadvantages like their high cost, large size, limited power capacity in addition to their harmful effects on the environment. One of the proposed solutions is to harvest energy from ambient sources to energize those sensors and then optimal energy management techniques are applied [1].

In the environment there are many renewable energy sources available that can be used to harvest energy from, like solar, wind, vibration and thermal energy but the question is which of them is better for WSN applications. It is clear that most of the sources depend on the environment which means that they are not predictable and the sensors cannot rely on them specially with their small power storage capabilities [2].

Radio frequency (RF) waves are a suitable source for such sensors to harvest energy from, because RF waves are controllable and can be turned on and off due to the power demand by the sensors [2]. Another advantage of the RF energy harvesting is that the sensors can work without battery at all unlike harvesting from uncontrollable sources like

the sun. Also the RF energy Harvesting comes with some limitations like low produced power.

In this chapter, we will go over a comparison between different energy harvesting sources followed by an introduction to RF energy harvesting discussing the availability of the RF energy sources and the power demand of the wireless sensors. The concept of the rectifying antenna (Rectenna) will be discussed briefly and then the thesis contributions will be listed.

1.1   Energy Harvesting Sources

Many ambient energy sources are available in nature that the energy can be harvested from. Solar energy is the most used ambient source for energy due to its high power that can be generated with an existing power density of up to 100 mW/cm^2. The solar energy is available for an average of 6 hours in a sunny day which represents a serious disadvantage as it is unpredictable, also solar panels need proper orientation to collect sufficient solar power [3]. The produced current and voltage depends on the solar panel size so it needs large size which is inefficient for some applications.

In 1823, Seebeck found that there is voltage drop across a material which has a temperature gradient [4]. This discovery was the start of thermoelectric energy harvesting. When there is temperature difference or heat flowing across a thermoelectric device there will be voltage generated. Usually thermoelectric devices are bulky and heavy and occupying large area.

Table 1.1 Comparison between energy harvesting sources [3]

Parameters	Solar Energy	Thermal Ener.	RF Energy	Vibration
Power density	100 mW/cm^2	60 μW/cm^2	1 μW/cm^2	200 μW/cm^2
Output (V)	1 (Single Si cell)	-	3 - 4	10 - 25
Availability	Day time (4-8 h)	continuous	continuous	Due Activity
Weight (g)	5-10	10-20	2-3	2-10
Pros	Large amount of energy Well developed technology	Always available	Small Size Widely available	Well developed technology
Cons	Large size Non continuous Orientation Issue	Large size Low power	Distance dependent Low power	Large Area Output Variability

Due to the technological advancement, there are many sources of RF waves that the energy can be harvested from such as cellular networks, TV signals, WiFi networks and AM/FM radio waves [3]. The advantage of RF energy harvesting is the small area of the harvester and the reliability of the RF sources. RF waves low power density makes the harvester design very challenging as the antenna preferred to be with high gain and also very good impedance matching between the antenna and the following RF circuitry is necessary.

Electrical generation using mechanical strains such as vibration caused by wind or human movement become a well developed technology through the years [3]. The volume of the harvester is less than the solar and thermoelectric harvesters and larger than RF waves harvesters but the output has a large dynamic range with irregular motions so voltage regulation circuitry is a must to protect the system from voltage overshooting. Table 1.1 compares between some of the well known ambient energy harvesting sources.

1.2   RF Energy Harvesting

RF energy harvesting is about harvesting radio frequency waves that radiated from sources with high electromagnetic fields generation capabilities such as cell phone towers, TV signals and wireless networks access points then convert it to suitable voltage levels that can be used or stored for later use. In the past, small scale energy harvesting techniques were not considered a suitable source of energy compared to large scale techniques like solar energy but for powering wireless sensors RF energy harvesting is preferable than the conventional techniques because it is controllable and predictable which is better for reliable operation [2].

Most of the communication base stations have omni directional antennas which radiate RF energy in all directions for better coverage and the power radiated by those sources is high and can up to 30 Watts [5]. The question is how much energy can be harvested from such sources, actually it is not that much due to the environment effects, as most of the power will be dissipated in the air as heat or absorbed. Table 1.2 shows the average power consumed by wireless sensor nodes from four different manufacturers. The average consumed power by the wireless sensor is few mill-watts which is not easy to obtain by RF energy harvesting so the need for ultra low power sensor nodes that work in the scale of micro watts is fundamental for the RF energy harvesting to be successful. Also, storing capacitors are essential to accumulate enough power to operate such devices for short periods of times (note that sensor nodes are idle most of the time).

Table 1.2 Power consumption of low power sensor nodes [5]

Parameters	Manufacturer			
	Crossbow MICAz	**Waspmote**	**Intel IMote2**	**Jennic JN5139**
Typical range	100 m	500 m	30 m	1000 m
Data rate	250 Kbps	250 Kbps	250 Kbps	250 Kbps
Sleep mode	15 μA	62 μA	390 μA	2.8 μA
active mode	8 mA	9 mA	31-53 mA	3 mA
Transmission	17.4 mA	50.26 mA	44 mA	34mA
Reception	19.7 mA	49.5 mA	44 mA	34 mA
Voltage supply	2.7 V	3.3 V	3.2 V	2.7 V
Average power	2.8 mW	1 mW	12 mW	3 mW

Ultra low power sensor nodes are defined to work with sleep current of nano amperes and their radio transceivers work with milli amperes for transmitting and receiving. Also they must work with low current peripheral circuits (clocks, voltage regulators…) where energy efficient radio protocols must be applied.

The available known wireless systems that RF energy can be harvested from and their frequency bands are [5]:

- GSM - 850 (869 - 894 MHz).

- GSM - 900 (935 - 960 MHz).

- GSM - 1800 (1805 - 1880 MHz).

- UMTS - 2100 (2110 - 2170 MHz).

- ISM - 2450 (2400 - 2500 MHz).

- ISM - 5200 (5150 - 5350 MHz).

1.3   Rectifying Antennas (Rectennas)

To harvest ambient RF energy, the rectifying antenna (Rectenna) concept is introduced. The rectenna consists of an antenna to harvest the RF energy followed by a rectifier to convert the RF energy to DC to be used within a practical application. Figure1 shows a block diagram of a rectenna [6]. The rectenna consists of an antenna that receives RF signals which will go through a band pass filter or matching network to then a rectifier to convert the AC signal to DC. The rectifier is represented by a diode, the diode characteristics has a significant impact on the rectenna performance such as the built in voltage which is preferred to be low to get high rectifying efficiency. The band pass filter between the diode and the antenna has a job to prevent harmonic signals created by the diode from going back again to the antenna and re-radiated again to the environment. If the antenna is not matched at the frequencies of the harmonics then the bands pass filter can be replaced with just matching network to match the impedance between the antenna and the rectifier. A low pass filter must be located between the diode and the load to pass the DC and block any AC signals from going to the load and also it is used as storage device for later use [6].
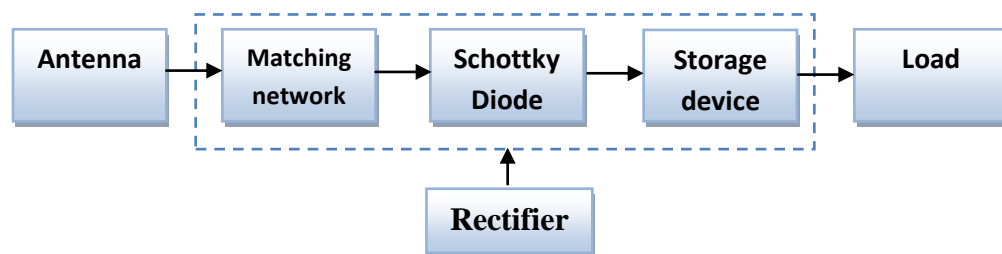
Figure 0.1 rectenna structure [6]

1.4   Thesis Contributions

In this thesis, different compact printed antennas are designed and tested for RF energy harvesting applications. Modeling, simulation and experimental results are presented. The thesis contributions can be listed as follows:

1. Design of a dual band meander line antenna (MLA) to cover the known wireless cellular standards such as GSM 900, GSM 1800 and UMTS. The meander line structure is used to reduce the antenna size. The antenna is an electrically small antenna (ESA) at 915 MHz with substrate size of 45x32.6 mm^2. The MLA is tested using Powercast P2110-EVAL-01 kit for RF energy harvesting capabilities.

2. Design of highly miniaturized dual band patch antenna to cover two industrial, scientific and medical radio (ISM) bands at 2.45 and 5.2 GHz. A 74% miniaturization ratio was achieved compared to conventional rectangular patch antenna at 2.45 GHz which is reported as the highest miniaturization ratio achieved thus far for dual band patch antenna.

3. An RF to DC converter circuits are designed at 2.43 and 5.2 GHz to test the proposed dual band patch antenna for RF energy harvesting operation as part of a rectenna configuration.

CHAPTER 2

THEORETICAL BACKGROUND

In this chapter, RF energy harvesting concepts and principles will be investigated and effect of the different parts of a rectenna will be discussed.

2.1   Rectenna Design Considerations

Modern RF energy harvesting systems depend on semiconductor diodes for RF to DC conversion. Diodes are the optimal choice when dealing with RF waves as diodes can handle small amounts of power with low cost and small form factor (small size). Schottky diodes are preferred over PN diodes due to their low built in voltage and small junction capacitance as the low built in voltage increases the rectenna sensitivity and the low junction capacitance increases the diode operational frequency so schottky diodes can operate with high frequency and they are known for fast switching capabilities [7].

2.1.1   Schottky Diode Characteristics

Diodes are nonlinear devices with an exponential relationship governing their voltage and the corresponding current [7],

$$I(V) = I_S(e^{\alpha_D V_D} - 1) \tag{2.1}$$

where I(V) is the current cross the diode terminals as a function of the diode voltage, I_s is the saturation current and α_D is the temperature factor of the diode. A diode has three main regions of operation as shown in the diode I-V curve shown in Figure 2.1. If the

diode voltage V_D is less than the diode break down voltage (V_{br}), then the diode will be in the reverse bias region and the current will flow in the reverse direction (from - to + as shown in Figure 2.1). If $V_{br}<V_D<V_T$ where V_T is the threshold voltage, the diode is off and there will be no current flow. If $V_D>V_T$, the diode is said to be in the forward bias region and the current will flow normally.
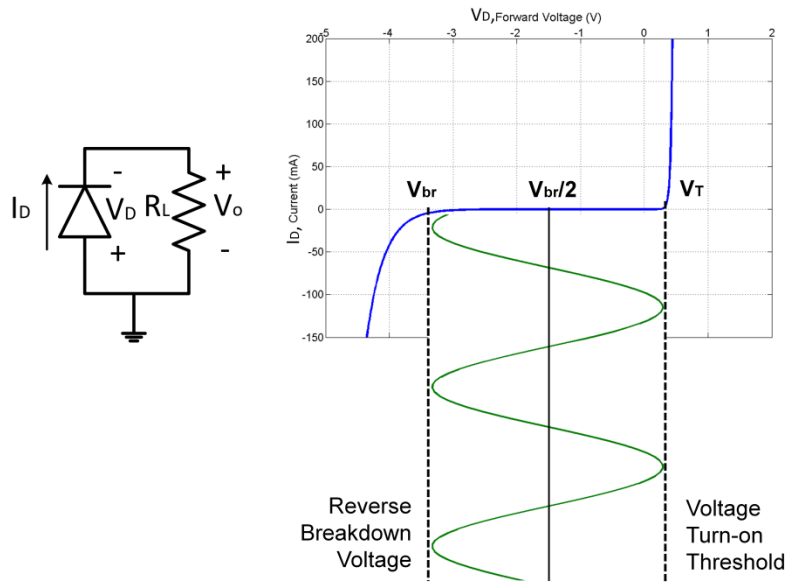
Figure 2.1 Diodes IV curve and regions of operation [8]

Rectification takes place when the coming RF signal with peak V_p is larger than the diode turn on voltage V_T as charges will transfer through the diode and build a DC bias V_D which will increase while $V_p >V_T$. If V_p continued to be larger than V_T, V_D will increase and goes toward the break down voltage V_{br} in the diode IV curve as shown in Figure 2.2, while $V_p >V_T$ there will be a point where $V_p +V_D>V_{br}$. At that point V_D will no longer increasing even with $V_p >V_T$, this happened because $|V_p| > |V_{br}|$. This scenario illustrates an important fact, the largest generated DC voltage from a diode is half the

9
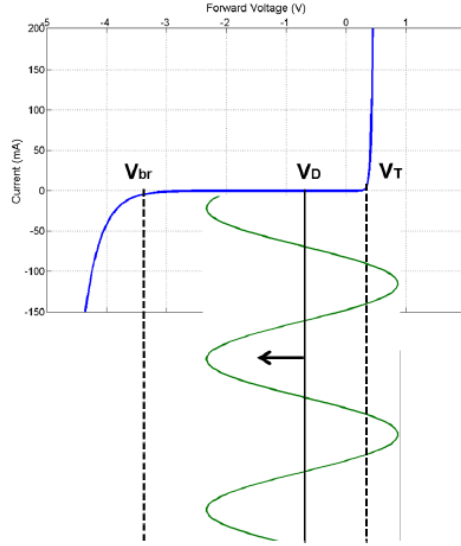
Figure 2.2 V_D goes toward V_{br} [8]

break down voltage of the diode. The maximum DC power $P_{DC\ max}$ generated across a load resistor R_L is

$$P_{DC\ max} = \frac{V_D^2}{R_L} = \frac{\left(V_{br}/2\right)^2}{R_L} = \frac{V_{br}^2}{4R_L} \tag{2.2}$$

2.1.2   Sources of Loss in Rectennas

Due to the diode nonlinear behavior, there are losses that affect the generated DC power and reduce its amount. There are three major sources of losses in a rectenna which are:

2.1.2.1   Diode turn on and breakdown voltages

Diode turn on voltage is the most important parameter to identify the rectenna sensitivity as the input RF signal must be larger than this voltage for the diode to operate and rectify the incoming signal so schottky diodes with low turn on voltage are preferred. Diode breakdown voltage will identify the largest input RF signal the diode can rectify so higher breakdown voltages are preferred as the largest DC voltage generated is equal to half of the diode breakdown voltage as discussed in section 2.1.1.

10

2.1.2.2 Impedance matching

Figure 2.3 shows schottky diode standard model in RF frequencies with its packaging parasitics. The diode package leads are modeled with series inductance L_S and shunt capacitance C_P, R_S represents the contact resistance and the diode junction is represented by a parallel resistance and capacitance. The diode junction resistance R_j and capacitance C_j are functions of the RF incoming signal as shown in Figure 2.3 which indicates that the diode impedance will change with the incoming RF signal and its frequency, this makes impedance matching between the antenna and the rectidier very challenging. It is impossible to match the rectifier and the antenna for a wide range of frequencies and input power levels, usually the designers aim to match them for an specific frequency and input power level specified by the desired application.
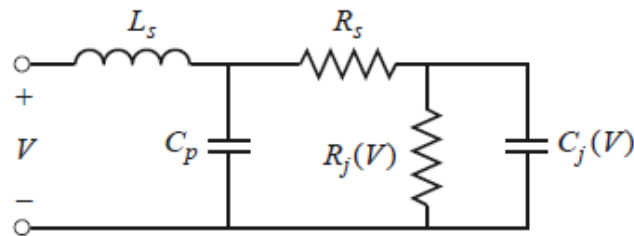
Figure 2.3 Schottky diode RF model [7]

2.1.2.3 Harmonic generation

While diodes are converting RF signals to DC, they generate harmonics from the RF input signal. The generated harmonics reduce the amount of the RF signal that is being converted to DC and as well reduce the conversion efficiency. When the input RF signal increases, the harmonics generation increases.

2.1.3 RF-DC conversion Efficiency

RF energy harvesting circuits are evaluated using two parameters, RF-DC conversion efficiency and sensitivity. RF-DC conversion efficiency represents the portion of the RF power that being converted to DC. The generated DC power is calculated as

$$P_{DC} = \frac{V_{DC}^2}{R_L} \qquad (2.3)$$

where V_{DC} is the generated DC voltage across the load resistor R_L. Then the conversion efficiency η_{DC} is calculated using

$$\eta_{DC} = \frac{V_{DC}^2 / R_L}{P_{in}} \qquad (2.4)$$

where Pin is the input RF power at the input the rectifier. As discussed in section 2.1.2, there are many sources of losses in a rectenna and these losses reduce the RF-DC conversion efficiency significantly which makes achieving high conversion efficiency very difficult. Figure 2.4 shows the losses effect on the conversion efficiency, the RF input power must be higher than the turn on voltage and lower than the diode
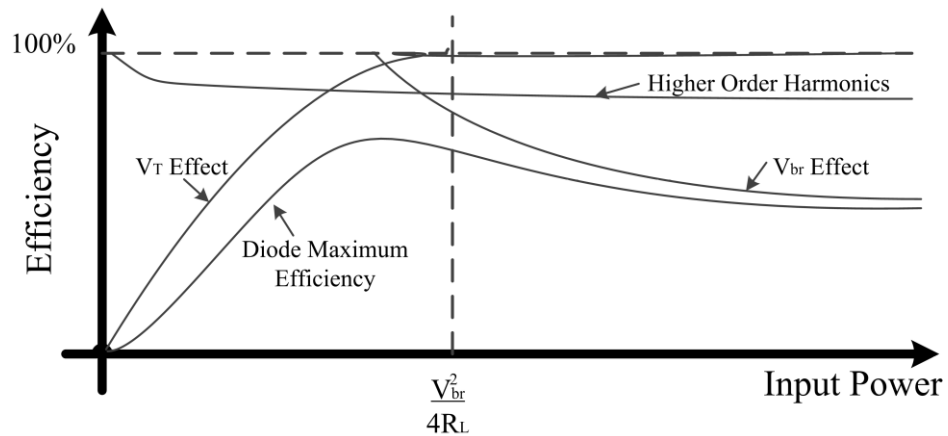
Figure 2.4 Rectenna RF-DC conversion efficiency characteristics [8]

12

breakdown voltage. The higher order harmonics also reduce the converted portion of the FR power which reduces the RF-DC conversion efficiency. Due to these losses there must be tradeoffs to get the optimal conversion efficiency.

2.2 Rectifier Circuit Topologies

There are many circuit topologies used to design RF rectifiers based on diodes. The choice of a certain topology depends on the application that the rectifier is designed for, if the target is to design a high sensitivity rectifier then a simple rectifier with one diode is the most suitable topology to work for low input RF signals. If high voltage is required then charge pump topologies are the most suitable options where cascaded diodes are used to get high voltage with low sensitivity but relatively high level RF input signal is needed to turn on the diodes.

The half wave rectifier is the simplest rectifier topology where one diode is used as shown in Figure 2.5. Half wave rectifiers are suitable for low frequencies as they are not preferred at RF due to many factors. One diode operation needs the input RF signal to be larger than the diode turn in voltage and the output DC voltage is bounded by the diode breakdown voltage as discussed in section 2.1.1. The full wave rectifier has the
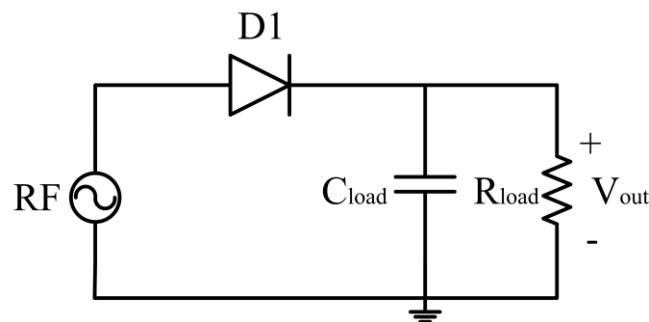
Figure 2.5 Half wave rectifier [8]

13

same problems as the half wave rectifier while using two diodes. The maximum conversion efficiency for the half wave rectifier is 40.6% [9] which is very low so this topology is rarely used in RF applications.

An efficient rectifier topology with high sensitivity is shown in Figure 2.6 which is called the single shunt rectifier. High sensitivity is achieved through using one shunt diode and the high efficiency is obtained by using a quarter wavelength transformer that will reflect the generated harmonics back again to the rectifier which will increase the overall DC power generated. It is not preferable with low frequencies due to the large length of the quarter wavelength transformer but at high frequencies this length is acceptable.
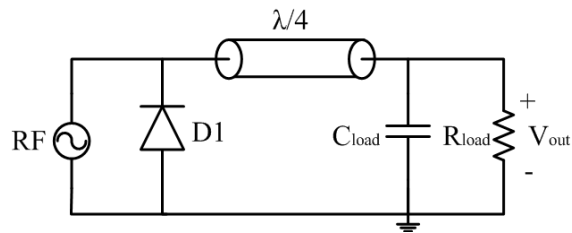
Figure 2.6 Single Shunt Rectifier [8]

When high voltage is required to operate electronic devices then voltage multipliers are used as single diode rectifiers will not provide enough voltage. Voltage multipliers are
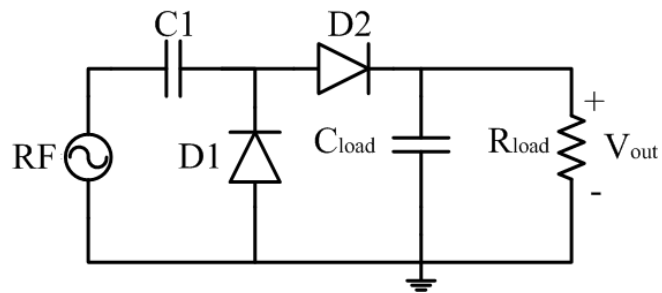
Figure 2.7 Single stage voltage multiplier [8]

14

the basic block in any charge pump rectifier such as Dickson and Greinacher pumps [10]. Figure 2.7 shows a single stage voltage multiplier and is sometimes called a voltage doubler because it doubles the peak RF voltage. The input RF signal turns on diode D1 that generates DC power which will be stored in capacitor C1 and biases diode D2.

Figure 2.8 shows Crockcroft Walton charge pump which is one of the well known charge pumps. Crockcroft Walton designed it to provide high voltage for their experiments. A high voltage up to 700 KV was achieved using multiple stages of voltage multipliers and other components [10]. This high voltage comes with many drawbacks that makes it impractical for some energy harvesting applications. When increasing voltage multiplier stages, the circuit output impedance will be high which introduce large losses before the DC power reaches the load. Also the capacitor values must be higher than the parasitic values so to bias the next stage this condition makes the circuit difficult for integrated designs.
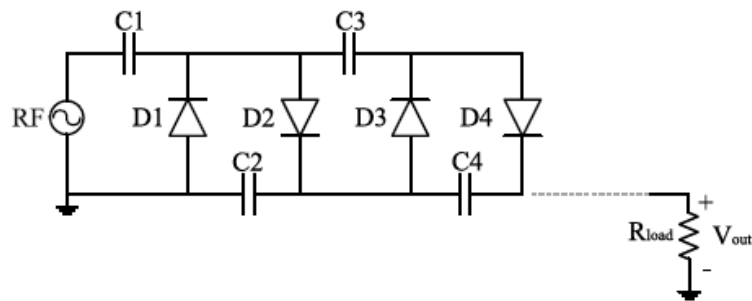
Figure 2.8 Cockcroft Walton charge pump [8]

2.3   Patch Antennas

Low profile antennas are required due to their light weight, low cost, small size and ease of fabrication [11]. They are a must in many applications such as wireless and satellite

communications. Patch antennas are the most known low profile printed antennas, they are used extensively in microwave frequencies due to their simple designs and their compatibility with the printed circuit technology.

2.3.1 Conventional Patch Antenna Geometry

Figure 2.9 shows the conventional rectangular patch antenna geometry. It consists of a thin metallic patch usually a rectangular patch but other shapes are reported in literature such as circular, triangular, elliptical and other shapes. The metallic patch resides on a substrate with height **h** as shown in Figure 2.9, then there is a ground layer at the bottom of the substrate. Many substrates with different dielectric constants can be used deign patch antennas. Thick substrate with low dielectric constant will result in patch antenna with wide bandwidth, high efficiency and small losses but this comes in expense of the antenna large which is undesirable in any applications. To get antenna with small size, thin substrate with high dielectric constant are used which will tightly coupled the fields and minimize undesired radiation but in expense of narrower bandwidth and less efficiency.
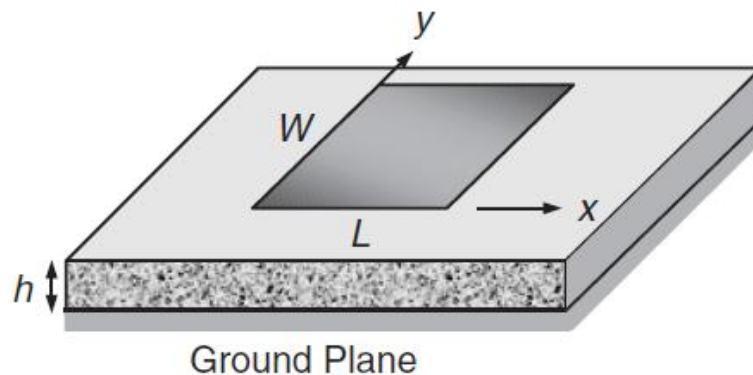
Figure 2.9 Conventional rectangular patch antenna geometry [12]

2.3.2 Patch Antenna Feed Methods

For microstrip patch antennas there are four major feeding methods which are coaxial probe feeding, microstrip line feeding, proximity coupled feeding and aperture coupled feeding [11]. These methods are shown in Figure 2.10. The first two methods depend on connecting a metallic feed part to the patch and the last two methods depend on noncontacting feeding using coupling through slots.

In coaxial probe feeding, the coax inner conductor is connected to the patch and the outer conductor of the coax is attached to the ground layer. Probe feeding has the advantage of easy fabrication and matching but it is not easy to model. Microstrip line feeding is the most popular feeding method for patch antennas. It is simple to model and also to match through proper inset positioning. However with the increasing of the substrate thickness, spurious radiation and surface waves will increase too which will result in narrow bandwidth.
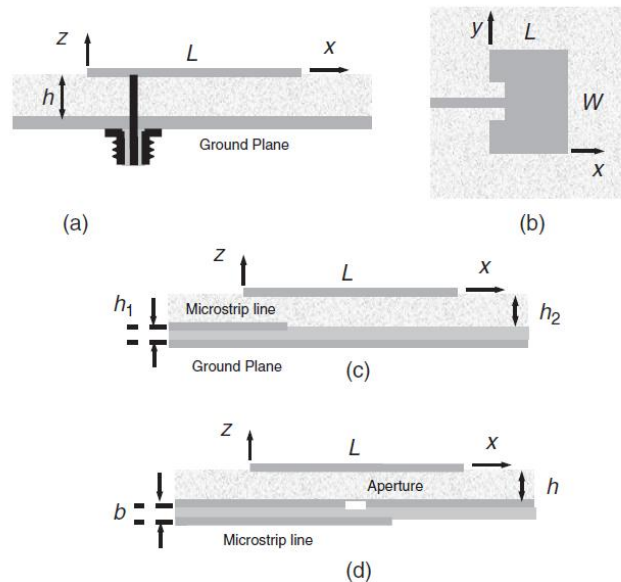
Figure 2.10 Patch antenna feeing methods: (a) probe feeding, (b) microstrip line inset feeding, (c) proximity coupled feeding, and (d) aperture coupled feeding [12]

17

To overcome the problem of spurious radiation in probe feeding and microstrip line feeding methods, aperture coupling and proximity coupling feed are introduced so that there are no metallic part attached to the patch. Aperture coupled feeding consists of two substrates with a ground layer in the middle which is difficult to fabricate and increase the antenna size. The patch on the top layer is coupled using slot to a microsrip line which is on the ground layer so that the feed line is completely isolated from the radiating patch. The antenna can be matched by changing microstrip line width, the slot position and size. For proximity coupled feeding, a feed line in the middle of two substrates in which the patch on the top layer and the ground is on the bottom layer. This method is reported to has the widest bandwidth among the methods discussed here.

2.3.3 Patch Antenna Analysis

Patch antenna is one of few printed antennas that have mathematical analysis to specify the antenna dimension and resonance frequency. Many methods for patch antenna analysis were reported, the most popular methods are the transmission line and cavity methods [11]. Transmission line analysis is the simplest method but with less accuracy compared to the cavity model.

In the transmission line method the patch antenna is represented using two slots separated by a transmission line with low impedance. For a rectangular patch antenna, due to the finite patch dimensions along its width and length the fields at the patch edges undergo fringing as shown in Figure 2.11. The fringing amount is a function of the patch dimension and the substrate height, for microstrip patch antennas the length is much larger than the substrate height so that the fringing effect is reduced but it is still can

18

change the antenna resonance. To take the fringing effect into account, the effective

dielectric constant ε_{reff} concept is introduced and it can be calculated using

$$\epsilon_{reff} = \frac{\epsilon_r+1}{2} + \frac{\epsilon_r-1}{2}\left[1 + 12\frac{h}{W}\right]^{-1/2} \tag{2.5}$$

where h is the height of the substrate, W is the width of the path and ε_r is the substrate

dielectric constant.
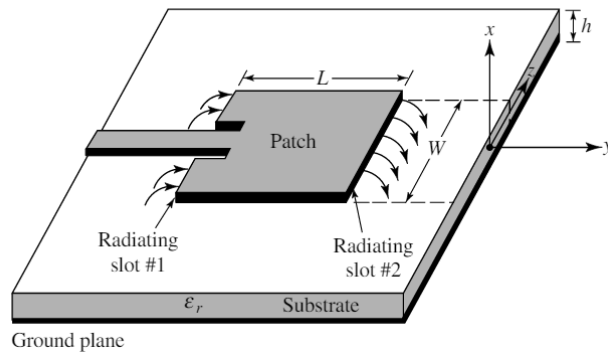
Figure 2.11 Patch antenna with fringing effect [11]

Due to the fringing effect, the patch antenna appears to has electrically larger size than its

original physical size as shown in Figure 2.12. The increase in the patch length ΔL can be

calculated using

$$\frac{\Delta L}{h} = 0.412\frac{(\epsilon_{reff}+0.3)\left(\frac{W}{h}+0.264\right)}{(\epsilon_{reff}-0.258)\left(\frac{W}{h}+0.8\right)} \tag{2.6}$$
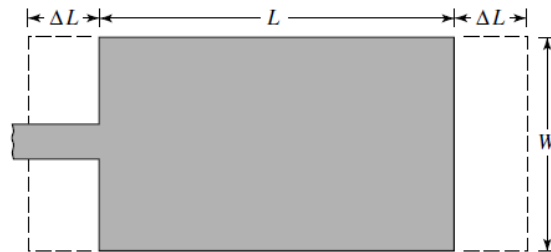
Figure 2.12 Patch antenna effective length [11]

19

The resonance frequency of the patch antenna fundamental mode TM_{010} can be calculated using

$$f_{r010} = \frac{v_0}{2L\sqrt{\epsilon_r}} \qquad (2.7)$$

where v_0 is the free space speed of light. Using transmission line model the rectangular patch antenna can be designed using the following steps

- The patch width W for a good radiation characteristics can be calculated using

$$W = \frac{v_0}{2f_r}\sqrt{\frac{2}{\epsilon_r+1}} \qquad (2.8)$$

- Calculate the effective dielectric constant ε_{reff} using (2.5).

- Calculate the patch length extension ΔL using (2.6).

- Calculate the physical length of the patch L using

$$L = \frac{1}{2f_r\sqrt{\epsilon_{reff}}\sqrt{\mu_0\epsilon_0}} - 2\Delta L \qquad (2.9)$$

2.4 Monopole Antennas

A monopole antenna is a half of a dipole antenna that mounted on infinite ground plane as shown in Figure 2.13. The theory of a monopole antenna depends on the image theory which states that the fields above the ground layer can be determined through using equivalent source in free space [11], this is means a monopole antenna with length L on an infinite ground plane is a dipole antenna with twice the length (2L). The monopole antenna has an input impedance equals half of the input impedance of a centered dipole antenna [12]. The monopole antenna radiation pattern is the same as the upper half of the equivalent dipole antenna, also the directivity of the monopole antenna is twice the

20

directivity of its corresponding dipole antenna as in the monopole case there is no radiation under the ground layer. All these comparisons apply when the monopole antenna ground plane is infinite but if it is finite the image theory will not hold any more.
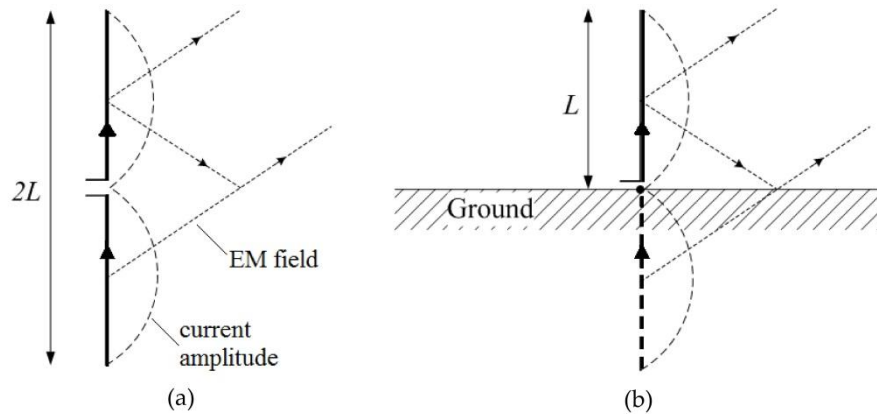
Figure 2.13 Monopole and dipole antennas with the same characteristics (a) dipole antenna, and (b) Monopole antenna

2.5   Summary

In this chapter, the design considerations for designing RF rectennas is discussed. The discussion focuses on the diode behavior as it is a nonlinear device which needs to be handled carefully. Then the main sources of losses in any RF energy harvesting system is investigated and their effect on the DC power generation is mentioned. The most well known rectifier circuit topologies that used for RF to DC conversion are investigated and their advantages and disadvantages are discussed. Patch and monopole antennas fundamentals are investigated and their main features are discussed.

CHAPTER 3

LITERATURE REVIEW

A literature survey is done for three different topics. The first section discusses printed rectennas found in literature, in the second section dual band meander line antennas (MLA) in literature are investigated. In the third section dual band patch antennas miniaturization techniques are listed.

3.1   Printed Rectennas

Research on rectennas is gaining bit of momentum due to the energy solution they might offer. In literature, many types of rectennas were reported based on different types of antennas such as wire antennas (dipoles, monopoles), antenna arrays, integrated solar cells rectennas and single element printed antennas. In this work, different types of rectennas from literature which are based on the single element printed antennas will be discussed.

3.1.1   Single Band Rectennas

In this section, rectennas which are working in a single frequency band are discussed. The frequency band is dependent on the application that the rectenna is designed for. For RF energy harvesting, most rectennas are working in the bands of GSM 900MHz, GSM 1800MHz, but for the wireless power transmission, most of them are working in the ISM bands (2.45 GHz, 5.8 GHz).

Patch antennas are the most used antennas for designing printed single band rectennas [13]–[20]. In [13], a 2.45 GHz dual polarized rectenna for energy harvesting applications is proposed. The rectenna is based on a square aperture coupled patch antenna. A 32.5% size reduction is achieved by introducing the cross shaped slot etched on the antenna surface as shown in Figure 3.1. Also the orthogonal coupling slots introduce a dual linearly polarization property for this antenna. The antenna size was 34x34 mm^2 and fabricated on two Arlon A25N substrates (20 mil thickness) separated by a Rohacell 51 foam layer (6 mm thickness). The antenna measured directivity was 7.5 dB. The rectenna maximum simulated RF-DC conversion efficiency was 15.7% and 42.1% for input power of -20 dBm and -10 dBm respectively.
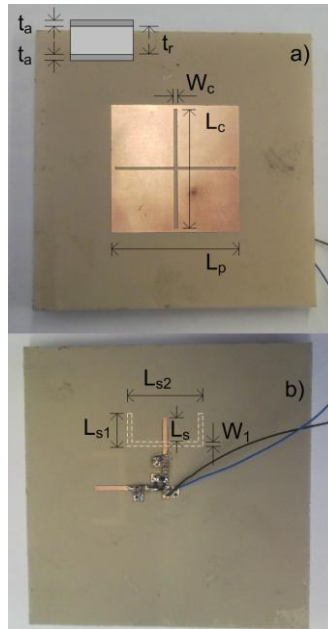
Figure 3.1 the fabricated rectenna with its (a)top view (b)Bottom view [13]

In [21] a 2.45 GHz rectenna based on miniature second iteration Koch antenna is proposed for battery less RFID sensors. This antenna geometry is applied to a patch

antenna to reduce its size as shown in Figure 3.2. The rectenna gain is 4 dB. Two-stage Dickson charge-pump configuration is designed and proposed, resulting in a DC that is four times larger than the peak RF voltage. RF-DC conversion efficiency up to 70% at RF power input of 3 dBm is achieved. But with low inputs, the RF-DC efficiency goes down to less than 10% for input power less than -20dBm. The rectenna was fabricated on RO3006 layer (50 mil thickness and dielectric constant = 6.15).
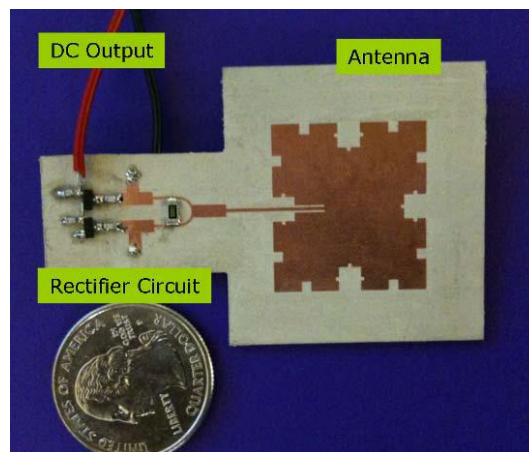
Figure 3.2 the fabricated Koch antenna [21]

In [22] a rectenna working at GPS L1 (1.575 GHz) band is proposed for low input power applications. The rectenna consists of an electrically small antenna (ESA) and a Schottky diode with a total size of 70x32 mm^2 as shown in Figure 3.3. The antenna size is 38x32 mm^2 and it is matched to the input impedance of the rectifying circuit. The results showed that when the input power is 1.0 mW (0 dBm), the rectenna efficiency measured on a load resistor 1540 Ω is 34.1% with a voltage of 0.73V cross the resistor. The rectenna was fabricated on Rogers DuriodTM 5880 material.
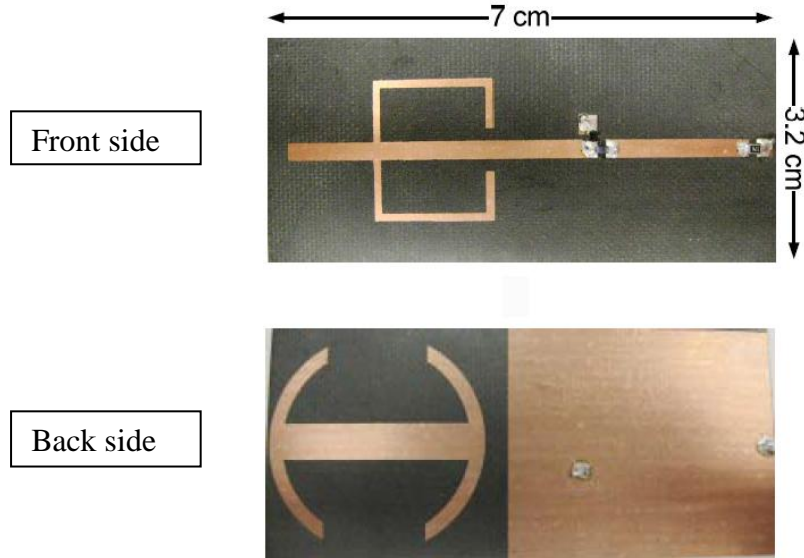
Figure 3.3 the front and the back sides of the rectenna [22]

A 2.45 GHz rectenna based on planar inverted-F antenna PIFA is proposed for energy harvesting systems in [23]. The PIFA size was 90x40x2 mm^3 as shown in Figure 3.4. The rectenna RF-DC conversion efficiency was 55.6% when the RF power density is 1.6 mW/cm^2. The rectenna can generate 1.9 V with a load of 200 Ω.
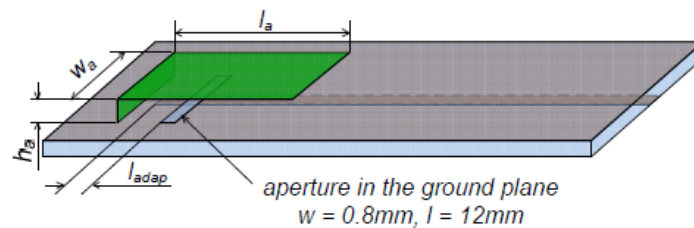
Figure 3.4 The geometry of the proposed PIFA [23]

In [24] a 2.45 GHz rectenna based on a simple structure antenna with high gain is proposed. The rectenna shown in Figure 3.5 has a size of 85x80 mm^2. The measured

antenna gain was 8 dBi. The rectenna efficiency was up to 50% when the input power is 1 mW (0 dBm).
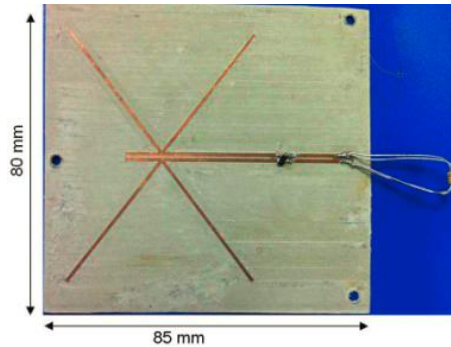
Figure 3.5 the proposed high gain rectenna [24]

In [25] a 2.45 GHz rectenna based on a dual polarization diversity antenna has been developed. The antenna is fed by two probes as shown in Figure 3.6 and an annular rectangular-ring slot is inserted on the antenna to enhance its isolation which is found to be higher than 30 dB. The antenna has a gain of 7 dB. The rectenna size was 80x80 mm^2. The rectenna was matched by stubs. The output voltages from the rectifier were 1.923, 1.842, 1.724, 1.172, 0.602, 0.301 and 0.166 V at 2.45 GHz, when a signal generator transmitting the RF power level: 10, 5, 0, -10, -15 and -20 dBm, respectively.
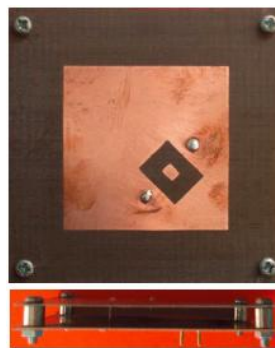
Figure 3.6 the fabricated dual polarized rectenna [25]

In [26] a 5.8 GHz bow-tie loop antenna was developed to be used in rectenna application. The proposed antenna has a broad beam width and a high gain of 9.5 dBi. The antenna size was 20x36 mm^2 and its geometry is shown in Figure 3.7. The antenna is printed on a substrate with 0.8mm thickness and a dielectric constant of 2.8.
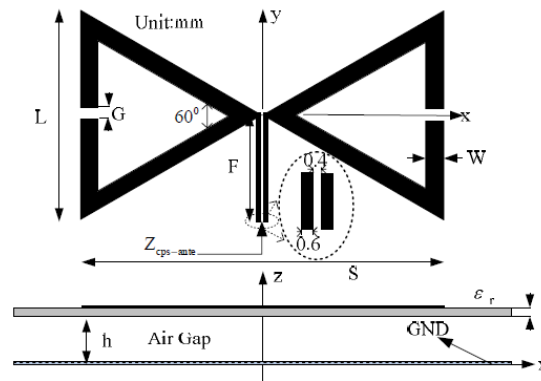
Figure 3.7 geometry of the Bow tie antenna [26]

In [27] a 2.45 GHz miniaturized tag antenna was developed for wireless sensors powering. The antenna is shown in Figure 3.8 and has size of 10x12x0.5 mm^3 with -5.9 dB gain. The antenna was fabricated on Rogers RO4003C (dielectric constant=3.55, thickness=0.5 mm). The rectenna achieved a maximum conversion efficiency of 29.5% when the input power to the rectifier was 6 dBm.
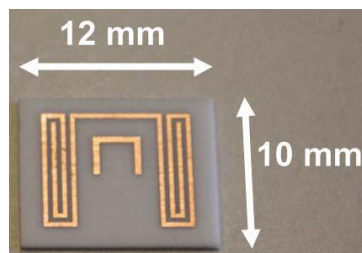
Figure 3.8 the miniaturized tag antenna [27]

A miniaturization technique by introducing a circular slot into the ground plane is proposed in [28] and [29]. The two antennas can be used in rectenna and active integrated antenna (AIA) applications. The two antennas had the same size which was 55x40 mm^2 and have a harmonic suppression property. In [28] a 2.45 GHz circular patch antenna is proposed. As shown in Figure 3.9, the slits which are on the antenna and the stub are introduced for harmonic suppression. The antenna is fabricated on an FR4 material (thickness =1.6mm and dielectric constant = 4.7). The circular patch antenna had a gain of 2.229 dB and radiation efficiency of 72.33%. In [29] a 2.45 GHz rectangular patch antenna was introduced. As shown in Figure 3.9, the curvature slots and the loaded notch with the open stub are introduced for harmonic suppression as well. The circular patch antenna has a gain of 2.817 dB and radiation efficiency of 83.55%. The discussion above shows the performance of the rectangular patch antenna introduced in [29] is better than the performance of the circular patch antenna introduced in [28].

(a)   (b)
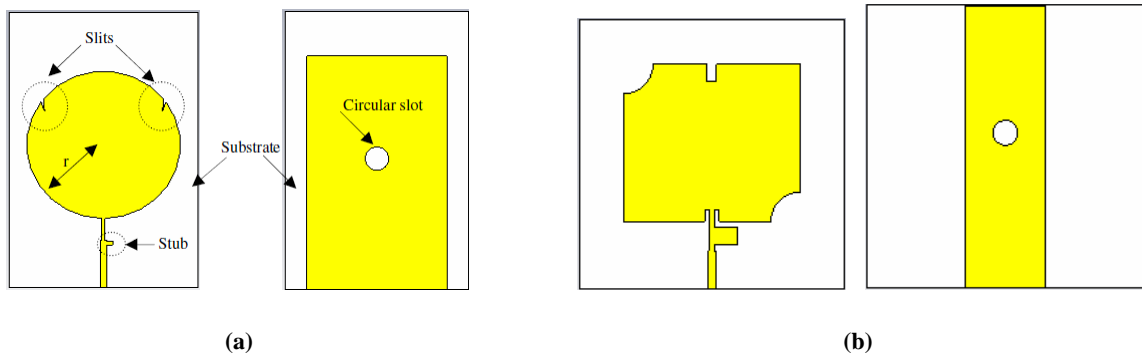
Figure 3.9 Patch antennas (a) Circular [28]**, (b) Rectangular** [29]

In [30] a 915 MHz meander circular PIFA is proposed for energy harvesting in a head mountable deep brain stimulation (DBS) device. As shown in Figure 3.10, the proposed antenna has a physical area of 3.14x102 mm^2. The antenna is fabricated on FR4 material

and had a gain of -18.28 dB. The antenna efficiency was 14.51% with 18 MHz bandwidth. A rectifier is designed to be integrated with the antenna, a conversion efficiency of 74 % is achieved when the input power is 37 dBm.
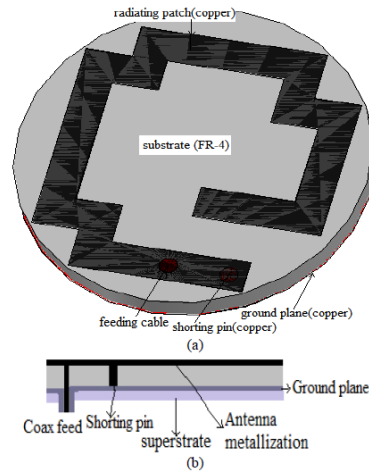
Figure 3.10 the geometry of the circular PIFA [30]

In [31] a 900 MHz rectenna based on a miniaturized loop antenna is proposed. By introducing the meander line structure, a 50% size reduction is achieved and the new size is 60x80 mm^2 as shown in Figure 3.11. The antenna gain is 4.22 dBi with 97% radiation efficiency. The rectenna is fabricated on a double side FR4 substrate. The RF-DC conversion efficiency was up to 47% when the received RF signal was 0 dBm and the load was 5 Kohm.
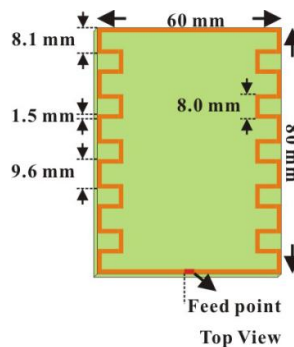
Figure 3.11 geometry of the loop antenna [31]

29

In [32] a 5.8 GHz bow-tie retrodirective rectenna is introduced as shown in Figure 3.12. The retrodirective array was used to steer the rectenna main beam towards the power source. The retrodirective rectenna has a size of 70x37 mm^2 and it was fabricated on Rogers Duroid 5880 substrate. The rectenna had two coplanar stripline (CPS)-fed bow-tie antennas, a rectifying diode, two bandpass filters, and a resistive load. The bow-tie patch antenna had higher gain than the ordinary patch antenna and the rectifying diode can be mounted easily between the two pairs of coplanar stripline, for those advantages the bow-tie was chosen. At 5.8 GHz, the bow-tie antenna had a gain of 5.8 dBi. The beam steering is controlled by two pairs of bow-tie antenna where one pair can serve as the receiver and the other pair serves as the transmitter. The rectenna conversion efficiency was up to 84% with a power density of 10 mW/cm^2.
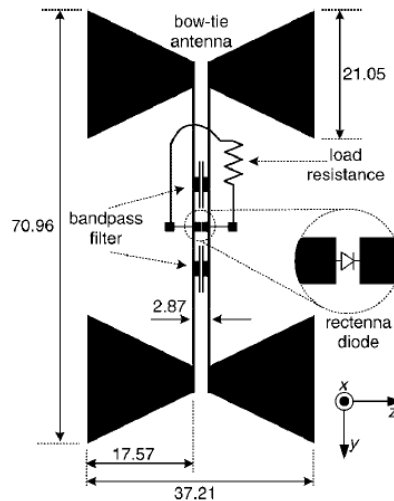
Figure 3.12 the retrodirective rectenna [32]

In [33] a 5.8 GHz a finite ground coplanar waveguide (FG-CPW) rectenna was proposed. The rectenna consists of a patch antenna, compact CPW resonant cell (CCRC) band stop filter and a Schottky barrier diode as shown in Figure 3.13. The antenna has 9 dBi gain

and 90% efficiency with size of 79x21 mm^2. The rectenna is fabricated on RT/Duroid 6002 substrate with a dielectric constant of 2.94 and has RF-DC conversion efficiency is 68.5% at 270Ω load when the input power is 18 dBm.
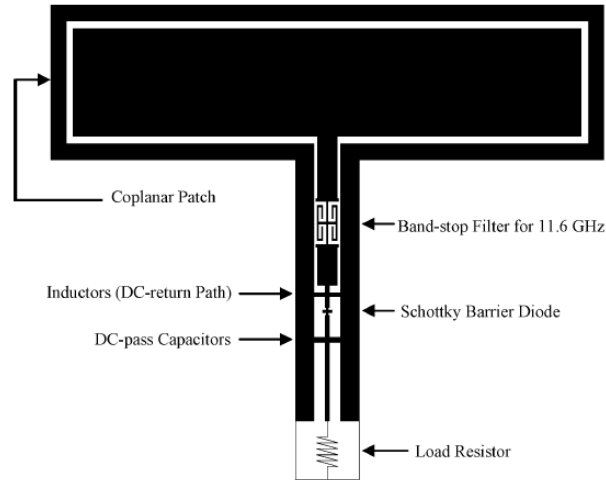
Figure 3.13 Geometry of FG-CPW rectenna [33]

In [34] a 5.8 GHz compact size rectenna based on an open ended diamond antenna is introduced. The proposed antenna had the same dimensions of a conventional patch antenna but with narrower half beamwidth (75 deg.) and higher gain which was not specified in the paper. The antenna size was 17x17 mm^2 as shown in Figure 3.14 and the rectifier size was 10x10 mm^2. The rectenna was fabricated on Resin substrate (0.5 mm thickness). The rectenna conversion efficiency was 59.5% and can achieve output DC voltage of 77 mV when the rectenna distance from the intentional source is 0.6 meter. The authors also fabricate a two element array with the proposed antenna and the measured output voltage is 177 mV when the distance was 0.6 meter.
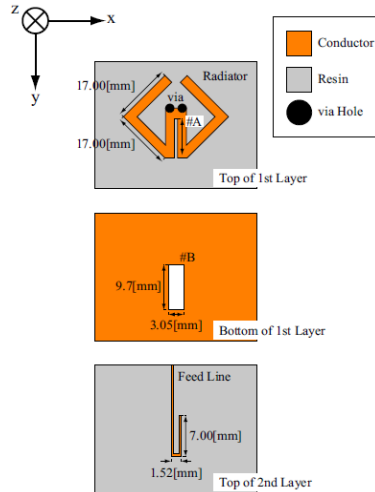
Figure 3.14 Geometry of the diamond antenna [34]

In [35] a 5.8 GHz stacked differential mode rectenna is introduced for large scale rectenna arrays. As shown in Figure 3.15, the rectenna consists of three microstrip patch antennas, two schottky diodes, four shorted stubs for harmonics suppresion and two capacitors for storing the energy. The fabricated rectenna has size of 120x40 mm^2 and it is printed on a teflon fiber substrate (0.8 mm thickness) with a dielectric constant of 2.15. The measurements stated that the rectenna has RF-DC conversion efficiency of 37.1 even with low received power density until 0.04 W/m^2. The proposed rectenna can be used for large scale rectenna arrays with the same conversion efficiency.

In [36] a 5.8 GHz rectenna with data communication property based on an aperture coupled dual linear polarized patch antenna is proposed. As illustrated in Figure 3.16, the vertical feed (V port) for the rectenna with 7.2 dBi gain and the horizontal feed (H port) for data communication with 7.6 dBi gain. The rectenna has a size of 38x38 mm^2. The reported conversion efficiency was 81% at input power of 10 mW.
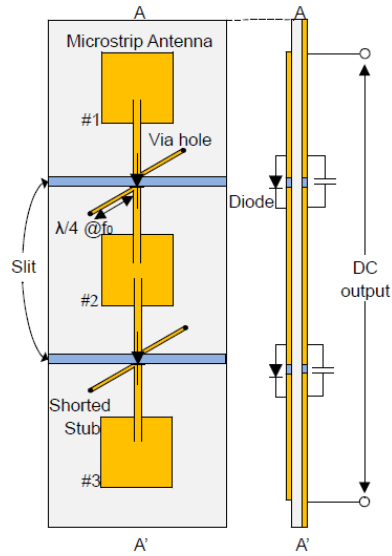
Figure 3.15 Structure of the stacked differential mode rectenna [35]
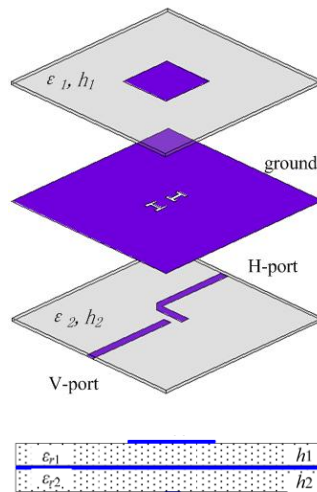
Figure 3.16 the proposed dual polarization antenna with its side view [36]

Most of the papers discussed earlier proposed antenna with linear polarization, but there are some novel designs based on a circular polarization antennas because with a circular polarization, the losses due to polarization mismatch will be minimum. The works in [37]–[43] discuss circular polarization rectennas.

In [37] a 2.45 GHz rectenna based on a circularly polarized printed shorted annular ring slot is proposed. The rectifier was located at the back side of the antenna to reduce its dimensions. The rectenna size is 95x95 mm^2 and its geometry is shown in Figure 3.17. The measured antenna gain was 4.7 dB. The rectenna was printed on ARLON 25N substrate with a dielectric constant of 3.38. The rectenna conversion efficiency was 56% at input power density of 20 μW/cm^2 and 2500 Ω as load, the output DC voltage was 1.1 V.
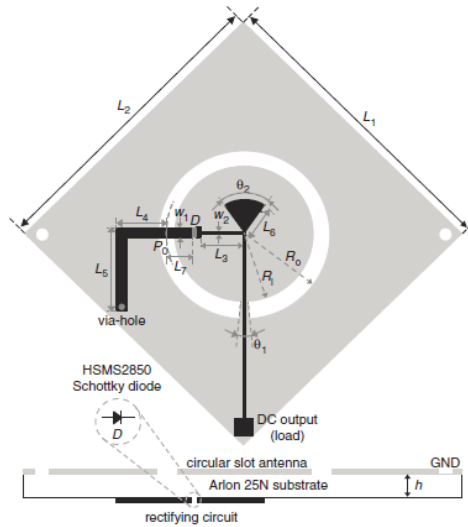
Figure 3.17 the annular ring slot rectenna geometry [37]

In [38] a 2.45 GHz circulary polarized rectenna with 2nd order harmonic rejection property was proposed. The rectenna is based on a circularly polarized patch antenna with introducing two unbalanced circular slots for size reduction (12% size reduction) and also for 2nd order harmonic rejection. The rectifier with the 3rd order harmonic rejection is on the back side of the antenna as shown in Figure 3.18. The rectenna size was 60x60 mm^2. The rectenna was fabricated on a two layer low cost FR4 substrate with

h1=1.6 mm and h2=0.8 mm with a dielectric constant of 4.4. The rectenna bandwidth was 137 MHz and provides up to 15.8 V with 78% conversion efficiency at input power density of 16.5 mW/cm^2 on 1 KΩ load.
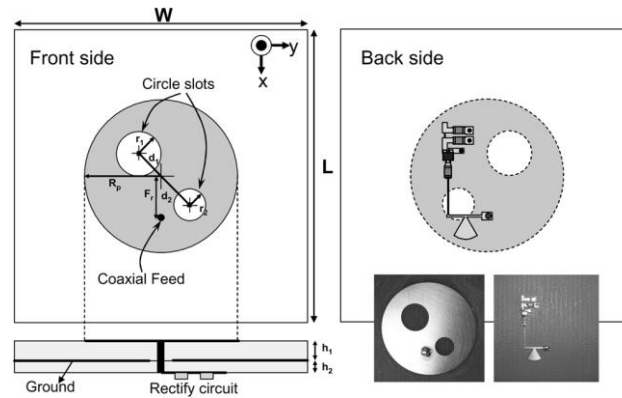
Figure 3.18 the rectenna with two unbalanced circular slots [38]

In [39] a 2.45 GHz square microstrip antenna with circular polarization and harmonic rejection was proposed. The harmonic rejection is achieved by introducing four slits on the antenna. Figure 3.19 shows the proposed antenna which had size of 60x60 mm^2 with maximum gain of 3.4 dBi and 137 MHz bandwidth. The rectenna conversion efficiency is 37.8% with 30 Kohm as a load.
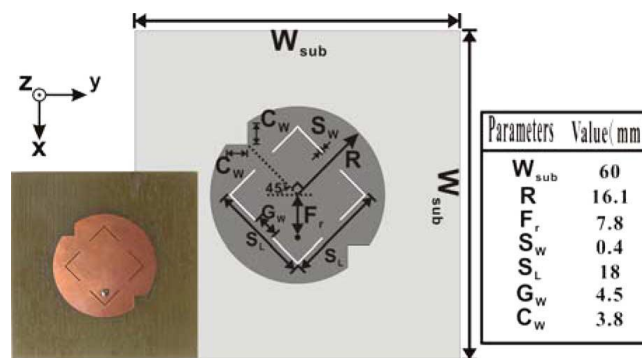
Figure 3.19 the proposed square microstrip antenna [39]

2.45 GHz rectennas based on a dual circularly polarized (DCP) patch antennas were introduced in [40] and [41]. A T-shape slot on the ground plane was introduced in [40] as shown in Figure 3.20. The T-shape is designed to provide circular polarization, second harmonic rejection and impedance matching. The antenna in [40] has LHCP and RHCP with gain of 8 dBic and 7.98 dBic, respectively. The antenna size was 100x100 mm^2 with a 40 MHz bandwidth.
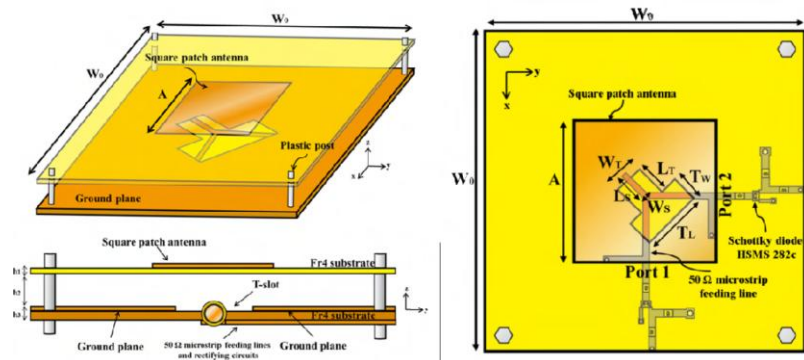
Figure 3.20 Layout of the T-shape slot DCP rectenna [40]
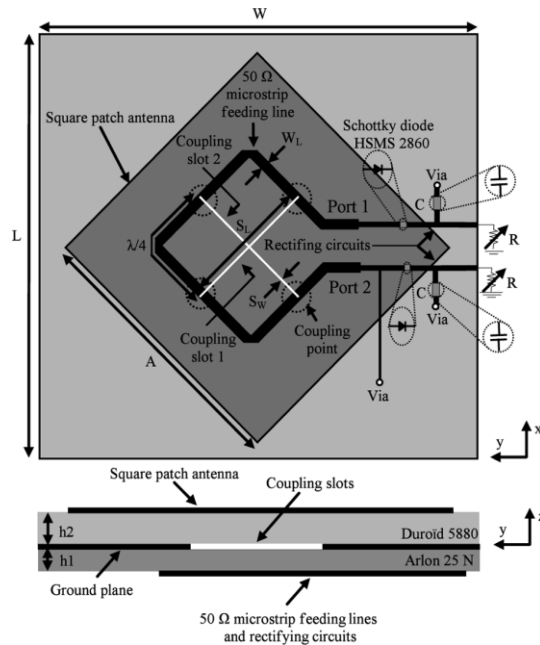
Figure 3.21 Layout of the of the DCP rectenna [41]

36

As shown in Figure 3.21, two orthogonal slots in [41] are introduced on the ground plane to provide LHCP and RHCP with gain of 6.8 dB and 25.24 dB, respectively. The rectenna size was 100x110 mm^2. A maximum conversion efficiency of 63% was achieved across a load of 1600 Ω when the power density is 0.525 mW/cm^2.

A circularly polarized patch antenna with data communication capability was introduced in [42]. The rectenna was working at 5.5 GHz and the data communication in the band 5.15–5.35 GHz. The antenna size was 14.8x14.8 mm^2. By manipulating the two slots on the patch as shown in Figure 3.22, we can get RHCP or LHCP. The rectenna maximum gain was 8 dBi and a conversion efficiency of 57.3% at load of 300 Ω was achieved when the power density is 2.55 mW/cm^2.
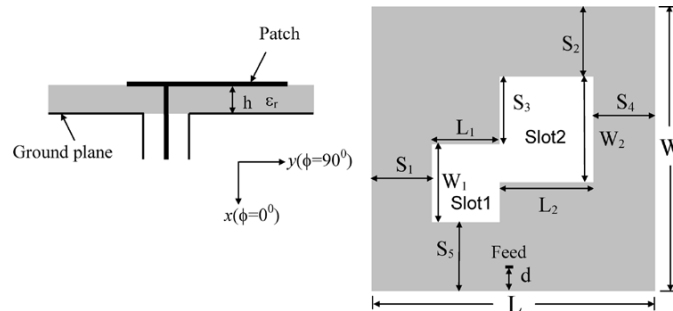
Figure 3.22 The circularly polarized patch antenna [42]
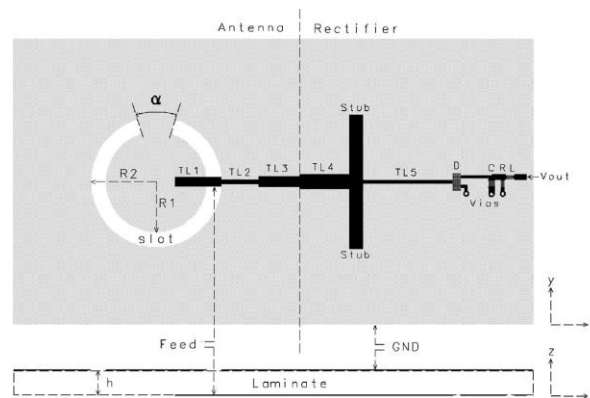
Figure 3.23 the proposed low profile rectenna [43]

37

In [43] a 5.8 GHz circularly polarized rectenna based on shorted annular ring slot antenna is proposed. The rectenna size was 57.4x57.4 mm^2 with 6.1 dB gain. The antenna structure is shown in Figure 3.23.

3.1.2 Wide Band Rectennas

In this section, wide frequency band rectennas will be discussed. There are a few wide band rectennas reported in literature.

The work in [44] represents a wideband composite Right/Left Hand (CRLH) rectenna. The rectenna operated at the band from 700 - 1000 MHz for energy harvesting applications. The rectenna has a size of 16.4 cm x 3.7 cm and consists of 3 CRLH units and is fed through a coplanar transmission line as shown in Figure 3.24. The antenna lies on an FR-4 substrate with 4.7 dielectric constant. The gap between the units represents a series capacitance. The antenna bandwidth was 290 MHz with 3.24 dBi gain at 900 MHz.
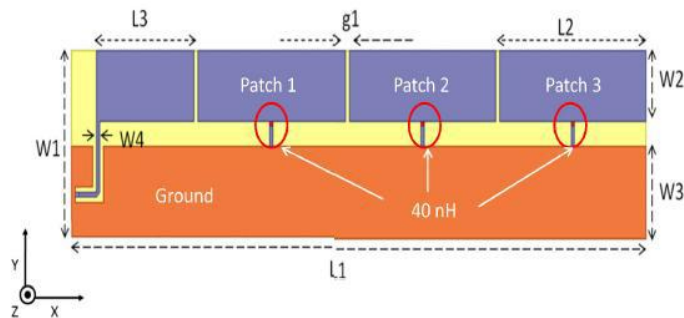
Figure 3.24 3 cell CRLH antenna [44]

An ultra wide band UWB antenna is introduced in [45] for wireless power transmission applications. The proposed antenna operates in the band from 2 - 6 GHz and has a size of 47.6 x 28 mm^2. The maximum gain of the antenna measured at different frequencies was

1.26 dBi at 2.5 GHz, 0.37 dBi at 3.8 GHz and 3.32 dBi at 5.8 GHz respectively. The rectenna conversion efficiency was up to 43.3% across a load of 1300 Ω when the input power was 0 dBm. The antenna structure is shown in Figure 3.25.
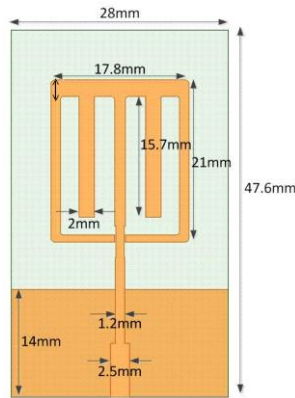
Figure 3.25 geometry of the planar ultra wide band antenna [45]

In [46] a wide band bow-tie antenna is proposed for energy harvesting applications. The antenna resonates in the band from 845-3500 MHz. As shown in Figure 3.26, by introducing a loaded ring, the antenna operating frequency band is shifted to lower frequencies. The proposed antenna has a gain in the range 2.5 - 5.5dB. As shown in Figure 3.26, the antenna outer ring had 4.7 cm radius which means that the antenna had a big size. A measured DC voltage of 1.2 V was achieved across 5 KΩ load when the power density was 0.07 W/m^2.
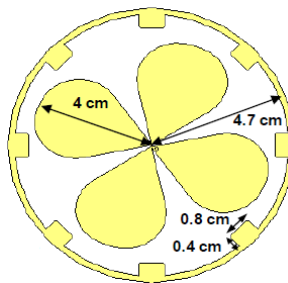
Figure 3.26 the proposed bow-tie antenna [46]

39

A broadband implantable rectenna with stacked PIFA structure was proposed in [47] for medical implants. The rectenna has a 50 MHz bandwidth and works in the band (377 - 427 MHz). The rectenna contains an implantable PIFA on the top side of the substrate and doubler rectifier consists of two schottky barrier diodes on the back side. Figure 3.27 shows the proposed stacked rectenna which consists of three top layers as the antenna and the bottom layer as the rectifier. Layer 1 is the ground plane and the radiating elements of the PIFA are in layer 2 and layer 3. The RF-DC conversion efficiency was up to 80% across a load of 20 KΩ when the input power was 2 dBm.
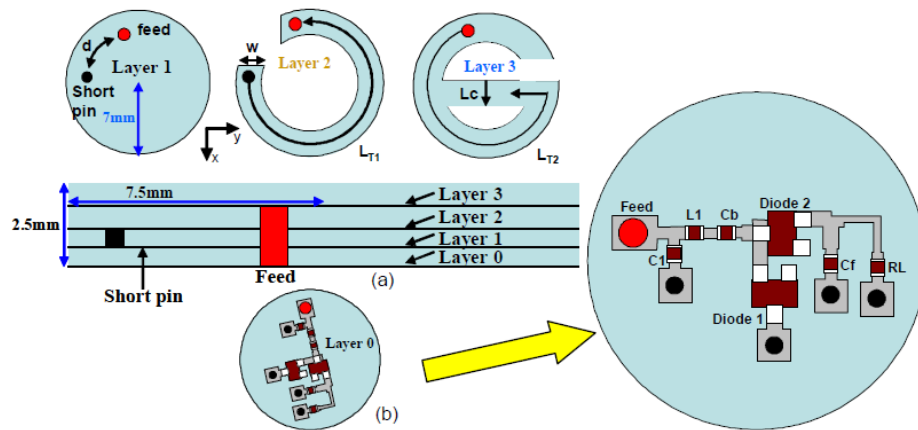
Figure 3.27 stacked antenna (a) implanted PIFA (b) The rectifier at the bottom [47]

In [48] a dual band rectenna based on a broadband 1x4 quasi Yagi antenna array is proposed for RF energy harvesting. The dual bands of the rectenna are 1800 MHz and 2100 MHz bands and the bandwidth of the 1x4 quasi Yagi antenna was 400 MHz which is from 1800 to 2200 MHz. To design the 1x4 quasi Yagi array antenna, first 1x2 subarray with 190 x 100 mm^2 is introduced as shown in Figure 3.28 and then the 1x4 array is fabricated by simply connecting two 1x2 subarrays with a T-junction power divider. The array is fabricated on RT/Duroid 5870 substrate. The array has a high gain

of 10.9 and 13.3 dBi at 1.85 and 2.15 GHz, respectively .A dual band rectifier is also designed. The rectenna conversion efficiency was 40% at input power density of 455 μW/m^2 with a 5 KΩ load to produce 224 mV DC voltages.
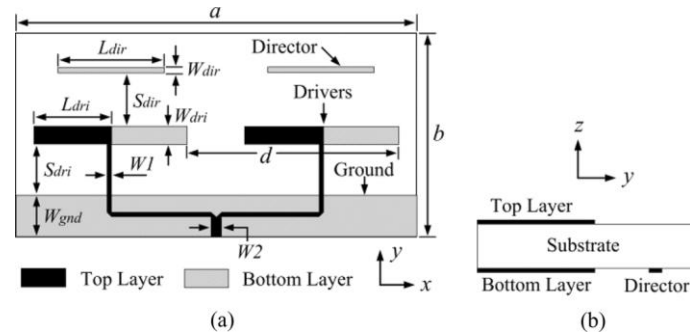
Figure 3.28 1x2 quasi Yagi subarray layout [48]

3.1.3 Multi Band Rectennas

In this section, multi-band rectennas that appeared in literature will be discussed for energy harvesting and wireless power transmission applications.

In [49] a multi-band annular ring antenna for energy harvesting applications is proposed. The antenna resonates at three frequencies (900, 1800 and 2450 MHz). By introducing the appropriate slots on the antenna as shown in Figure 3.29, the antenna can operate in these bands and with circular polarization. The antenna has high gain of 5.5, 7.1, and 9.4 dB at 900, 1750, and 2450 MHz, respectively and also a good efficiency of 61%, 54%, and 85% at 900, 1750, and 2450 MHz, respectively. The outer radius of the ring is 71 mm which means that the proposed antenna has a big size. This antenna was designed to be wearable. The antenna proposed in [50] is working on the same frequency bands and the same polarization as the antenna introduced in [49]. The proposed antenna of [50] is shown in Figure 3.30 and has a size of 140 x 154 mm^2.

41
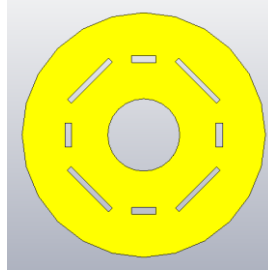
Figure 3.29 Geometry of annular ring antenna [49]
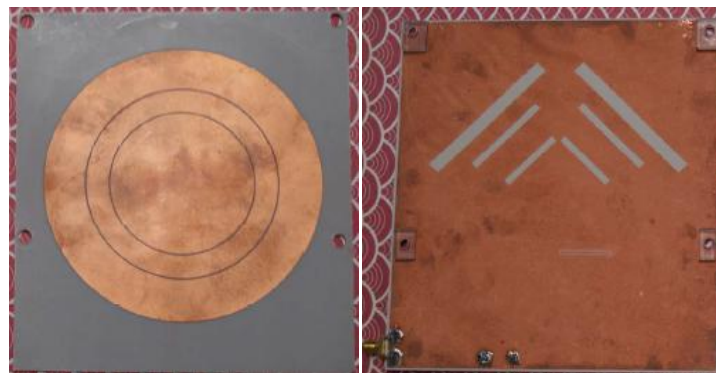
Figure 3.30 the triple band circularly polarized antenna [50]

The antenna has three circular resonators that are coupled with the feed network by three pairs of perpendicular slots that are etched on the ground plane, each slot covering a certain frequency band. There is no gain or efficiency values reported. [51] suggests a triple band antenna that is very close to that proposed in [49]. The two antennas have the same dimensions, same resonance frequencies and same polarization state but the only difference is that in [51], two orthogonal slots in the ground plane are been introduced for circular polarization property.

In [52] dual band rectenna based on two ring slot antennas is proposed. The two bands covered were 2.45 and 5.8 GHz. As shown in Figure 3.31, by introducing a meander line

42

structure, 52% size reduction is achieved. The rectenna conversion efficiency is 65% and 46% at 2.45 and 5.8 GHz when the power density was 10 mW/cm^2, respectively. The rectenna size was 40 x 43 mm^2 with maximum gains of 2.2 and 3.6 dBi at 2.45 and 5.8 GHz, respectively.
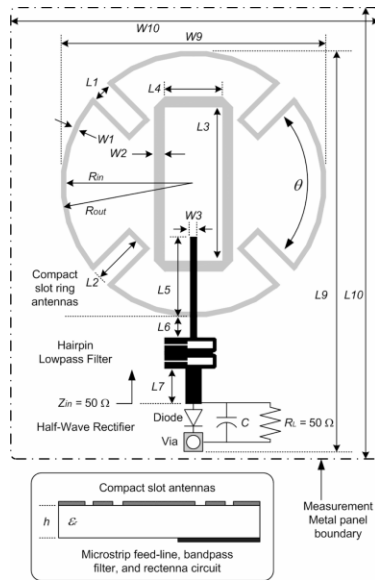
Figure 3.31 dual band rectenna geometry [52]

In [53] a triple band rectenna based on multi resonators is proposed. The frequency bands covered were 900, 1800 and 2450 MHz. As shown in Figure 3.32, each antenna will resonate in a different frequency. The proposed antenna has good efficiency which was higher than 60% at the center frequency of each band but has a relatively big size, because as reported the outer ring radius of the first antenna was 57 mm which means the antenna has big size.
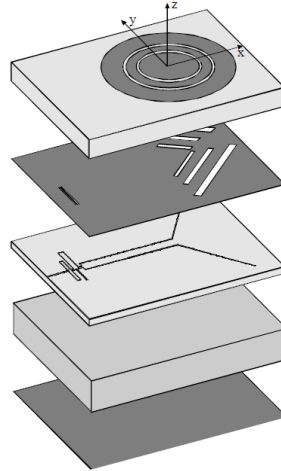
Figure 3.32 The layout of the multi resonator rectenna [53]

In [54] a dual band rectenna based on a shorted circularly polarized ring slot antenna which resonates at 2.45 GHz and 5.8 GHz was proposed. The antenna had a gain of 0.7 and 1.5 dB at 2.45 and 5.8 GHz, respectively. The radius of the outer ring was 26.5 mm as shown in Figure 3.33 by R4. The rectenna conversion efficiencies were 65% and 46% at 2.45 GHz and 5.8 GHz respectively when the power density was 10 mW/cm^2.
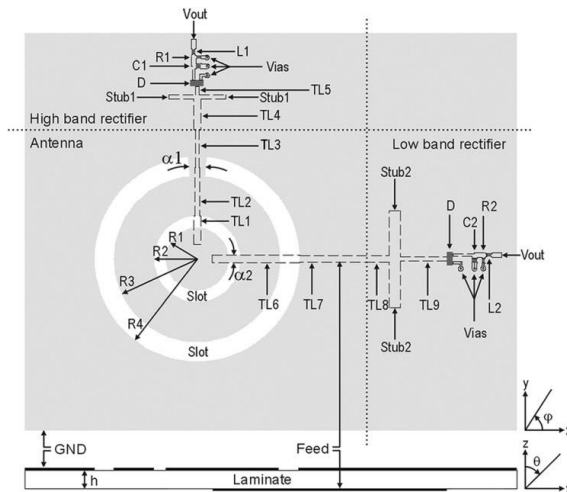
Figure 3.33 Geometry of the dual band ring slot antenna [54]

In [55] a miniaturized triple band PIFA implantable antenna used for rectenna and data communication applications was introduced. The three bands were the medical implant communications service (MICS) band at 402 MHz for data communication and the ISM band at 433 and 2450 MHz for wireless power transmission. For the antenna, a ∏-shaped radiator with stacked and spiral structures as shown in Figure 3.34 is proposed. The antenna has a large bandwidth of 113 and 70 MHz in the MICS and ISM bands respectively. The antenna has a size of 10 x 10 mm^2. The rectenna conversion efficiency was up to 86% across a 5 kΩ load with input power of 11 dBm.
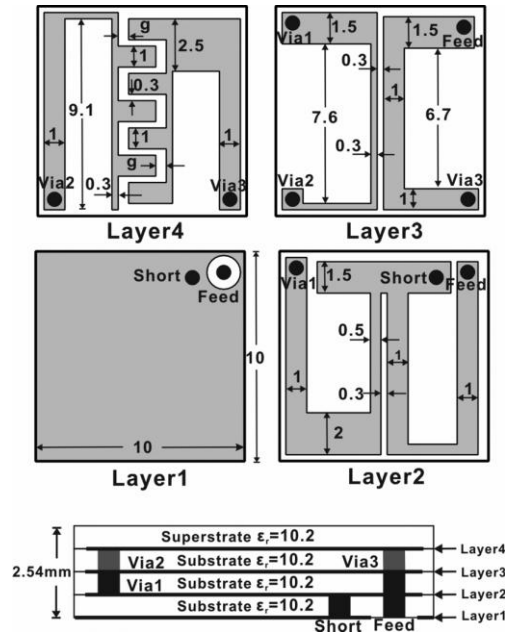
Figure 3.34 Geometry of the stacked implantable antenna [55]

To conclude, a tree that classifies rectennas in literature in terms of their frequency bands is shown in Figure 3.35. Most of the rectennas cover a single band and few of them cover wide band and multiband. Figure 3.36 shows a tree that classifies rectennas due to their size. Showing that most of them have size larger than 40x40 mm^2 and only four rectennas

out of that have size less than 40x40 mm^2. These four antennas rely on stacked design which uses many layers stacked together. This research focuses on designing a dual band rectenna that has a size less than 40x40 mm^2. This is done in [55] which is implantable rectenna using a complicated design consists of 4 layers.

```
                        ┌─────────────┐
                        │  Rectennas  │
                        └─────────────┘
        ┌───────────────────┼───────────────────┐
        ▼                   ▼                   ▼
┌───────────────┐   ┌───────────────┐   ┌───────────────┐
│  Single Band  │   │   Wide band   │   │   Multiband   │
│  [13] - [43]  │   │  [44] - [48]  │   │  [49] - [55]  │
└───────────────┘   └───────────────┘   └───────────────┘
        ▼                   ▼                   ▼
┌───────────────┐   ┌───────────────┐   ┌───────────────┐
│ [13], [14], [15], │ │ [44], [45], [46], │ │ [49], [50], [51], │
│ [16], [17], [18], │ │   [47], [48]  │   │ [52], [53], [54], │
│ [19], [20], [21], │ └───────────────┘   │     [55]      │
│ [22], [23], [24], │                     └───────────────┘
│ [25], [26], [27], │
│ [28], [29], [30], │
│ [31], [32], [33], │
│ [34], [35], [36], │
│ [37], [38], [39], │
│ [40], [41], [42], │
│     [43]      │
└───────────────┘
```
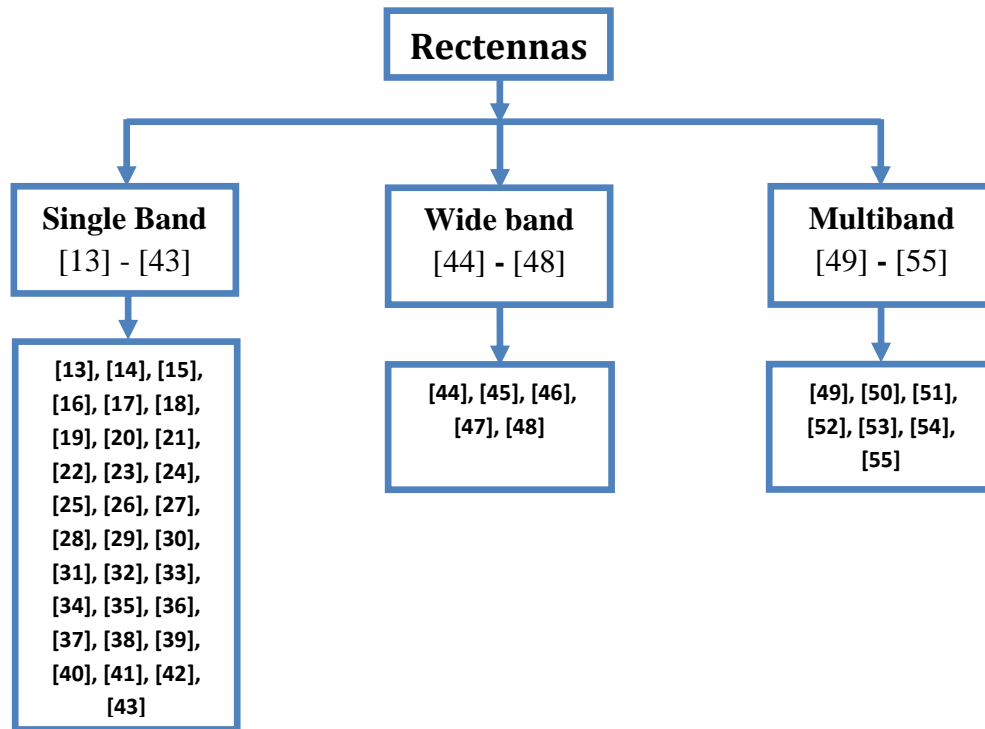
Figure 3.35 Tree of rectennas classification by frequency band

```
                        ┌─────────────┐
                        │  Rectennas  │
                        └─────────────┘
              ┌──────────────────┴──────────────────┐
      ┌───────────────┐                      ┌───────────────┐
      │  Size > 40x40 │                      │  Size < 40x40 │
      └───────────────┘                      └───────────────┘
              │                                      │
   ┌─────────────────────┐              ┌─────────────────────┐
   │   [13], [14], [15], │              │   [34], [36], [47], │
   │   [16], [17], [18], │              │         [55]        │
   │   [20], [22], [23], │              └─────────────────────┘
   │   [24], [25], [27], │
   │   [29], [30], [31], │
   │   [32], [33], [35], │
   │   [37], [38], [39], │
   │   [40], [41], [42], │
   │   [43], [44], [45], │
   │   [46], [48], [49], │
   │   [50], [51], [52], │
   │        [53], [54]   │
   └─────────────────────┘
```
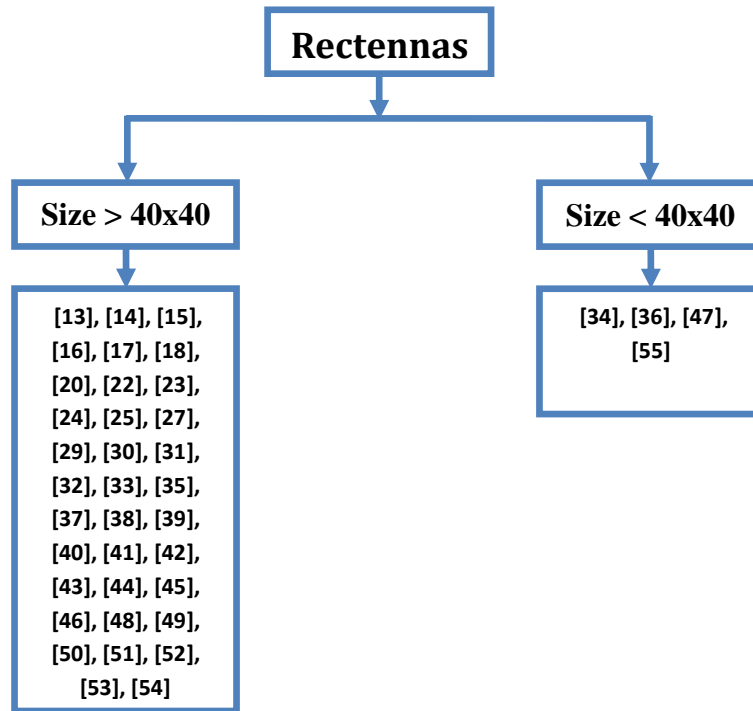
Figure 3.36 Tree of rectennas classification by size

3.2   Dual band Meander Line Antennas

The meander line or folded monopole antennas have been used extensively in literature to reduce the antenna size. In this section, dual band meander line antennas that are found in literature are investigated.

One way to make the meander line resonates at dual band is to extend a conductor line as shown in [56]–[58]. In [56], [57] a dual band meander line antenna is introduced by using a conductor line as shown in Figure 3.37. The antenna is fed by a 50 ohm coplanar waveguide (CPW) transmission line, it resonates at 910 and 1800 MHz with 90 MHz (875 - 965) bandwidth at the lower band and 218 MHz (1706 - 1924) bandwidth for the higher band. The antenna is fabricated on FR4 substrate with 1.6 mm thickness and dielectric constant of 4.4.

The gain of the antenna is 1.3 and 3 dBi for the lower and higher bands respectively. The antenna size is not reported but with rough estimation based on provided dimensions it is more than 58 x 60 mm^2.
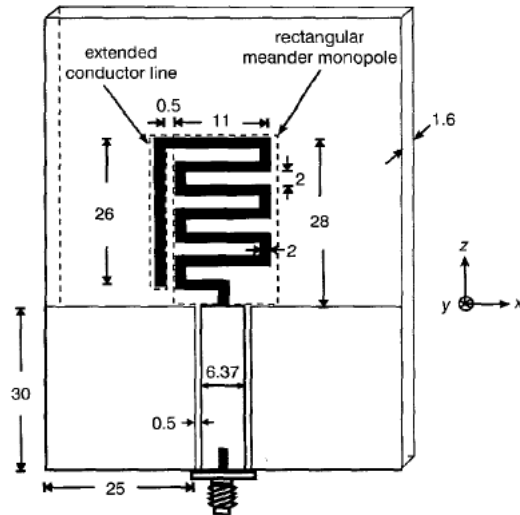
Figure 3.37 dual band meander line antenna geometry that fed by CPW [56]

In [58], a dual band folded monopole antenna is proposed for energy harvesting applications. The dual resonance behavior is due to the extended conductor line as shown in Figure 3.38. The proposed antenna works at 915 and 1800 MHz and it is fed with 50 ohm coplanar waveguide transmission line. The antenna is fabricated on FR4 substrate with dielectric constant of 4.4 and 1.6 mm thickness. The measured bandwidth is 59.3 and 114.2 for the lower and the higher bands respectively. The measured gain is -0.23 and 1.14 for the lower and higher bands respectively. The antenna size without its ground is more than 30x30 mm^2 based on rough estimation due to the provided dimensions.

48
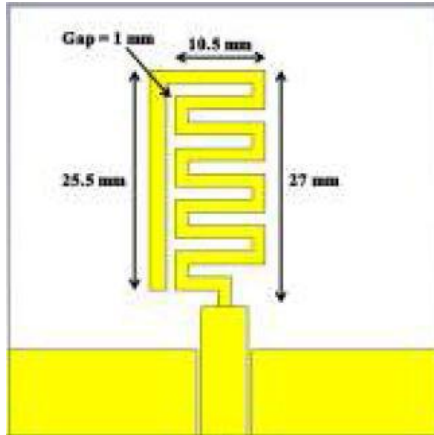
Figure 3.38 folded monopole antenna geometry [58]

Another dual band meander line antenna that relied on extending a conductor line is introduced in [59]. This antenna resonates at 900 and 1800 MHz with a narrow bandwidth. The antenna is miniaturized for system in package applications as shown in Figure 3.39, the antenna size (in mm) without the ground plane is 14 x 17 x 0.76 and it is printed on TMM4 substrate with dielectric constant of 4.5.
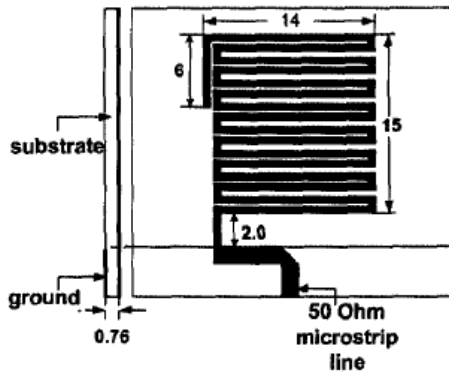
Figure 3.39 the miniaturized dual band meander line antenna [59]

In [60], a dual band meander line antenna is proposed for MIMO antenna systems. The antenna has two portions as shown in Figure 3.40, the meander line portion is responsible for the lower frequency resonance and the small arm is responsible for the higher one. This

antenna resonates at 870 MHz and 2.6 GHz with a measured -6 dB bandwidth of 75 and 90 MHz at the lower and higher bands respectively. The gain is 0.72 and 0.3 dB for 870 and 2600 MHz respectively.
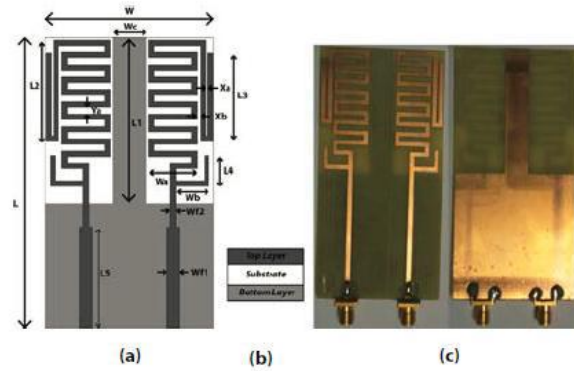
Figure 3.40 MLA for MIMO antenna systems (a) geometry, (b) Stackup and (c) the fabricated antenna [60]**.**

A dual band meander line antenna is proposed in [61] to work in UMTS/HSDPA bands. This antenna is operating at 1200 and 1900 MHz with experimental -6 dB bandwidth of 200 and 300 MHz for 1200 and 1900 MHz respectively. The antenna is shown in Figure 3.41 and has size (in mm) of 30 x 5 x 8 and it is printed on FR4 substrate with dielectric constant of 4.4.
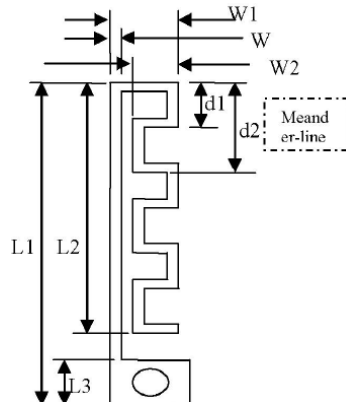
Figure 3.41 folded monopole antenna suitable for UMTS/HSDPA operation [61]

A wearable dual band folded monopole antenna is proposed for biomedical applications in [62]. The proposed antenna is shown in Figure 3.42 and it is targeting the ZigBee dual band (868 - 928 MHz) and (2400 - 2500 MHz). This antenna is printed on LTCC substrate with a dielectric constant of 7.1 and it has a size (in mm) of 16.5 x 17 x 0.8. The antenna shows a good bandwidth of 500 MHz for both of its bands with gain of -16 and -11 dB for the lower and higher bands respectively.

Front view   **Back view**
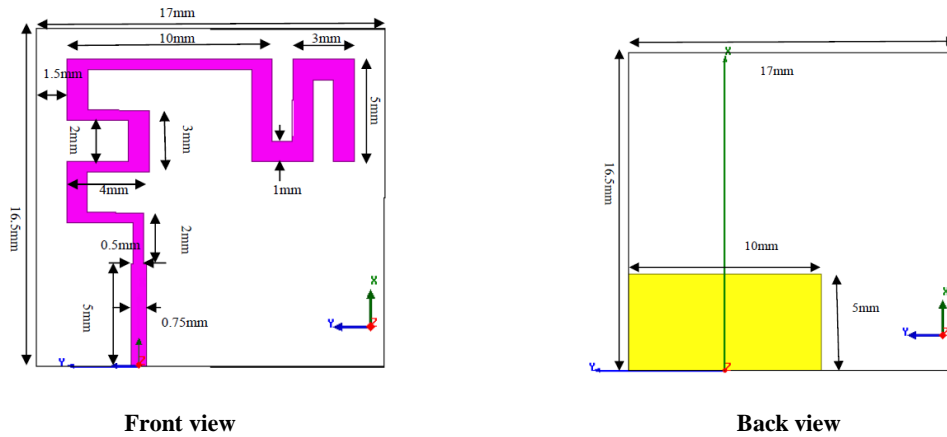
Figure 3.42 geometry of the dual band wearable antenna [62]

In [63] - [64], a dual band meander line antenna is introduced with a shaped ground and a rectangular patch as shown in Figure 3.43. The proposed antenna in [64] is targeting the wireless LAN bands which are 2.5 and 5.2 GHz. The shaped ground provides good impedance matching for the lower band and the coupled patch helps in matching the higher band also the patch controls the higher band resonance, it can change the frequency from 5.2 to 7 GHz. The antenna has experimental bandwidth of 270 and 315 MHz for the lower and higher bands respectively. The antenna size (in mm) is 31 x 8 x 1.6 and it is printed on FR4.
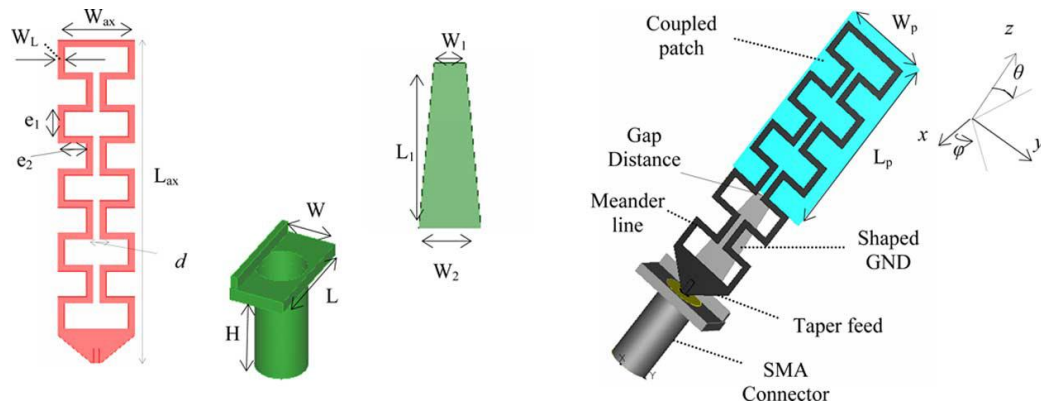
Figure 3.43 MLA with shaped ground and a coupled patch [64]

A dual band printed monopole antenna is introduced in [65]for WCDMA and the 2.5 GHz extension band. The proposed antenna resonates at 2 and 2.5 GHz by using two different monopoles as shown in Figure 3.44. The shorter monopole is responsible of the higher band and the other one is responsible of the lower band. The slots etched in the longer monopole to enhance the bandwidth, the -10 dB measured bandwidth is 300 MHz for both frequency bands. The antenna is fabricated on RO4350B substrate with dielectric constant of 3.48 and thickness of 1.52 mm. The antenna simulated gain is 2.7 and 2.5 dBi at the lower and higher bands respectively. The size of the antenna is not reported but by looking to the dimensions in Figure 3.44, the size (in mm) will be more than 52 x 10.

In [66], a dual band monopole with two arms is proposed for WLAN and WiMAX applications. The dual band behavior achieved by using two symmetric arms as shown in Figure 3.45. The antenna resonates at 3.5 and 5.3 GHz with impedance bandwidth of 100 for both the bands. The antenna has a good gain which is more than 5 dB for both lower and higher bands. The antenna size (in mm) is 30 x 35 x 1.6 and it is fabricated on FR4 substrate.
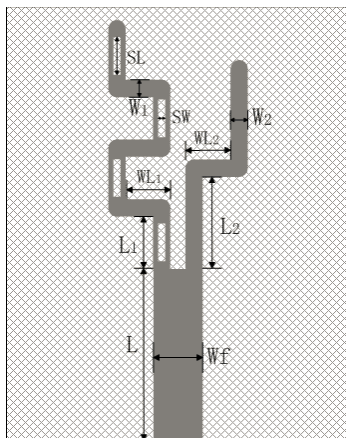
Figure 3.44 dual band printed monopole antenna geometry [65]
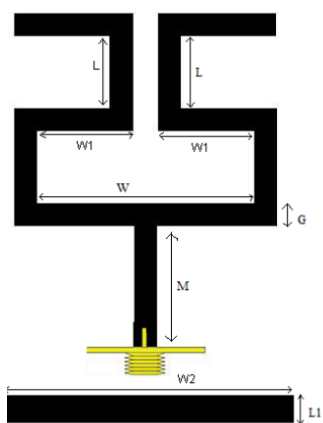
Figure 3.45 the proposed monopole antenna geometry [66]

A miniaturized dual band meander line antenna is introduced in [67] by using two portions of the meander line on the two sides of the substrate as shown in Figure 3.46. The antenna resonates at 1440 and 2440 MHz. the bottom meander line is connected to the transmission line and the upper meander line is excited parasitically. The antenna size seems to be large because the ground plane alone is 50 x 50 mm^2.
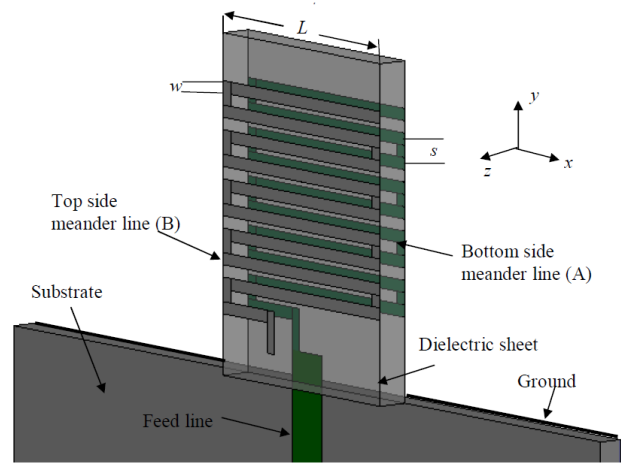
Figure 3.46 the proposed compact size MLA [67]

In [68], a dual band antenna is proposed with electromagnetic band gap (EBG) structure to reduce specific absorption rate (SAR) in mobile devices. The antenna is based on meander line antenna that resonates in wide bandwidth dual bands which are (587- 977 MHz) and (1670- 8630 MHz) as shown in Figure 3.47. The EBG structure provides a good impedance matching that results in the wide bands. The antenna size (in mm) is 27 x 25 x 0.8 and it is fabricated on FR4 substrate.
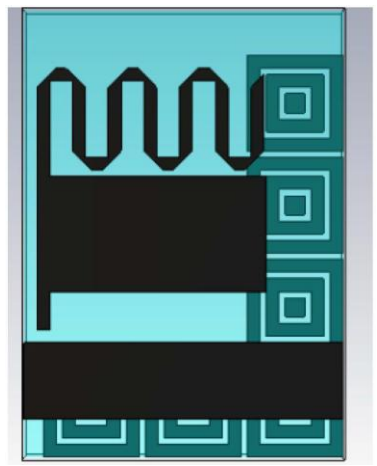
Figure 3.47 the proposed antenna with EBG structure [68]

54

A dual band T-shaped printed monopole antenna for WLAN operation is presented in [69]. The antenna resonates at 2.4 and 5.2 GHz by tuning the asymmetric short and long arms as shown in Figure 3.48. The antenna maximum gain is 0.8 and 3 dB for the lower and higher bands. The size of the antenna (in mm) is 20 x 38.5 and it is fabricated on FR4 substrate.
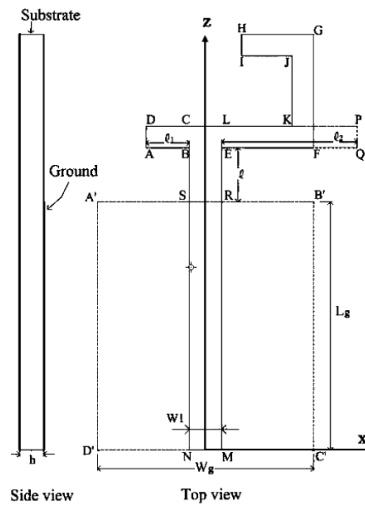
Figure 3.48 geometry of the T-shaped antenna [69]

In [70], a dual band meander line antenna designed on two FR4 substrate sides is proposed and the antenna geometry is shown in Figure 3.49. The antenna resonates at 900 and 1900 MHz. The simulated results showed a narrow band at 900 MHz and a wide band at 1900 but the measured results were different in terms of bandwidth, measured bandwidth is 120 and 900 MHz for the lower and higher bandwidth. The antenna size (in mm) is 40 x 70 and has a gain of 1.8 and 2.9 dB for the lower and higher bands respectively.
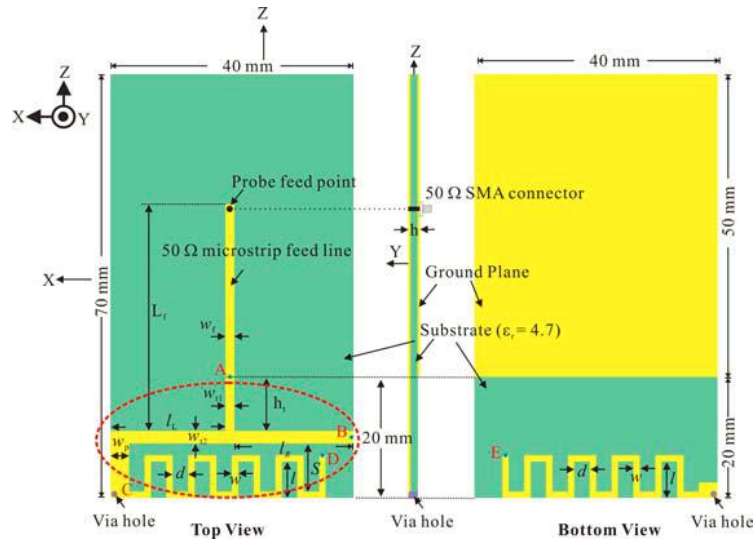
Figure 3.49 the proposed dual band MLA [70]

To conclude, many dual band meander line and folded monopole antennas are found in literature for many applications due to their small size and ease of fabrication. Also many ways of designing a dual band meander line antenna by extending a conductor line or using separate portions where each will be responsible of a certain band. A tree compares the reported antennas in terms of their frequency coverage and size is shown in Figure 3.50. The tree shows that most of the antennas resonates at less than 1 GHz have size more than 40 x 40 mm^2 and few of them have size less than 40 x 40 mm^2 and even these antennas are for special applications (i.e. wearable antenna and system in package applications). In [59] and [68] the antenna gain and radiation efficiency are not reported. In [62], the antenna maximum gain is -16.3 and -11.6 dB at 915 and 2450 MHz, respectively.

```
                                    ┌──────────┐
                                    │   MLA    │
                                    └──────────┘

              ┌──────────────┐              ┌──────────────┐
              │ Size > 40x40 │              │ Size < 40x40 │
              └──────────────┘              └──────────────┘

    ┌──────────────┐ ┌──────────────┐ ┌──────────────┐ ┌──────────────┐
    │ Freq. < 1GHz │ │ Freq. > 1GHz │ │ Freq. < 1GHz │ │ Freq. > 1GHz │
    └──────────────┘ └──────────────┘ └──────────────┘ └──────────────┘

    ┌──────────────┐ ┌──────────────┐ ┌──────────────┐ ┌──────────────┐
    │ [56], [57],  │ │ [65], [67]   │ │ [59], [62],  │ │ [61], [63],  │
    │ [58], [60],  │ │              │ │    [68]      │ │ [64], [66],  │
    │    [70]      │ │              │ │              │ │    [69]      │
    └──────────────┘ └──────────────┘ └──────────────┘ └──────────────┘
```
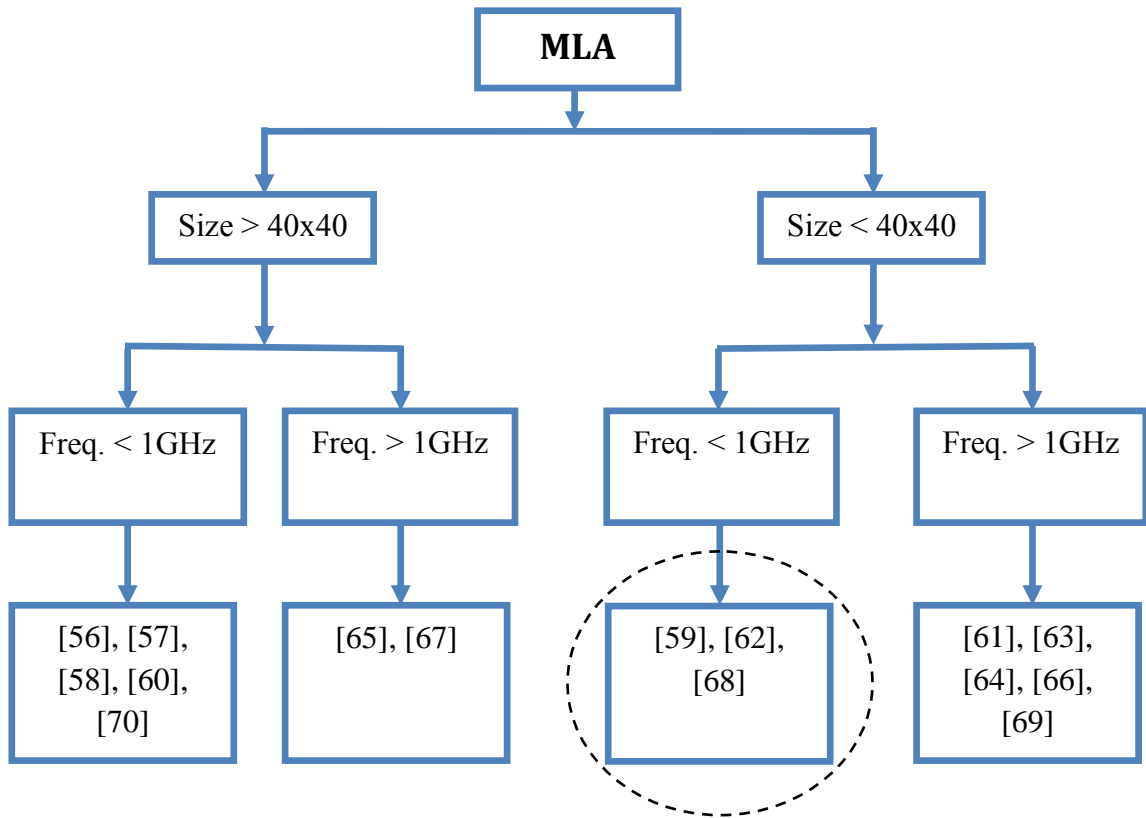
Figure 3.50 Tree compares reported MLAs based on the size and frequency

3.3   Miniaturized dual band Patch Antennas

Patch antennas are widely used due to their attractive properties such as light weight, low profile and ease of fabrication. In this section, miniaturized dual band patch antennas that approved in literature are investigated and the miniaturization methods used and the miniaturization ratio achieved are listed. The calculations of miniaturization ratios depend on calculating the ratio for each dimension (length and width) separately and then taking the average of them.

The most used method for miniaturizing dual band patch antennas is using slots to increase the current path so that the resonance frequency will be lower. The slots were used in [71]–[76] and the highest miniaturization ratio obtained was 64% [75]. In [75] many slits are etched on the top of the patch to increase the current path as shown in Figure 3.51. The antenna is designed to resonate at 2.7 and 4.5 GHz with patch size of 16x14x1.6 mm^3. It is fabricated on FR4 substrate and the measured gain is -4.3 dBi at 4.5 GHz. The gain at the lower band and the radiation efficiency for both bands were not mentioned.
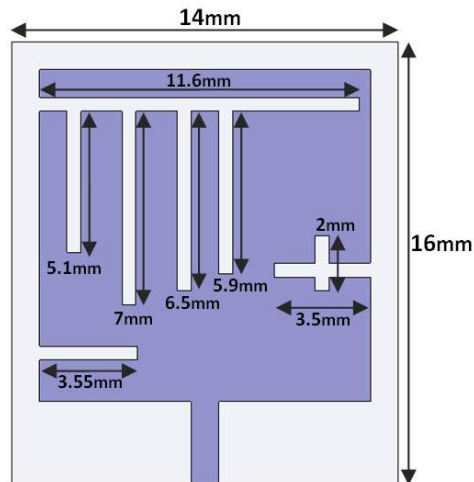
Figure 3.51 Miniaturized Patch antenna with slits [75]

Miniaturization through shorting patch via a shorting post or a shorting wall is used extensively as in [77]–[80] and the highest size reduction achieved was 65% [79]. In [79] a shorted dual band N shaped patch antenna is proposed as shown in Figure 3.52. The antenna radiates at 3.5 and 8.5 GHz with wide bandwidth of 1.46 and 2.17 GHz at the lower and higher bands, respectively.

Front view   **Back view**
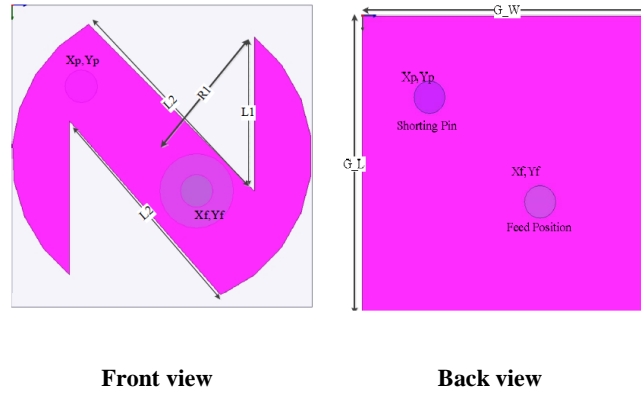
Figure 3.52 Shorted N shape patch antenna [79]

Using coplanar waveguide (CPW) feeding with slots for miniaturization is reported in [81]–[84] and 62% size reduction was achieved [82]. The proposed antenna in [82] consists of a rectangular patch and a notch cut fed with CPW as shown in Figure 3.53.
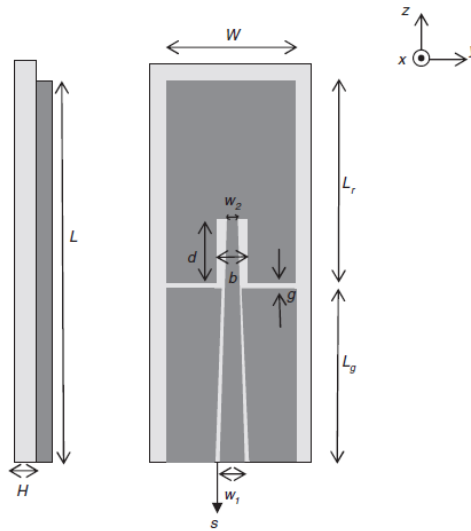
Figure 3.53 Dual band Microstrip antenna with CPW feeding [82]

Defected Ground Structures (DGS) were used to miniaturize and achieve dual band patch antennas as reported in [85], [86] and the highest miniaturization ratio obtained was 68% [85]. In [85] a circularly polarized patch antenna with a novel DGS is designed to

resonate at 900 and 2450 MHz as shown in Figure 3.54. The antenna has a compact size of 38x40x1.58 mm^3 and it is simulated on FR4 substrate. The antenna has a gain of 2.6 and 3.5 dBi for the lower and higher bands, respectively.

Front view   Back view
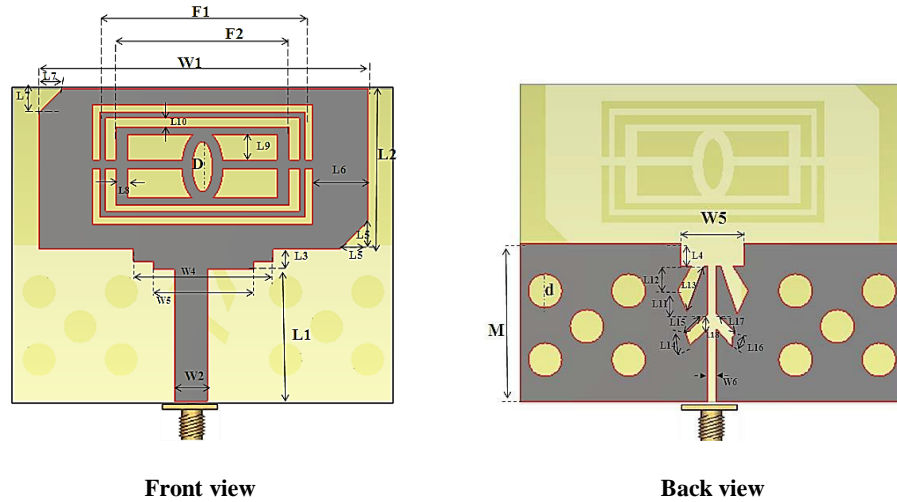
Figure 3.54 Dual band patch antenna with DGS [85]

Miniaturizing dual band circular patch antennas through using annular rings is reported in [54], [87] and 53% size reduction was achieved [54]. An annular ring dual band patch antenna is proposed as shown in Figure 3.55. The antenna resonates at 1.22 and 1.48 GHz with very narrow bandwidth which represents small frequency ratio. The antenna has a measured gain of 1.35 and 3.5 dB at the lower and higher bands, respectively.
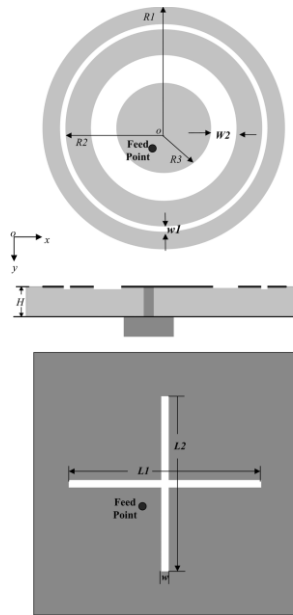
Figure 3.55 Annular ring circular patch antenna [54]

Figure 3.56 shows a rectangular dual band patch antenna miniaturized using 4 symmetrical V grooves [88]. The proposed antenna resonates at 2.46 and 5.46 GHz with patch size of 24.8x24.8 mm^2 which means 39% size reduction was achieved.
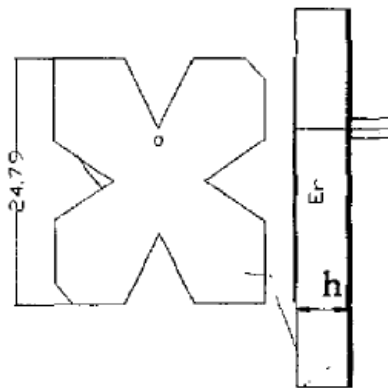
Figure 3.56 Patch antenna with V grooves [88]

Figure 3.57 represents a dual band patch antenna that miniaturized using two stubs, one on the upper layer and the other one is connected to the ground layer [89]. The proposed

antenna radiates at 2.45 and 5.8 GHz with bandwidth of 148.5 and 205 at 2.45 and 5.8 GHz, respectively. The patch size is 15.6x8.8 mm^2 with 64% size reduction compared to a conventional rectangular patch. The antenna maximum gain is 1.92 and 3.385 dBi at the lower and higher bands, respectively.
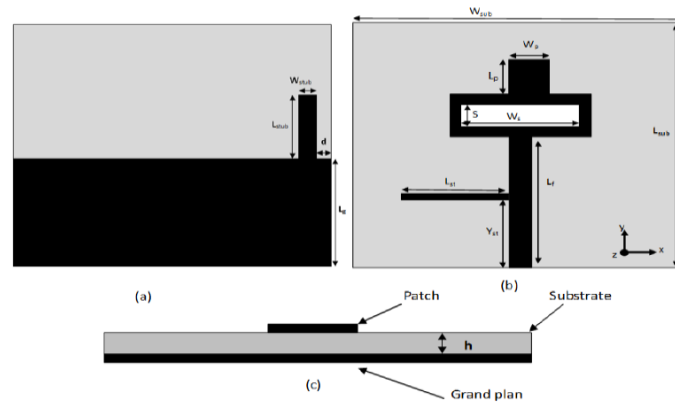
Figure 3.57 patch antenna with stubs [89]

Using metamaterials for dual band patch antennas miniaturization was reported in [90] with 58% miniaturization ratio. Figure 3.58 shows the proposed metamaterial based patch antenna with mushroom like transmission line metamaterial (TL-MTM) structures. The antenna radiates at 2.76 and 5.23 GHz with narrow bandwidth of 40 and 160 MHz at the lower and higher bands, respectively. The antenna measured gain is 1 and 6.8 dBi at 2.76 and 5.23 GHz, respectively with good radiation efficiency of 79 and 90% at the lower and higher bands, respectively.
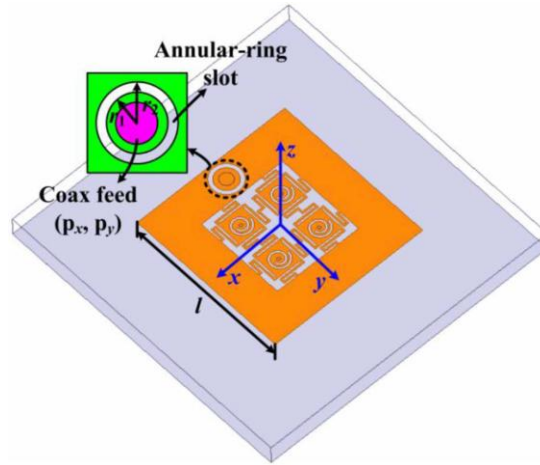
Figure 3.58 Mushroom like TL-MTM patch antenna [90]

In this section, miniaturized dual band patch antennas in literature are investigated and the miniaturization methods used were listed. The highest miniaturization ratio reported for dual band patch antennas thus far is 68% [85], but for single band patch antennas the miniaturization ratio is higher and can be higher than 83% as achieved in [91].

3.4 Conclusions

A comprehensive literature review is done for three topics. For printed rectennas, it is found that one multi band rectennas with size less than 40x40 mm^2 this antenna is stacked implantable rectenna that has a complicated design with four layers. For dual band meander line antennas, three antennas were found that have size less than 40x40 mm^2 and working with frequency less than 1 GHz, these antennas have poor gain and radiation efficiency. Finally the miniaturized dual band patches were investigated and found that the highest miniaturization ratio is 68%.

CHAPTER 4

DUAL BAND MLA DESIGN AND MEASUREMENTS

In this chapter, a miniaturized dual band meander (MLA) line antenna is designed for RF energy harvesting applications. Different MLA designs were fabricated tested to get the optimal results, all these designs will be discussed. The proposed antenna is designed to cover the cellular standard bands such as GSM 900, GSM 1800 and UMTS. The antenna is tested for RF energy harvesting applications using the Powercast P2110-EVAL-01 kit. The proposed MLA performance is compared to the powercast dipole antenna in terms of the received DC power and the maximum distance from the transmitter that the antenna can still receiving from.

4.1   Different Dual-band MLA Designs

In this section, different dual band MLA designs will be discussed. All these designs have good simulated results, when measured lower matching levels are achieved for the lower band. Several MLA designs were optimized, then fabricated to get measured results closer to the simulated ones. All the antenna designs were simulated and optimized using HFSSv15.

4.1.1   Shorted MLA with Two Sleeves

The first design is a shorted dual band MLA with extended conductor line and two sleeves in the ground as shown in Figure 4.2. The dual band behavior is obtained by extending a conductor line which helps in miniaturizing the antenna by increasing the

current path so that the antenna can resonate at 915 MHz and at the same time introducing the higher resonance at 1800 MHz. The shorting post which is connected to the meander line portion through a stub is for matching the antenna at the desired bands. Usually the meander line antennas have narrow band so that two identical sleeves shorted to the ground are added to the right and to the left of the antenna to introduce another resonance close to the higher resonance to enhance the bandwidth. The antenna designed on Rogers 3003 substrate with dielectric constant of 3, loss tangent of 0.0013 and thickness of 1.52 mm. The size of the antenna is 50 x 36.9 mm^2.
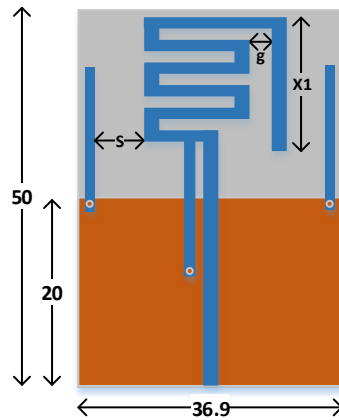
Figure 4.1 the geometry of the MLA with sleeves

The fabricated antenna is shown in Figure 4.2 and the simulated and measured resonance of the antenna is shown in Figure 4.3. The measurements were conducted at Antennas and Microwave Structure Lab (AMSDL) at the Electrical Engineering Department at KFUPM using Agilent N9912A FieldFox VNA. The results show that there is no agreement between the simulated and measured resonance as the matching levels in the measurement resonance are low. The antenna is so sensitive for any changes in its geometry as appeared in simulation so this difference in the results is due to the

65
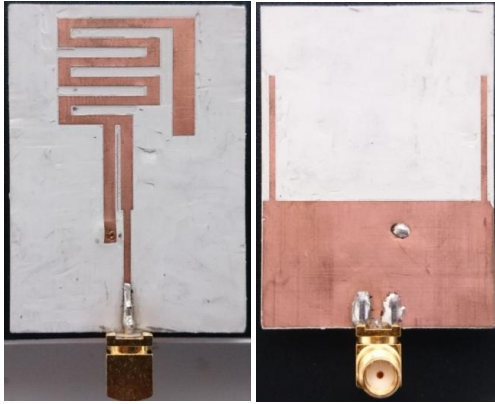
Figure 4.2 Fabricated MLA with two sleeves

fabrication tolerances. Also the sleeves are acting as radiators as they are connected to the ground layer which is shorted to the meander line so they will affect the lower band directly. This results show that this antenna is not stable for dual band operation.
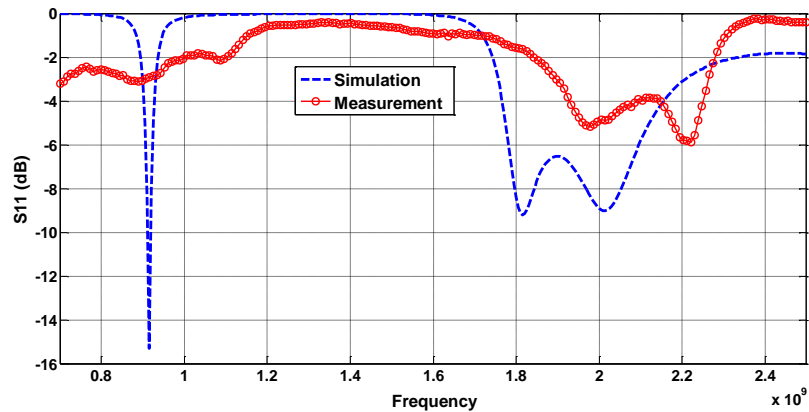
Figure 4.3 Measured and simulated resonance for MLA with sleeves

4.1.2 Shorted MLA with Two Radiators

The second dual band MLA design is a shorted MLA with two different radiators each radiator is responsible for one band as shown in Figure 4.4. The long meander line with the extended line is responsible for the radiation at 915 MHz and the shorter meander line is responsible for the radiation at 1800 MHz. The antenna is shorted to match it at dual bands as impedance matching with the antenna small ground is challenging.
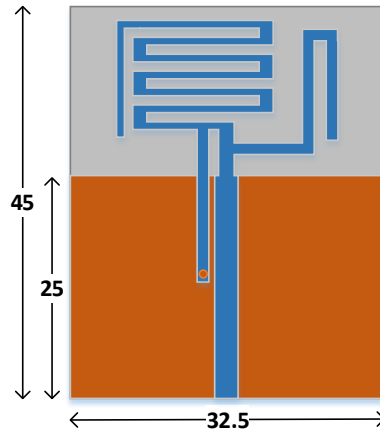
Figure 4.4 the geometry of the shorted MLA with two radiators

The antenna is designed and fabricated on Rogers 3003 substrate with dielectric constant of 3, loss tangent of 0.0013 and thickness of 1.52 mm as shown in Figure 4.5. The size of the substrate is 45 x 32.5 mm^2 which represents electrically small antenna (ESA) at 915 MHz. Figure 4.6 shows the antenna simulated and measured resonance, better agreement between the measured and simulated results is achieved compared to the MLA with sleeves discussed in section 4.1.1. The resonance frequency of the simulated and
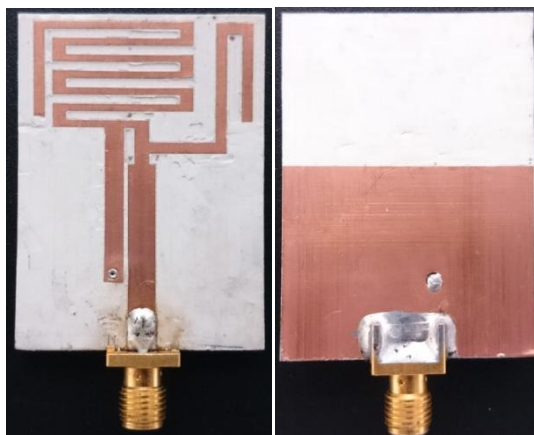
Figure 4.5 Fabricated shorted MLA with two radiators fabricated on RO3003
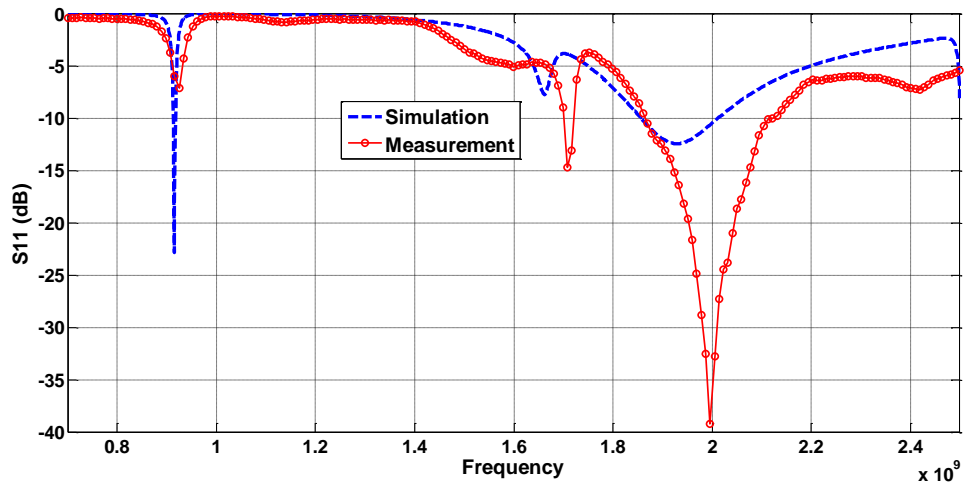
Figure 4.6 Resonance of the shorted MLA with two radiators fabricated on RO3003

measured is almost the same but the matching level is different as the simulated resonance has better matching at the lower band and the measured resonance has better matching at the higher band. The lower band measured resonance is -7 dB which is acceptable for ESAs but it is low matching level which will introduce losses and poor radiation efficiency and gain.

To improve the lower band matching levels, the same antenna shown in Figure 4.4 is optimized and designed on FR4 substrate with dielectric constant of 4.4, loss tangent of 0.02 and thickness of 1.52 mm. Rogers RO3003 is a soft material and there is possibility that the material can be bended while it is fabricated so FR4 substrate was chosen because it is rigid and strong. Figure 4.7 shows the fabricated MLA designed on FR4 substrate. The resonance results shown in Figure 4.8 illustrate the same behavior with the MLA shown in Figure 4.5 as the measured lower band matching is much lower than the simulated one.

68
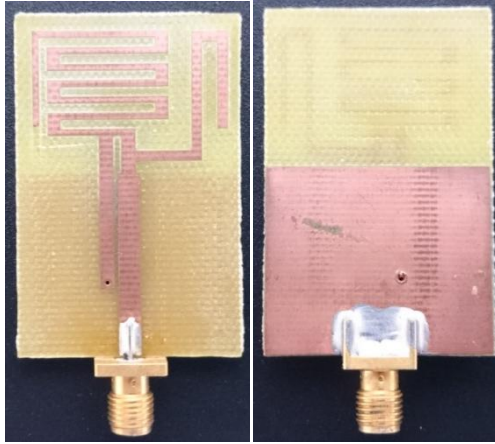
Figure 4.7 Fabricated shorted MLA with two radiators fabricated on FR4
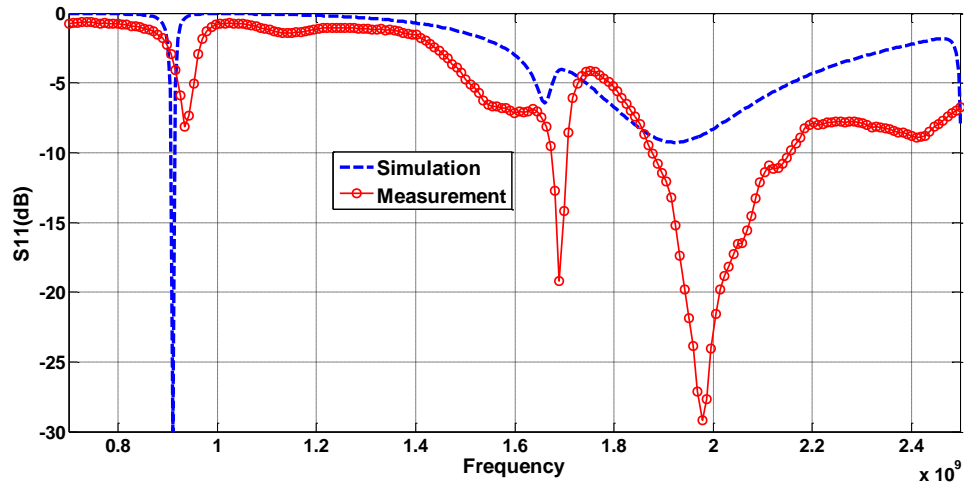
Figure 4.8 Resonance of the shorted MLA with two radiators fabricated on FR4

4.1.3   MLA with Two Radiators and λ/4 Transformer

To enhance the dual band MLA matching levels at the lower band, a third design is simulated and fabricated as shown in Figure 4.9. The new design depends on matching the antenna at 915 MHz using meandered quarter wavelength transformer to match the real impedance of the antenna as the imaginary part is almost zero in the simulation. The proposed design also relies on two different radiators to obtain the dual band property.
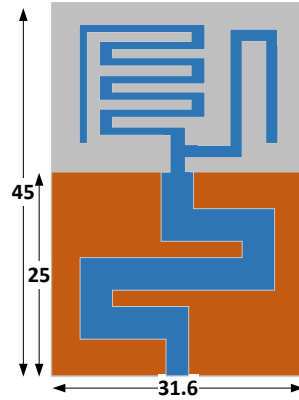
Figure 4.9 Geometry of the MLA with λ/4 transformer

The antenna is fabricated on FR4 substrate as shown in Figure 4.10 with substrate size of 45x31.6 mm^2 which is an ESA at 915 MHz. The antenna resonance is shown in Figure 4.11, as in the previous designs the measured matching level of the lower band is lower than the simulated matching levels, for the higher band the measured resonance is better than the simulated one. Using λ/4 transformer improved the lower band matching by 2 dB as previously it was -7 dB but in Figure 4.11 it is -9 dB.
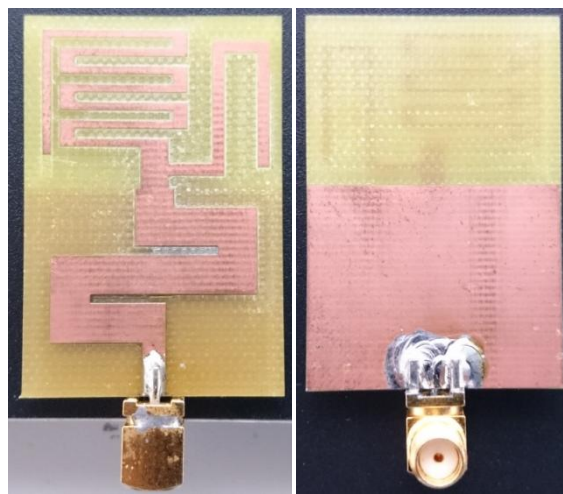
Figure 4.10 Fabricated MLA with λ/4 transformer fabricated on FR4
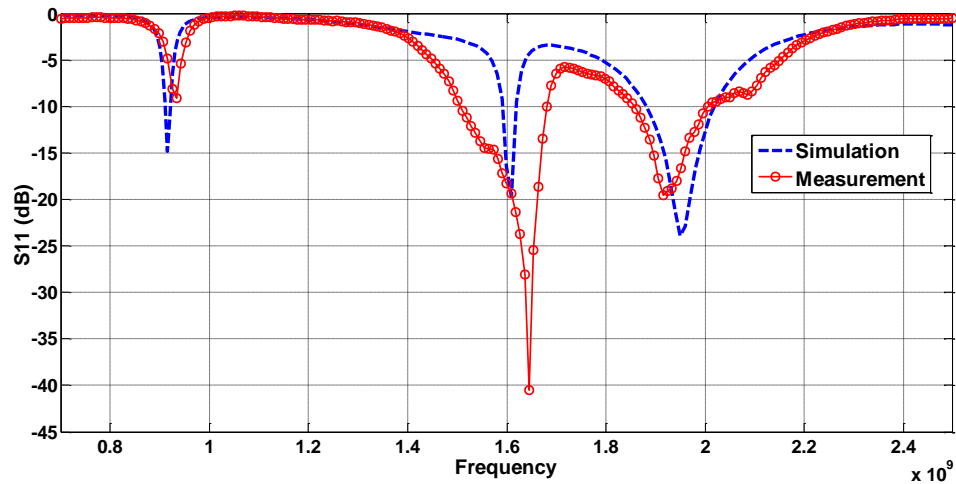
Figure 4.11 Resonance of the MLA with λ/4 transformer fabricated on FR4

4.2 Optimized Dual-band MLA Design

Different dual band MLA designs were shown in section 4.1, in this section the final optimized design will be shown and its' results will be discussed.

4.2.1 MLA Design and Geometry

The final optimized dual band MLA consists of two separate radiators, each of them is responsible of one band. The long meander line is responsible of the radiation at the lower band at 915 MHz and the short meander line is responsible of the radiation at the higher band at 1900 MHz. The geometry of the proposed antenna is shown in Figure 4.12 and the detailed antenna dimensions are shown in Table 4.1. The antenna is fed through a 50 Ω transmission line which is connected to λ/4 transformer to match the antenna at the lower band. This antenna is designed to cover the most known cellular bands such as GSM 900, GSM 1800 and UMTS.
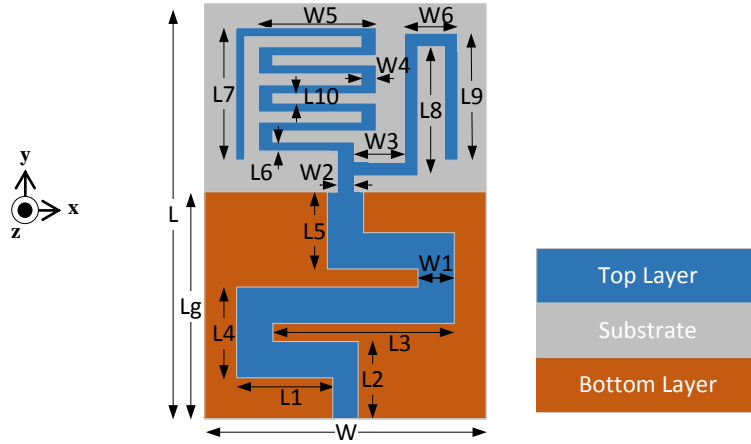
Figure 4.12 Geometry of the optimized dual band MLA

Table 4.1 Antenna detailed geometry parameters

Parameter	Value (mm)	Parameter	Value (mm)
L	45	L8	15
Lg	25	L9	14
W	32.6	L10	1.2
L1	10.8	W1	5.8
L2	9.5	W2	2
L3	19.2	W3	6.8
L4	12.6	W4	1.8
L5	7.7	W5	17
L6	1	W6	7
L7	17		

The antenna is fabricated on a double sided Rogers RO4350 substrate with dielectric constant of 3.48, loss tangent of 0.004 and thickness of 1.52 mm as shown in Figure 4.13. The antenna has a compact size of 45 x 32.6 x 1.52 mm^3 that makes it suitable for use on top of typical WSN nodes. The antenna is an ESA at 915 MHz as **ka**=0.21 as the definition of ESA is **ka** < 1 [92] where **k** is the wave number ($2\pi/\lambda$) and **a** is the radius of the smallest sphere inclosing the antenna radiating part at the desired frequency. The radius **a** of the smallest circle containing the long meander line is 11 mm.

72
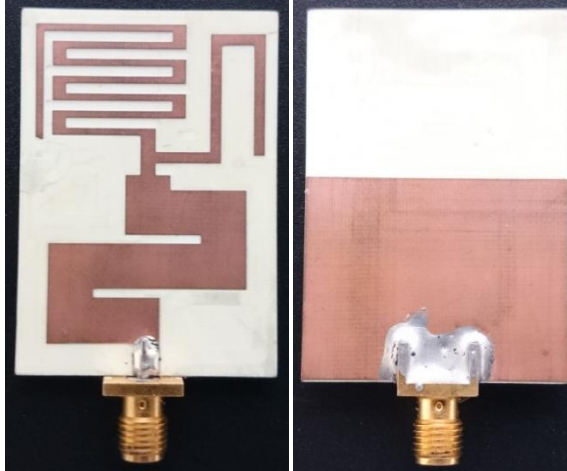
Figure 4.13 Fabricated MLA with λ/4 transformer fabricated on RO4350

4.2.2 MLA Results and Discussions

Figure 4.14 shows the MLA current distribution, at 915 MHz the current intensity is high in the long meander line which is responsible for the radiation at this band. For the higher band, the intensity is higher in the short meander line which is responsible for the radiation at 1900 MHz.
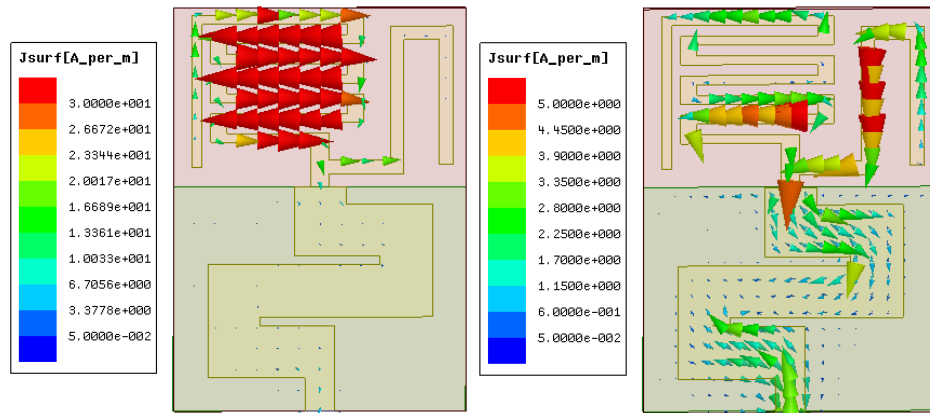
Figure 4.14 MLA current distribution at (a) 915 and (b) 1900 MHz

The simulated and measured antenna reflection coefficients are shown in Figure 4.15. For the lower band at 915 MHz, the measured resonance had a poor matching of -8 dB compared to a simulated resonance of -23 dB but it is acceptable for electrically small antennas. For the higher band at 1900 MHz, the measured and simulated resonance have good matching at the desired band. The antenna resonance at 1.6 GHz is due to a higher mode of the long meander line in which the current doesn't go through all the long meander line and the combination of the two radiators can generate another resonances. The antenna has -6 dB measured bandwidth of 20 and 320 MHz centered at 915 and 1900 MHz, respectively. The wide upper frequency band covers most of the known cellular bands. Figure 4.16 shows the antenna impedance (real and imaginary parts), at 915 MHz the real impedance is 55 ohm with the imaginary part goes to zero which is a good resonance. At 2.02 GHz, the real part is 85 ohm with the zero imaginary part. At the higher band the real part is high compared to 55 ohm of the lower band but in the measured results the higher band has a good matching compared to the lower matching is at 915 MHz.
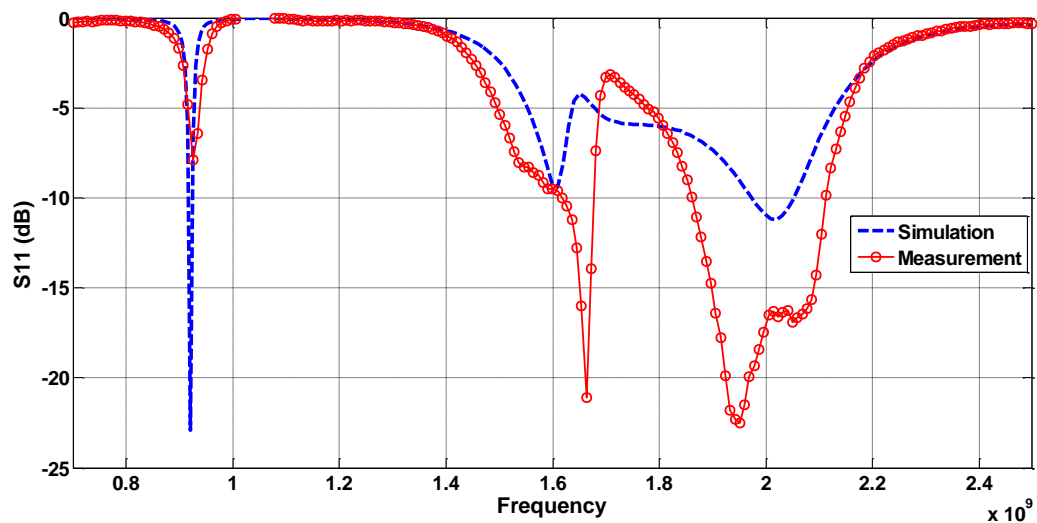
Figure 4.15 Optimized MLA resonance

74
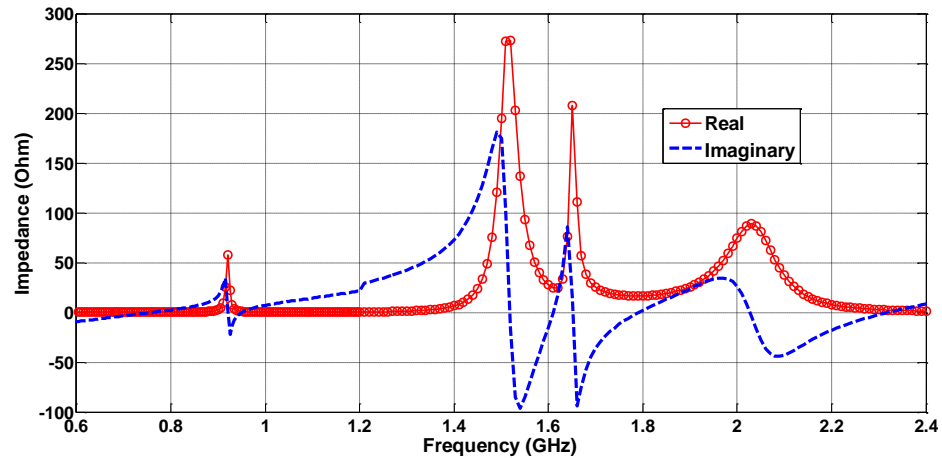
Figure 4.16 Optimized MLA simulated impedance

The antenna radiation characteristics were measured at MVG-Italy, in a Satimo Star-Lab near field chamber as shown in Figure 4.17. Figure 4.18 shows the measured maximum efficiency and gain. For the lower band at 915 MHz, the antenna has measured efficiency of -5.7 dB (27%) and simulated efficiency of 79%. This difference between the simulated and measured results is due to the different matching levels as shown in Figure 4.15. For the higher band the situation is different as the measured efficiency is -1.47 dB (71%) compared to simulated efficiency of 90%.
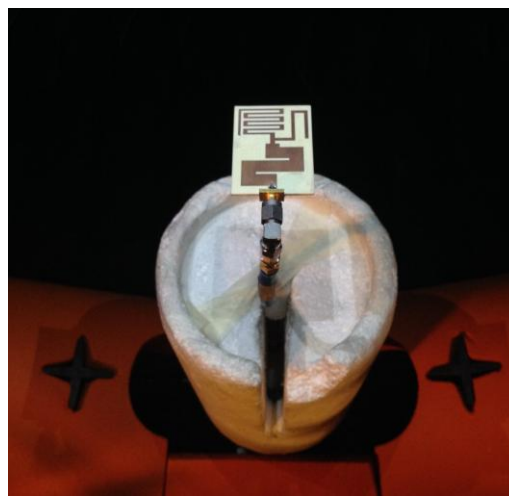
Figure 4.17 MLA near field measurements setup

75

The gain follows the same criteria as the efficiency as the measured gain at the lower band is -2.6 dB compared to simulated gain of 0.8 dB and this due to the lower matching levels of the fabricated antenna. For the higher band, the maximum measured gain is 3.14 dB at 2 GHz compared to maximum simulated gain of 2.8 dB.
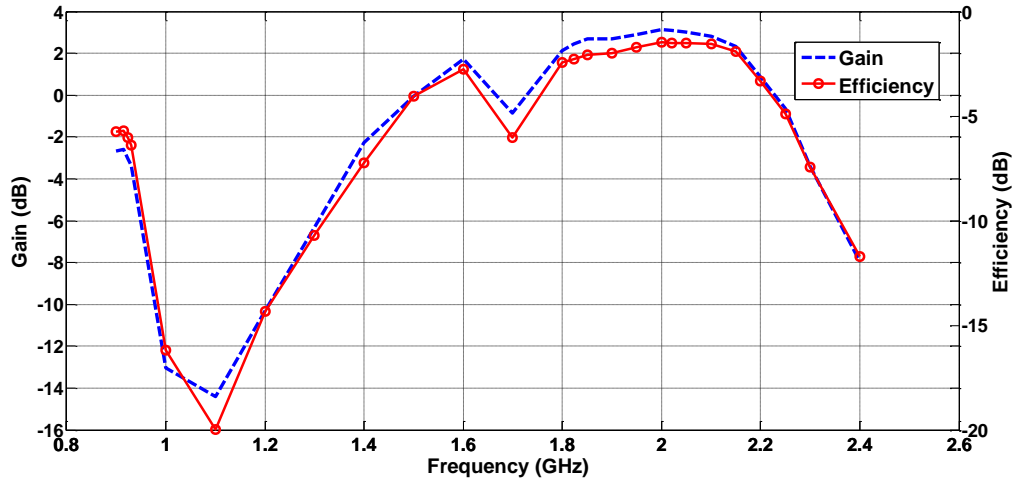
Figure 4.18 MLA measured maximum gain and efficiency

Figure 4.19 shows the simulated and the measured 2D radiation patterns in xz and yz planes at 915 and 1900 MHz. The antenna has almost omnidirectional pattern as expected for small antennas. For the lower band, the yz direction simulated and measured curves have small differences due to the SMA connector which is acting as a reflector in the measurements as its size is one third if the antenna size.
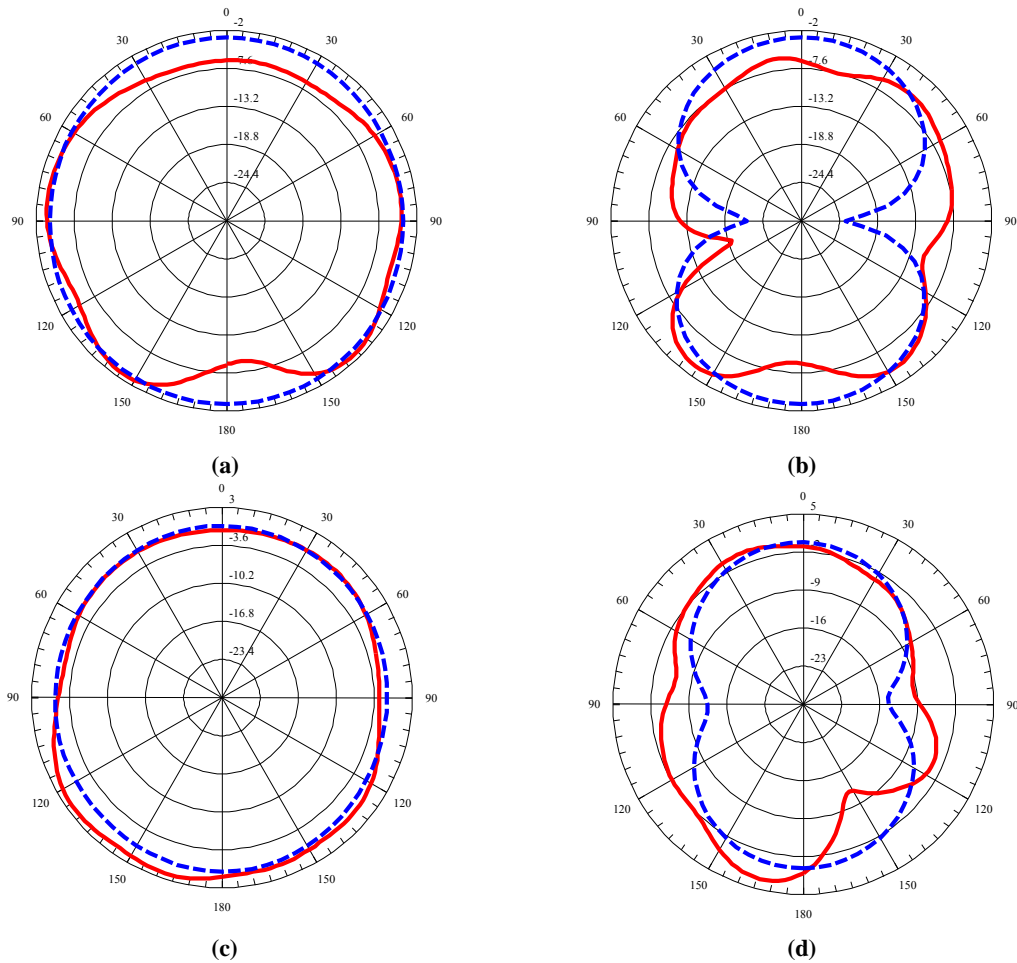
Figure 4.19 Simulated and measured 2-D radiation pattern. Simulated: Dashed lines. Measured: Solid lines. (a) xz-plane at 915 MHz. (b) yz-plane at 915 MHz. (c) xz-plane at 1.9 GHz. (d) yz-plane at 1.9 GHz.

4.3   Powercast Energy Harvesting Kit (P2110-EVAL-01)

Powercast energy harvesting kit for wireless sensors is a complete development kit for low power battery free wireless sensors applications powered by RF [93] energy . The kit consists of a transmitter, dipole antenna, patch antenna, rectifier, capacitors to store energy, sensor and access point to be connected to the computer. All the components of the kit are shown in Figure 4.20 and they will be discussed in the following sections.

Figure 4.20 Powercast energy harvesting kit components [93]

4.3.1 RF transmitter (TX91501-3W-ID)

The Powercast kit transmitter is 3 watt transmitter radiates at 915 MHz with integrated antenna which has gain of 8 dBi [94]. The transmitter is a black box as shown in Figure 4.21, it comes with fixed output power and no user adjustable settings.
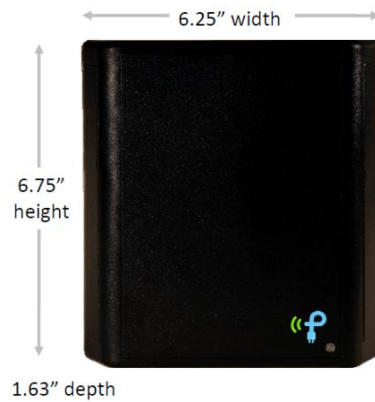
Figure 4.21 Powercast transmitter for energy harvesting kit [94]

4.3.2 P2110 Evaluation Board (P2110-EVB)

The evaluation board consists of SMA connector in which the antenna will be connected, a rectifier to convert the RF energy into DC, two different capacitors for storing energy and the user can choose any of them by means of jumpers, also there is an empty space for the user to connect additional capacitor. The board has 10-pin connector in which the wireless sensor will be connected to be powered by the harvested energy [95].

Figure 4.22 Powercast Evaluation Board (P2110-EVB) [95]

4.3.3 Powercast Antennas

Powecast kit comes with two printed antennas to be connected to the evaluation board through the SMA connector. The two antennas are the dipole antenna and patch antenna as shown in Figure 4.23. The dipole antenna has RF connector at the bottom and it is an omnidirectional antenna with vertical polarization and it has a gain of 1 dBi. The dipole antenna can receive the signal until 6 meters far from the transmitter. The patch antenna has RF connector in the middle. It is a directional antenna with vertical polarization. The

antenna gain is 6.1 dBi. The patch antenna can receive the signal until 12 meters far from the transmitter [95].

Figure 4.23 Powercast antennas (a) Dipole antenna (b) Patch antenna [93]

4.3.4 Wireless Sensor Board (WSN-EVAL-01)

This board contains sensors for light, temperature, humidity and an external input sensor [93]. The sensor will be connected to the evaluation board through the 10-pin connector by which the sensor board will be powered using the harvested energy. The data of the sensor will be transmitted to the access point by an antenna radiating at 2.4 GHz as shown in Figure 4.24. The user can select the sensor ID by changing the ID SELECT switch which has 3 switches so that the ID will be from 0 to 7.

Figure 4.24 Wireless Sensor Board [93]

4.3.5 Powercast Access Point

The powercast access point consists of two boards as shown in Figure 4.25. The Microchip 16-bit XLP shown in Figure 4.25 (a) is a development kit that is programmed to work as an access point to receive the data sent by the wireless sensor board and sends the data to the computer using USB cable. The board shown in Figure 4.25 (b) is the Microchip MRF24J40 PICtail which is 2.4 GHz radio that will be plugged into the Microchip 16-bit XLP board for receiving from the sensor.

a   b
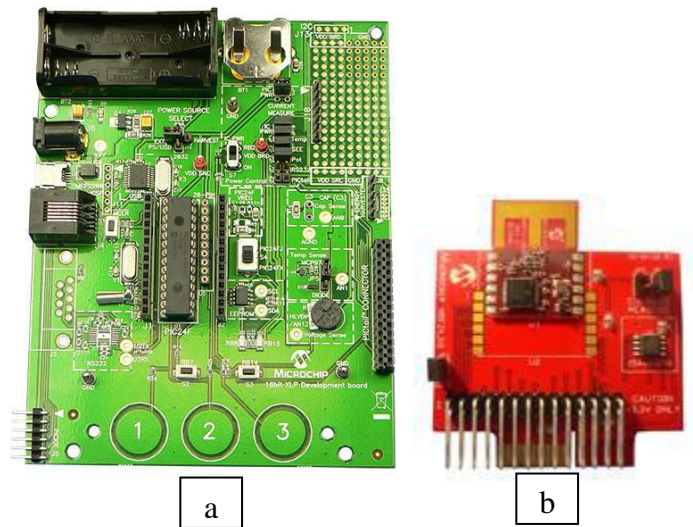
Figure 4.25 Powercast Access Point (a) 16-bit XLP (b) MRF24J40 PICtail [93]

The setup of the Powercast energy harvesting kit is shown in Figure 4.26. The TX91501 transmitter must be plugged in for line of sight (LoS) operation with the evaluation board and the distance between the transmitter and the receiver should in the range of the connected antenna as discussed earlier. The desired antenna is connected to the P2110 evaluation board through the SMA connector and the desired energy storing capacitor is selected using jumper J1. After that the wireless sensor is attached to the 10-pin connector in the P2110 evaluation board as shown in Figure 4.26. The access point is connected to a computer to receive and display the results.
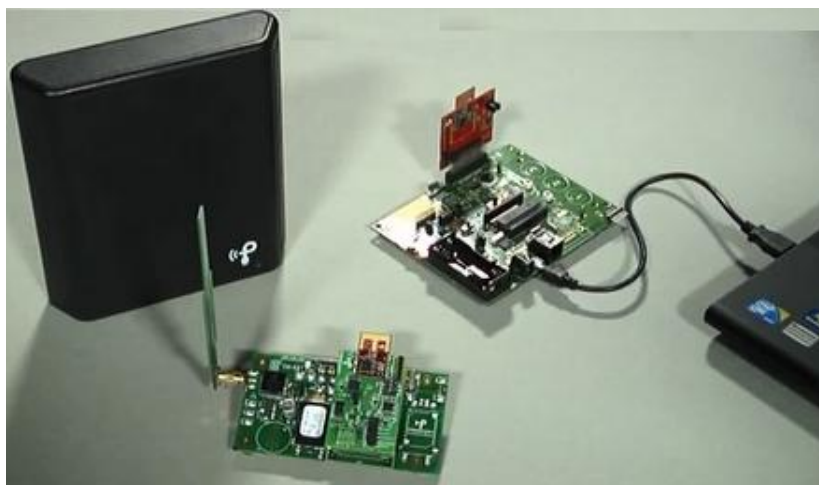
Figure 4.26 Powercast kit ready to work

4.4 Performance Comparison between the proposed MLA and the Powercast Dipole Antenna

In this section, the proposed dual band MLA will be tested for energy harvesting capabilities through using Powercast (P2110-EVAL-01) kit. Then the Powercast dipole antenna will be set as a reference antenna so that the proposed MLA will be compared to it in terms of the maximum distance that the antenna can still receive and the amount of harvested power.

4.4.1 Powercast Measurements Setup

Measurements are done by the Powercast kit to see the antenna and link performance in terms of received power and the distance between the transmitter and the receiving antenna. The original kit documentation lacks a lot of details about the performance of its antennas, thus a detailed measurement campaign has been conducted.

Figure 4.27 Measurement setup with 1 meter distance between the receiver and the transmitter

The proposed dual band MLA was tested using the powercast RF energy harvesting kit to check its ability to harvest RF energy and then being compared it with the dipole antenna that comes with the powercast kit. The measurements were conducted outdoors at King Fahd University of Petroleum and Minerals (KFUPM), Saudi Arabia. The transmitter and the receiving antennas were placed on metal stands with 1.5 meter height as shown in Figure 4.27 and the receiving antenna was connected to the rectifier board as shown in Figure 4.28. The distance between the transmitter and the receiver was varied and the corresponding harvested RF power was recorded for the two antennas.
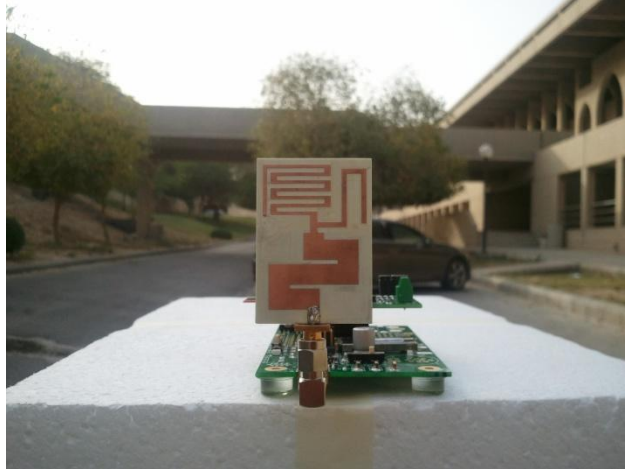
Figure 4.28 The proposed MLA connected to the kit

4.4.2 Powercast Measurements Results and Discussions

4.2 shows the dipole antenna measurements results at 915 MHz. The reference dipole antenna was able to receive the signal up to 5 meters away from the transmitter with maximum power of 2.33 mW. The measurement results for the proposed MLA at 915 MHz is shown in Table 4.3. The results shows that the MLA can receive up to 3 meters away from the transmitter with maximum harvested power of 0.6 mW. This difference in the receiving distance and the harvested power between the two antennas is due to the lower matching levels of the proposed MLA which resulted in low measured gain of -2.6 dB compared to 1 dB gain for the dipole antenna not to mention that the MLA small aperture leads to low captured RF waves.

Table 4.2 Dipole Antenna Measurements

Distance (m)	1	2	3	4	5
Power (mW)	2.33	0.7	0.26	0.2	0.07

Table 4.3 The Proposed MLA Measurements

Distance (m)	1	2	3
Power (mW)	0.6	0.06	0.04

The size of the dipole antenna is very big compared to the MLA size as shown in Figure 4.29. The length of the dipole antenna is 165 mm while the length of the dual band MLA is 45 mm which means the dipole antenna is about 3.5 times bigger than the proposed MLA and then it is acceptable to have half the distance with a quarter size of the antenna. Not to mention that a large antenna will not be suitable for integration with small sensor nodes. The lower power level harvested is due to the smaller aperture of the proposed antenna. Thus the tradeoff between having 75% size reduction is 1/2 covered range and approximately 75% reduction in actual captured power.

Figure 4.29 Size comparison between the proposed MLA and the Powercast dipole antenna

4.5   Conclusions

In this chapter, different dual band MLA design with different matching techniques are discussed to enhance the matching levels. Figure 4.30 shows these different designs with different matching techniques and different substrate materials. Each antenna in Figure 4.30 has different geometry from the other antennas. The Powercast energy harvesting kit components and measurements were discussed. The proposed MLA is compared with the Powercast dipole antenna in means of the harvested power and the maximum distance between the transmitter and the antenna that the antenna can still receive.
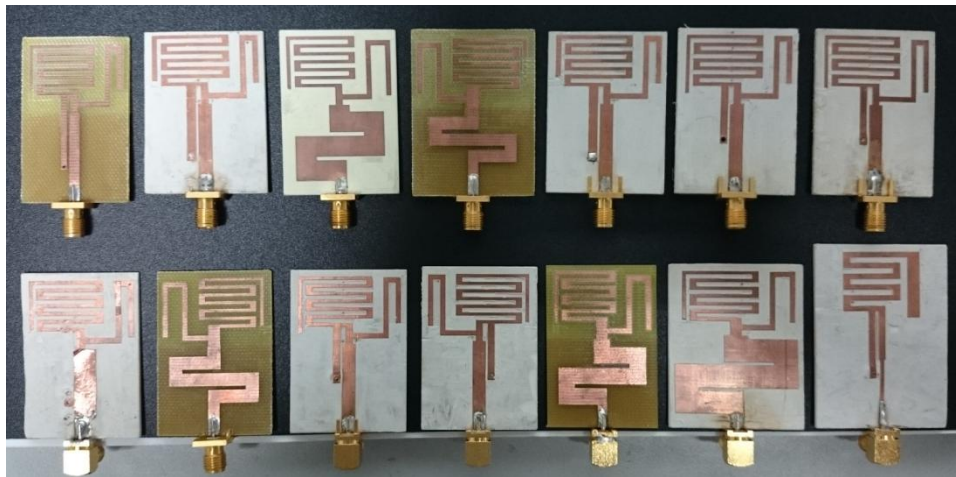
Figure 4.30 Different Fabricated MLA Designs

CHAPTER 5

MINIATURIZED DUAL BAND PATCH

RECTENNA

In this chapter, a highly miniaturized dual band patch antenna is designed to cover two WLAN bands at 2.45 and 5.2 GHz. The proposed patch antenna is miniaturized using a shorting post and a novel defected ground structure (DGS) to achieve 74% size reduction compared to conventional rectangular patch antenna at 2.45 GHz. The antenna design and the measurements results will be discussed in details. To check the proposed antenna RF energy harvesting capabilities, two rectifiers for RF to DC conversion are designed at 2.43 and 5.2 GHz and connected to the patch antenna to test the antenna both band.

5.1   Miniaturized Dual-band Patch Antenna Design

In this section, the proposed dual band patch antenna design and geometry will be shown and miniaturization techniques used will be discussed. The simulated and measured results of the antenna will be illustrated and compared.

5.1.1   Antenna Design and Geometry

The proposed antenna is simply a patch antenna miniaturized using a shorting post close to the feeding position with a novel DGS. The shorting increases the antenna size and the

current path by making the ground layer as a part of the radiator. Figure 5.1 shows the proposed patch antenna geometry and the detailed dimensions are listed in Table 5.1.The dual-band property is achieved by etching a U-slot in the ground as the current goes to the ground through the shorting post, this makes the ground part of the antenna. The patch antenna is fed with an SMA connector acting as a feeding probe at its edge.

(a)   (b)
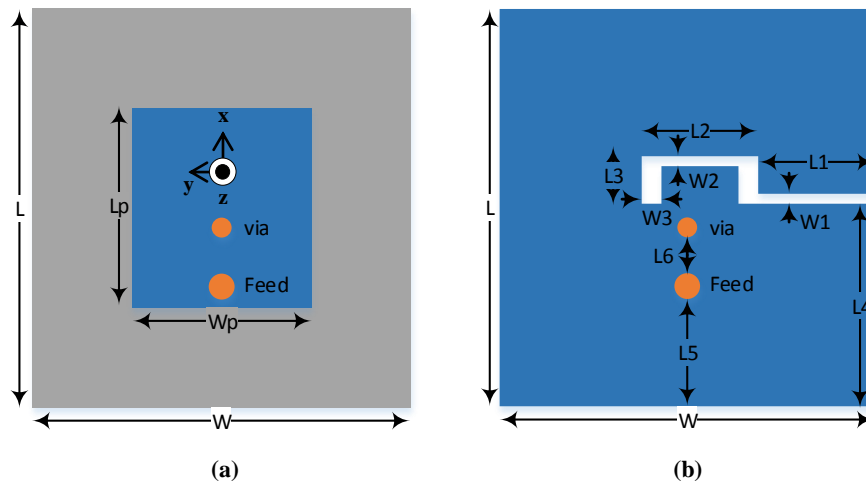
Figure 5.1 The patch antenna geometry (a) top layer, (b) bottom layer

Table 5.1 Detailed dimensions of the proposed patch

Parameter	Value (mm)	Parameter	Value (mm)
L	20	L4	8.9
W	18.8	L5	6
Lp	10	L6	1.8
Wp	8.8	W1	1
L1	6	W2	1.2
L2	5.9	W3	0.6
L3	2.6		

The antenna is fabricated on a double sided Rogers RO4350 substrate with dielectric constant of 3.48, loss tangent of 0.004 and thickness of 0.76 mm as shown in Figure 5.2. The antenna is compared with a European 50 cents to show its small size. The total

antenna size along with its GND plane is 18.8x20x0.76 mm^3 which represents an ESA at 2.45 GHz even when the circle surrounds all the substrate as shown in Figure 5.3. The radius a of the circle is 13.86 mm so that ka = 0.7 < 1 [92].
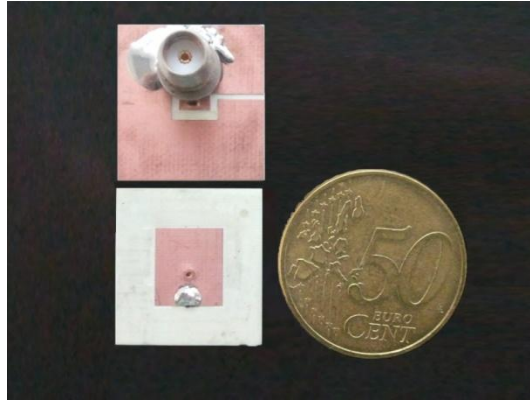
Figure 5.2 the fabricated patch antenna top and bottom layers
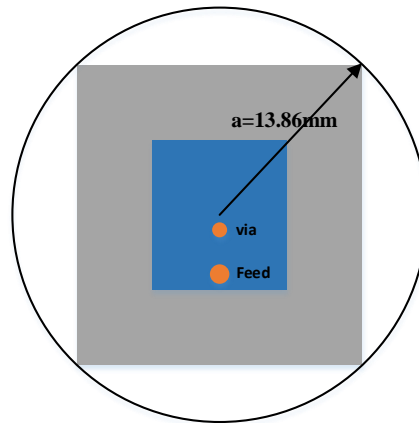
Figure 5.3 Circle surrounding whole the antenna

5.1.2 Results and Discussions

The proposed patch antenna was modeled, optimized and simulated using HFSS$^{\text{TM}}$ (version 15). Figure 5.4 and Figure 5.5 show the proposed patch antenna current distributions at 2.43 and 5.2 GHz, respectively. At 2.43 GHz, the highest current intensity traces two of the patch edges. Although the U-slot is etched on the ground, but it affects

89

the current on the patch as the current goes around the corresponding U-slot position in the ground layer showing current concentration around it thus explaining the miniaturization rule of the DGS.

(a)   **(b)**
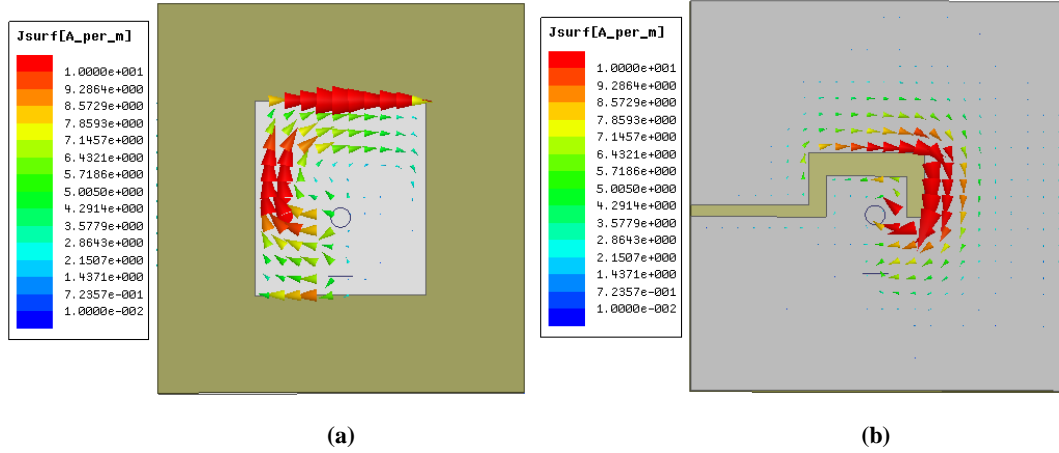
Figure 5.4 Current distribution for the patch antenna at 2.43 GHz (a) top layer, (b) bottom layer

At 5.2 GHz, the current is over all the patch and in the ground layer is surrounding the DGS.

(a)   **(b)**
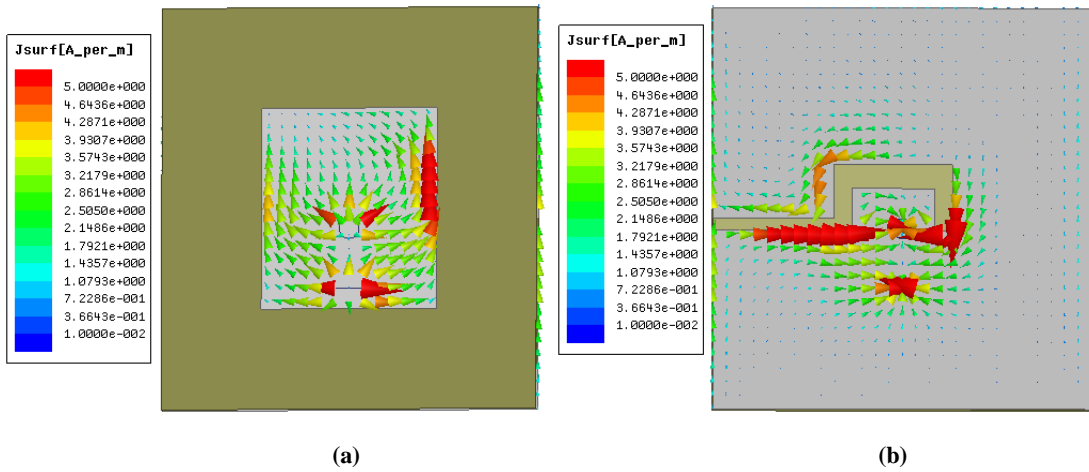
Figure 5.5 Current distribution for the patch antenna at 5.2 GHz (a) top layer, (b) bottom layer

To investigate more how the U-slot can control the antenna resonance, parametric studies on the U-slot width and arm's length were conducted and their effect on the antenna resonance was observed. The sweeps were conducted when all other parameters were set to the values in Table 5.1. Figure 5.6 show the effect of the U-slot width (L2) when it is changed from 4 to 8 mm. Changing L2 will affect the lower band and has no effect on the higher band which indicates that the frequency difference between the lower and higher band can be controlled by changing L2 and this conclusion is shown with exact numbers in Table 5.2.
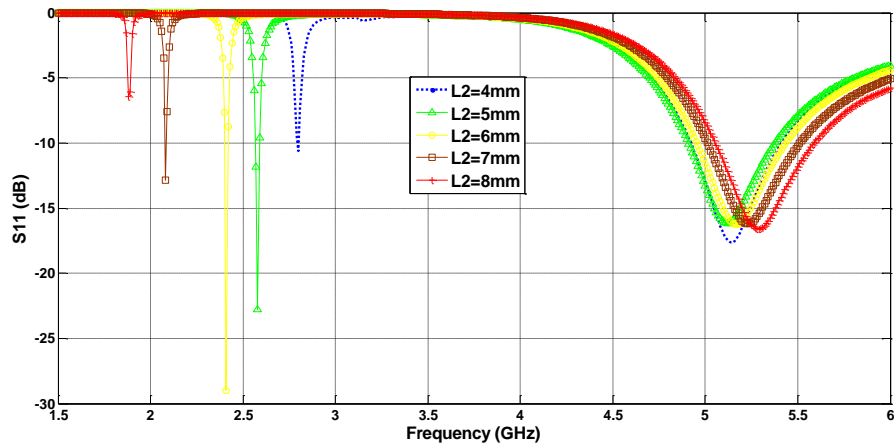
Figure 5.6 Effect of the U-slot width (L2)

Table 5.2 Effect of the U-slot width (L2) on the antenna resonance

L2 Value (mm)	1st resonance (GHz)	2nd resonance (GHz)	Freq. Difference (GHz)
4	2.8	5.14	2.34
5	2.58	5.12	2.54
6	2.41	5.17	2.76
7	2.1	5.23	3.13
8	1.88	5.3	3.42

Figure 5.7 shows the effect of the U-slot arm's length (L3) when changing it from 1 to 5 mm. Changing L3 will affect both frequency bands with the same amount of frequency

and this is shown clearly in Table 5.3 as all numbers in frequency difference column are almost the same. To conclude, by increasing L2 the lower band resonance can be reduced with reduced matching levels which is clear from the current distribution as at 2.43 GHz the current path will increase with the increase of L2 but at 5.2 GHz the current distribution is not affected with changing L2. Changing L3 will shift both bands with the same amount of frequency and this is expected from current distribution, such that larger L3 values will give lower resonance frequency with worse matching levels.
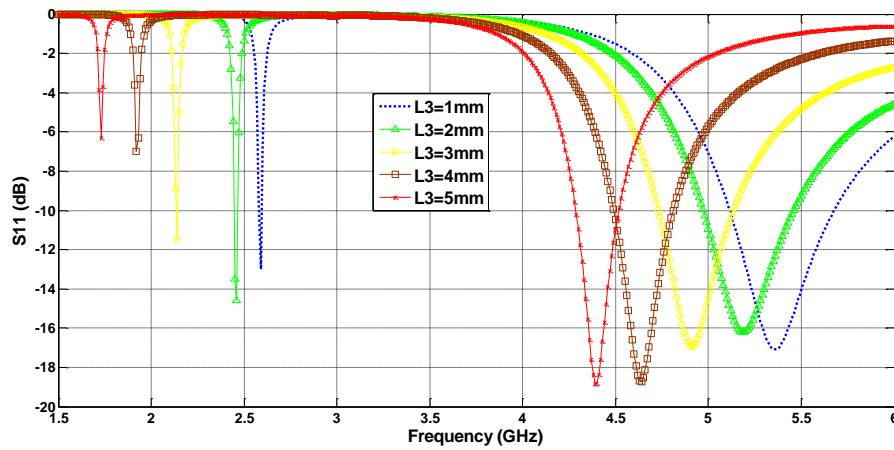
Figure 5.7 Effect of the U-slot arm's length (L3)

Table 5.3 Effect of the Arm's length (L3) on the antenna resonance

L3 Value (mm)	1st resonance (GHz)	2nd resonance (GHz)	Freq. Difference (GHz)
1	2.6	5.35	2.75
2	2.45	5.2	2.75
3	2.23	4.9	2.67
4	1.92	4.64	2.72
5	1.72	4.4	2.68

The fabricated antenna resonance was measured using an Agilent N9912A FieldFox VNA. The simulated and measured resonances of the antenna are shown in Figure 5.8 for the optimum values in Table 5.1. For the resonance frequency, there is a good agreement

between the simulated and measured results as in both the antenna resonates at 2.43 and 5.2 GHz. For the matching, in the lower frequency band the measured resonance has lower matching than the simulated one but it is acceptable for ESA. Please note that the connector model was not incorporated in the simulation model which might have contributed to the lower matching levels. The antenna has measured -6 dB bandwidth of 40 MHz at 2.43 GHz and 1.2 GHz at 5.2 GHz.
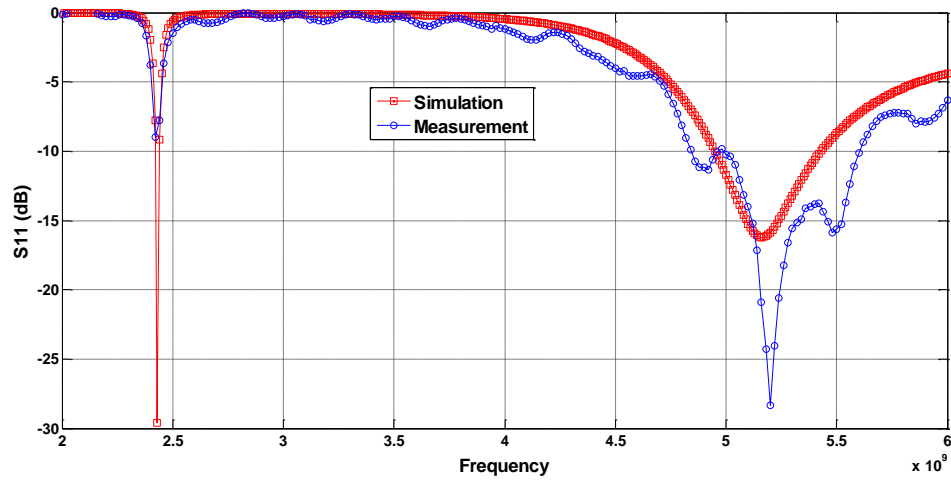
Figure 5.8 The patch antenna measured and simulated resonance

Figure 5.9 Patch antenna near field measurement setup

The antenna radiation characteristics were measured at MVG-Italy, in a Satimo Star-Lab near field chamber as shown in Figure 5.9. The measured maximum gain and efficiency are shown in Figure 5.10. The antenna had measured maximum gains of -1.7 and 2.4 dB at 2.43 and 5.2 GHz, respectively. The gain at 2.43 GHz is lower than the simulated gain of 0.8 dB and this due to the lower matching levels (lower total efficiency) between the simulated and the fabricated antenna. For the higher band at 5.2 GHz, the measured gain and the simulated one are in very close agreement as the maximum simulated gain value was 3 dB. The measured efficiency of the antenna was -5.27 dB (30%) and -0.9dB (81%) at 2.43 and 5.2 GHz, respectively, which is considered acceptable for miniaturized dual band patch antennas.
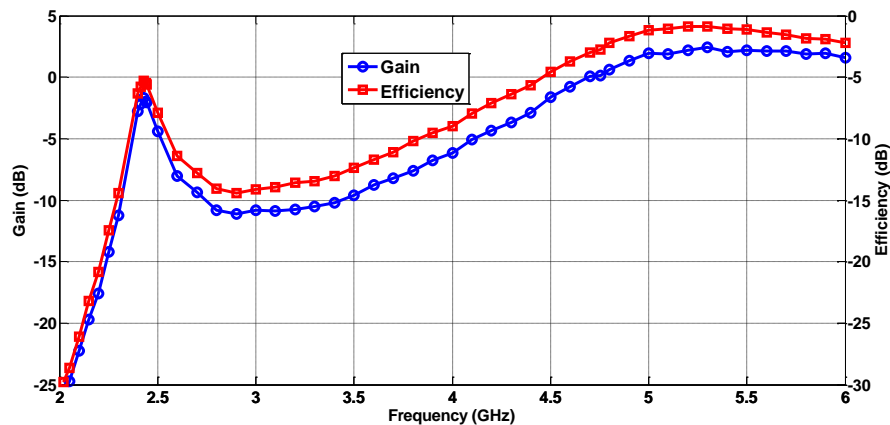
Figure 5.10 Patch Antenna measured maximum gain and efficiency

Figure 5.11 shows the simulated and the measured 2D radiation patterns in xz and yz planes at 2.43 and 5.2 GHz. The antenna has almost omnidirectional pattern as expected for small antennas.

94
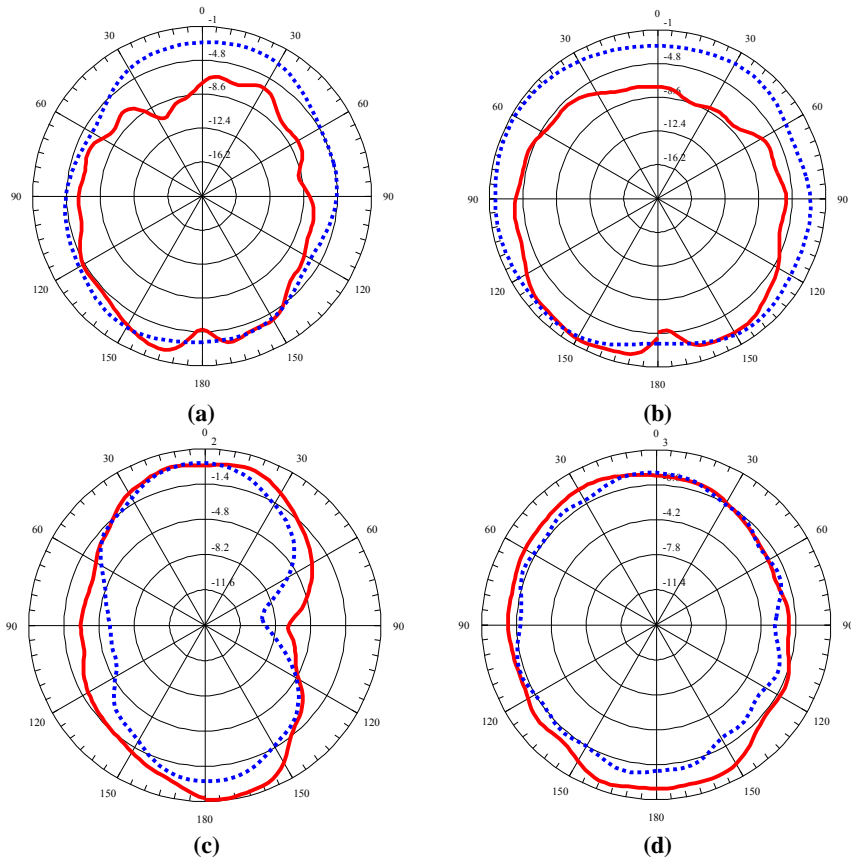
Figure 5.11 Simulated and measured 2-D radiation pattern. Simulated: Dashed lines. Measured: Solid lines. (a) xz-plane at 2.43 GHz. (b) yz-plane at 2.43 GHz. (c) xz-plane at 5.2 GHz. (d) yz-plane at 5.2 GHz

5.2   RF Energy Harvesting Circuit Design and Measurements

In this section, two rectifier circuits (RF to DC converter) are designed at 2.43 and 5.2 GHz to test the antenna energy harvesting abilities. The rectifiers design and their measurements when they are connected to the patch antenna will be discussed in details and this constitutes a rectenna configuration.

5.2.1   Single Shunt Rectifier Design

A single shunt rectifier is chosen to build a rectenna at 2.43 GHz. The single shunt rectifier consists of a parallel diode and a series λ/4 transformer at the operating frequency as shown in Figure 5.12. The idea behind using a λ/4 transformer is to reflect

95
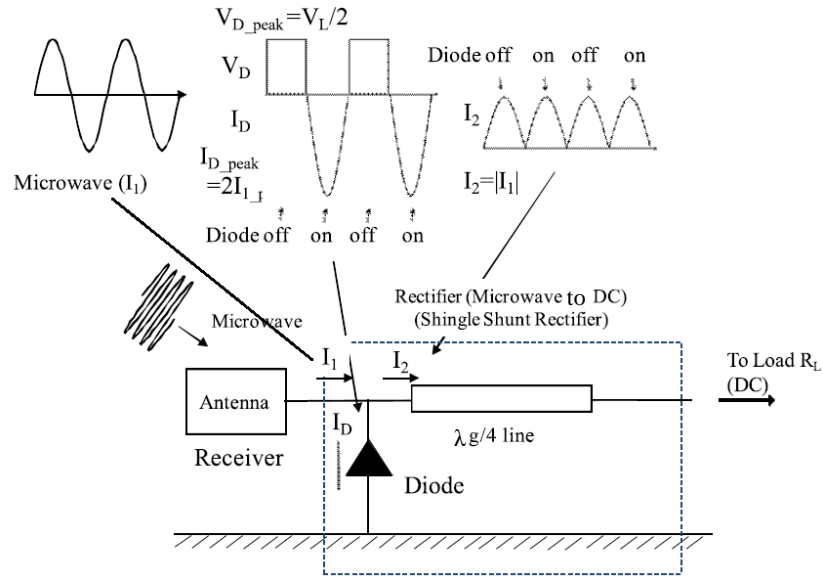
Figure 5.12 Single shunt rectifier [94]

back the odd harmonics to be rectified again by the diode and this will enhance the RF-DC conversion efficiency of the rectifier. The impedance Z to the right side of the diode is given by [94]

$$Z = \frac{Z_L + jZ_0 \tan{(\beta * \lambda/_4)}}{Z_0 + jZ_l \tan{(\beta * \lambda/_4)}} Z_0 \qquad \text{eq(5.1)}$$

where Z_L is the load impedance which is a pure resistance R_L, Z_0 is the $\lambda/4$ transformer characteristic impedance and β is the phase $(2\pi/\lambda)$. When the harmonics are odd, the impedance $(Z = Z_0{}^2/Z_L)$ will be ∞ for high characteristic impedances, when the harmonics are even the impedance $(Z = Z_L)$ will pass the DC to the load [94].

The single shunt rectifier is fabricated on FR4 substrate with dielectric constant of 4.4, loss tangent of 0.02 and thickness of 1.52 mm as shown in Figure 5.13. The rectifier is fabricated manually using copper strips. SkyWorks SMS7630-079LF schottky diode is
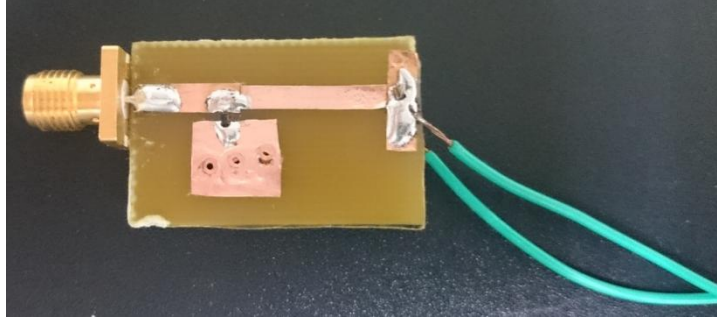
Figure 5.13 Fabricated 2.43 GHz single shunt rectifier

used to design the rectifier, this diode has low built in voltage starts from 60 to 240 mV and a breakdown voltage of 1 V when the current across it is 0.1 mA. The diode can be used up to 24 GHz but its performance starts to degrade after 5 GHz. The diode can be matched at a single point meaning that for a certain frequency and a certain RF input power because its impedance will change according to these two parameters so we chose not to match the diode at 2.43 GHz as the matching network can present losses at the other RF input power values that the diode is not matched to them.

5.2.2 Half Wave Rectifier Design

Figure 5.14 shows the schematic of the proposed half wave rectifier. It consists of a matching network to match the diode to 50 Ω, a schottky diode connected in series and a variable resistor that acts as a load. SkyWorks SMS7630-079LF schottky diode is used for designing this rectifier.

Specifying the diode input impedance at 5.2 GHz is not a simple task because in a simulation package parasitics cannot be fully embedded and it has huge effect in determining the diode package impedance, so for RF measurements are prefered to determine the diode input impedance. SkyWorks gives S parameters measurements for
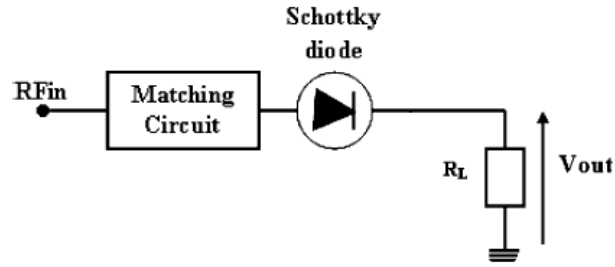
Figure 5.14 Half wave rectifier schematic

the diode with 0 dBm input power and large range of frequencies. Figure 5.15 shows the

smith chart for matching the diode with 0 dBm and frequency of 5.2 GHz. The diode

impedance is in position 1 on the Smith chart, by adding 50 Ω microstrip transmission

line with 3 mm length as shown in Figure 5.16 the impedance moves to position 2. Then

by adding a short circuit stub the impedance moves to position 3 where the impedance is

50 Ω. The rectifier final geometry is shown in Figure 5.16 and the fabricated rectifier is

shown in Figure 5.17 where a potentiometer is connected to measure the output DC

voltage for different load values.
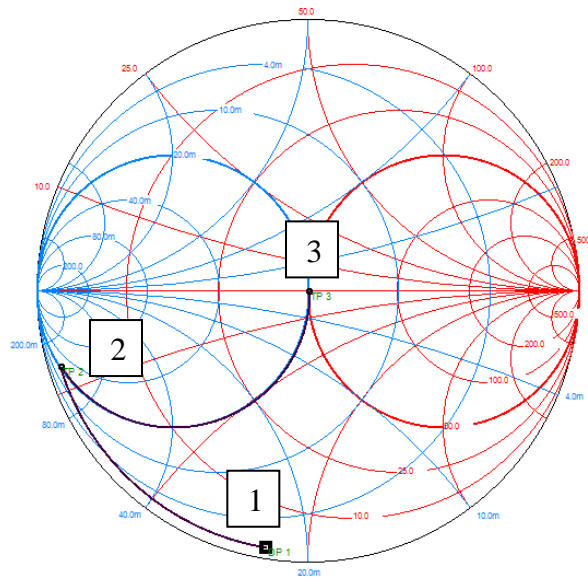
Figure 5.15 Matching network for SMS 7630 schottky diode

98
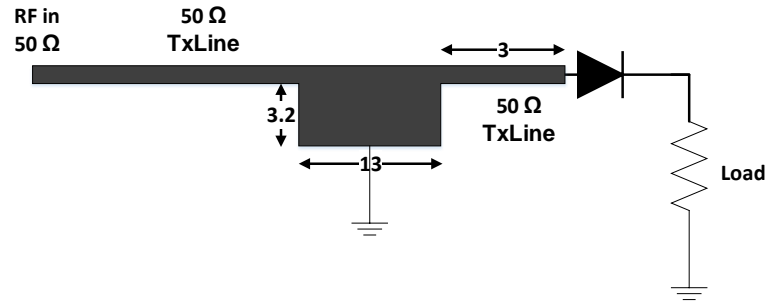
Figure 5.16 The proposed half wave rectifier geometry
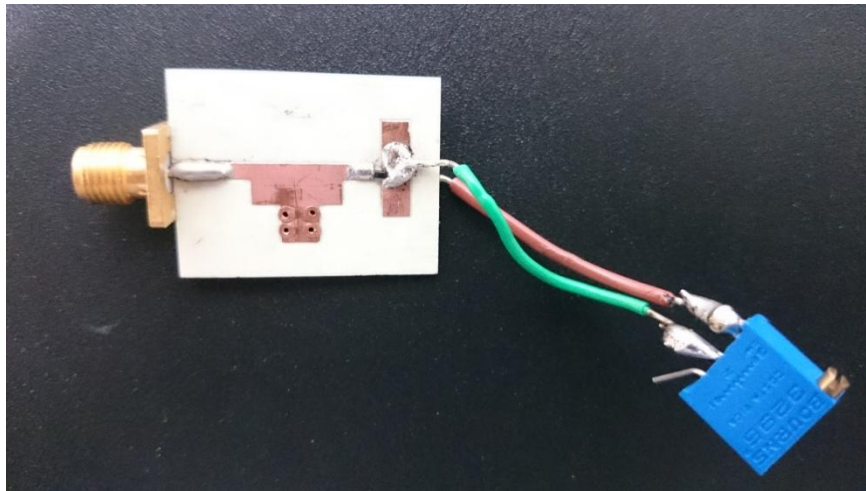
Figure 5.17 5.2 GHz fabricated rectifier

5.2.3 Measurements Setup

RF energy harvesting measurements were conducted to test the performance proposed patch antenna energy harvesting capabilities. Figure 5.18 shows the measurements setup. The components used are an RF signal generator to generate the RF signal at 2.43 and 5.2 GHz followed by a power amplifier (Pasternack PE 15A4019) to boost the signal power then connected to broadband horn antenna (A-INFO LB-10180-NF) for signal radiation. At the other side the miniaturized patch connected to the RF to DC circuit is resided 1 meter away from the horn antenna

Figure 5.18 Measurements Setup with 1 meter difference between the transmitter and the receiver

The power amplifier is used to boost the signal as the path loss is very high, the free space path loss (FSPL) can be calculated from

$$\text{FSPL (dB)} = 20 \log(d) + 20 \log(f) + 32.4 - G_T \text{ (dB)} - G_R \text{ (dB)} \tag{5.1}$$

where d is the distance in Kilometers, f is the frequency in MHz, G_T is the horn antenna gain which is 11 dB and G_R is the patch antenna gain which is-1.7 and 2.4 dB at 2.43 and 5.2 GHz, respectively. FSPL is found to be 30.8 and 34 dB 2.43 and 5.2 GHz, respectively which is very high for this small distance. A Pasternack PE 15A4019 broadband power amplifier is used. It has a gain of 36 dB while the signal from the signal generator had amplitude of -5 dBm. The power amplifier was connected between the signal generator and the horn antenna is shown in Figure 5.19. A Spectrum analyzer (Agilent N9912A FieldFox) is used to measure the captured signal at the output of the antenna which is the input signal to the rectifier.

Figure 5.19 The power amplifier connected

Figure 5.20 and Figure 5.21 show the proposed rectenna (patch antenna connected to the rectifiers).

Figure 5.20 Fabricated 2.43 GHz rectenna

Figure 5.21 Fabricated 5.2 GHz rectenna

5.2.4   Results and Discussions

In this section the RF energy harvesting measurements of the patch antenna will be showed and discussed for the two frequency bands.

5.2.4.1 Rectenna at 2.43 GHz

Figure 5.22 shows the generated DC voltage across different load values when the RF input power is 0 dBm at 2.43 GHz. The DC voltage will increase with increasing of the load, for the low load values the DC voltage will increase gradually but for the high load
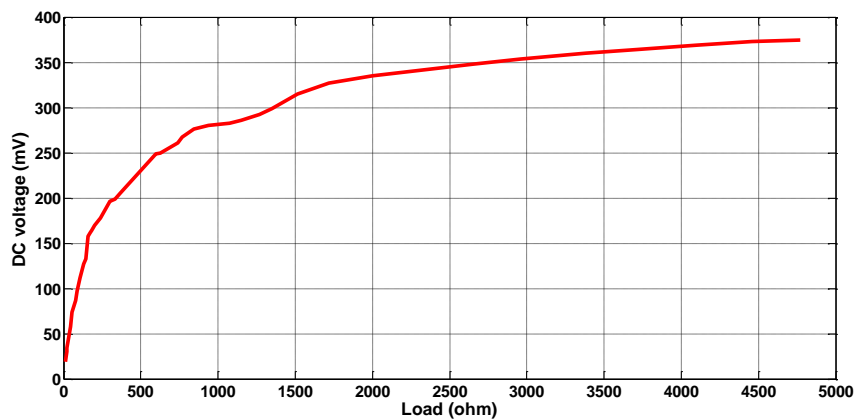
Figure 5.22 The generated DC voltage versus the load at 0 dBm input

values the DC voltage will increase slowly until the generated DC voltage is equal to the half of the diode breakdown voltage as discussed in Section 2.1.1. Figure 5.23 shows the generated DC power across different load values when the RF input power is 0 dBm. The optimal load in which the highest DC power is generated is 156 Ω.
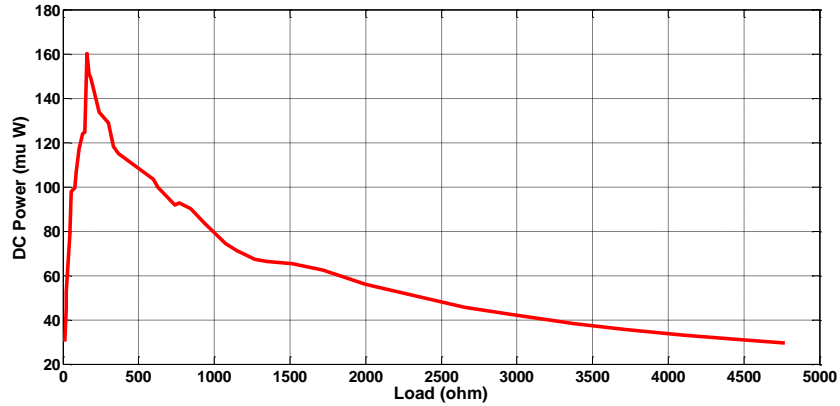
Figure 5.23 DC power versus the load at 0 dBm input

Figure 5.24 shows the DC voltage generated using different RF input power values when the load is fixed to 156Ω. The DC voltage increases with the increase of the input RF power and 0.9 V is achieved with input power of 15 dBm.
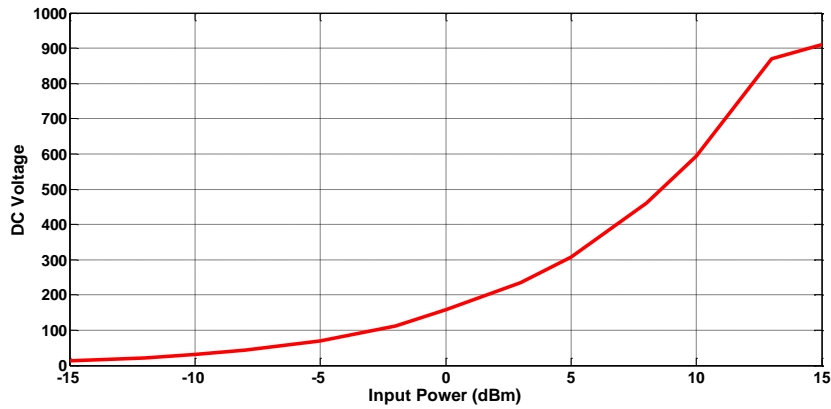
Figure 5.24 Output DC voltage across 156 Ω load versus the RF input power

103
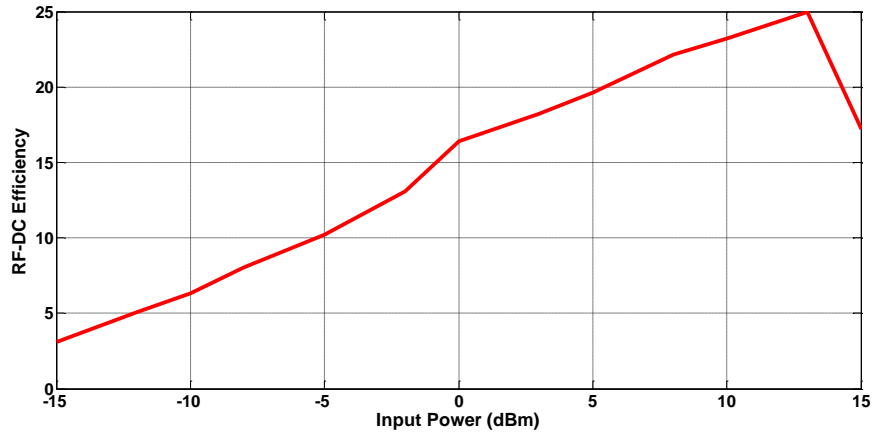
Figure 5.25 Rectifier conversion efficiency versus the RF input power for a load of 156 Ω

Figure 5.25 relates the RF-DC conversion efficiency to the input power when the load fixed to 156 Ω. The conversion efficiency is calculated using equation (2.4) using the measured DC voltage across the load. The highest conversion efficiency is 25% obtained when the input power is 12 dBm, this value is low due to the low precision of the dimensions during the rectifier fabrication as it is fabricated manually.

5.2.4.2 Rectenna at 5.2 GHz

Figure 5.26 shows the output DC voltage and the corresponding load values at 0 dBm input power to the rectifier input. The voltage begins to increase gradually for the low values of the load then the increment will be slow for the higher values. This happens because the generated DC voltage goes towards the maximum possible DC voltage which equals to the half of the diode breakdown voltage as discussed in Section 2.1.1.
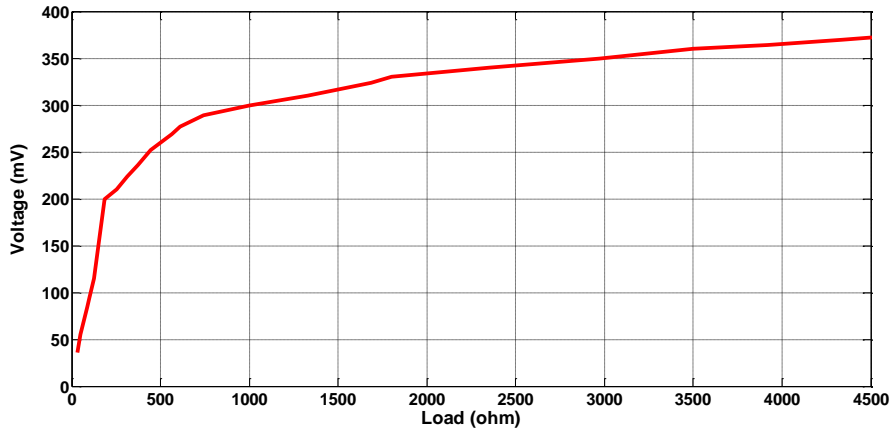
Figure 5.26 The generated DC voltage versus the load at 0 dBm input

Figure 5.27 shows the generated DC power across different load values when the RF input power is 0 dBm. The optimal load in which the highest DC power is generated is 185 Ω.

Figure 5.28 shows the output DC voltage with different input power values at 185 Ω. As expected the DC voltage increases with the increase of the input power as it reached 400 mV at 5 dBm. 5 dBm was the maximum input power that we can get from the measurements setup were conducted.
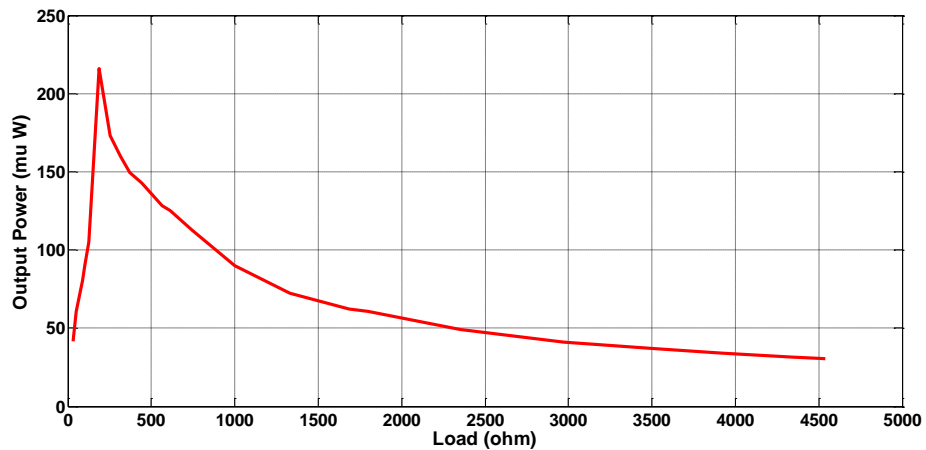
Figure 5.27 DC power versus the load at 0 dBm input

105
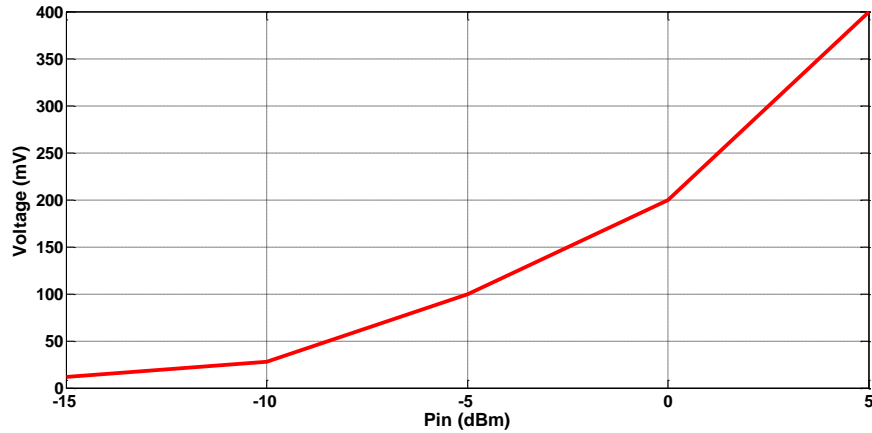
Figure 5.28 Output DC voltage across 185 Ω load versus the RF input power

Figure 5.29 shows the conversion efficiency versus the input power with load of 185 Ω. The smallest signal that the rectifier can receive is -15dBm which is 31µW. The efficiency is increasing with the input power increase as the highest efficiency found to be 26.5% at 5 dBm. The highest efficiency is expected to be at 0 dBm due to the matching there but one cannot be sure that the input power is exactly 0 dBm due to the losses from the cables, connectors and the surrounding environment. 26.5% conversion efficiency is acceptable for this rectifier topology as the half wave rectifier maximum efficiency is 40.6%
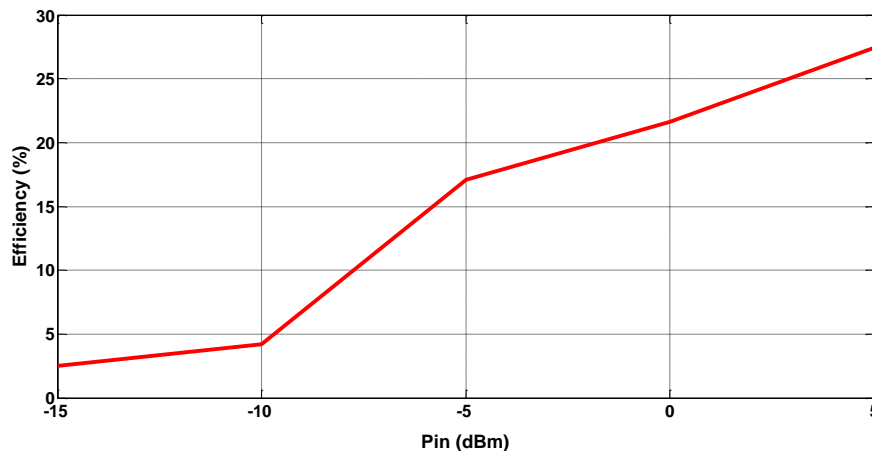
Figure 5.29 Rectifier conversion efficiency versus the RF input power for a load of 185 Ω

5.3   Conclusions

In this chapter, A highly miniaturized dual band patch antenna is designed to resonate at 2.45 and 5.2 GHz. 74% miniaturization ratio is achieved compared to conventional patch at 2.45 GHz. Two rectifiers are designed to be connected to the patch antenna to give a rectenna at both frequency bands. At 2.43 GHz, 0.9 V is achieved at 12 dBm across a load of 156 Ω with highest conversion efficiency of 25%. For 5.2 GHz, 0.4 V is measured across 185 Ω load at 5 dBm, this voltage results in 26.5 % conversion efficiency. Table 5.4 shows a comparison between the proposed patch antenna and other dual-band miniaturized patch antennas that appeared in literature in terms of miniaturization ratio, gain and efficiency. The proposed patch antenna has the highest miniaturization ratio with acceptable gain and efficiency, notice that no measured radiation efficiency was mentioned in almost all previous works.

Table 5.4 Comparison between the proposed patch antenna and other antennas from literature

Reference	Band 1 (GHz)	Band 2 (GHz)	Miniaturiza tion Ratio (%)	Maximum Gain (dB)		Efficiency (%)	
				Band 1	Band 2	η 1	η 2
[78]	2.45	5.8	60	0.5	1.5	-	-
[77]	1.7	8.1	46	-	-	-	-
[85]	900	2.45	68	2.6	3.5	-	-
[86]	3.5	5.8	58	5.4	6.4	-	-
[75]	2.7	4.5	64	-	-4	-	-
[81]	2	5.32	60	2.5	4.3	-	-
[84]	1.8	3.4	60	-	-	-	-
This work	2.43	5.2	74	-1.7	2.4	30	81

CHAPTER 6

CONCLUSIONS AND FUTURE WORK

6.1   Conclusions

Wireless sensors have been used in our daily life applications for monitoring physical phenomena as in medical applications and industry in general. Most of the wireless sensors use limited power batteries as an energy source, these batteries have their high cost, also they will add to the sensor size and their disposal is harmful to the environment. The proposed solution to overcome battery disadvantages is to harvest energy from ambient sources and use it to energize wireless sensors instead of the batteries. There are many sources in nature that energy can be harvested from such as the sun and the wind but these sources depend on the environment which is unpredictable and the sensors cannot rely on them specially with their small power storage capabilities. Radio frequency (RF) waves are reliable energy harvesting source for low power devices as dedicated RF sources can be assigned for RF energy harvesting purposes. In this work, two miniaturized dual band printed antennas are designed and tested for RF energy harvesting capabilities.

The first antenna is a miniaturized dual-band meander line antenna (MLA) that was designed to resonate at 915 and 1900 MHz to cover the most known cellular frequency bands. The dual-band property is achieved using two different radiators and it is matched by a quarter wavelength transformer at 915 MHz. The antenna is an electrically small

antenna (ESA) at 915 MHz. The antenna is tested using the Powercast energy harvesting kit to measure the maximum distance from the powercast transmitter that the proposed antenna can receive and then the antenna was compared and benchmarked with the Powercast reference dipole antenna. The proposed MLA was able to receive power for up to 3 meters away from the transmitter compared to 5 meters for the reference antenna, knowing that the length of the dipole antenna is about 4 times larger than the length of the proposed antenna.

The second antenna is a highly miniaturized dual-band patch antenna which resonates at two WLAN bands at 2.45 and 5.2 GHz. The patch has a compact size of 8.8x10 mm^2 which means 74% miniaturization ratio is obtained by using a shorting post and a novel DGS. The DGS consists of U-slot for dual-band operation and a rectangular slot to increase the current path and matching the antenna at the desired frequencies. This is the smallest dual band patch reported in literature so far. Two rectifiers are designed to be connected to the patch antenna to give a rectenna at both frequency bands. At 2.43 GHz, 0.9 V is achieved at 12 dBm across a load of 156 Ω with highest conversion efficiency of 25%. For 5.2 GHz, 0.4 V is measured across 185 Ω load at 5 dBm, this voltage results in 26.5 % conversion efficiency.

6.2   Future Work

Suggestions for future work include:

- Investigate more types of miniaturized antenna geometries to enhance the matching levels and investigate more on the relation between the small ka factor and the lower matching levels of small antennas.

109

- Embedding the SMA connector in the simulation to make the simulation more close to reality by coming up with 3D models for each connectors.

- Enhance the rectifier conversion efficiency with other circuit topologies and discuss the importance of the diode impedance matching as the matching for one input power will introduce losses for the other input power, thus investigating wide of multiband implementations.

REFERENCES

[1]   Z. G. Wan, Y. K. Tan, and C. Yuen, "Review on energy harvesting and energy management for sustainable wireless sensor networks," IEEE 13th International Conference on Communication Technology, pp. 362–367, 2011.

[2]   J. P. Olds and W. K. G. Seah, "Design of an active radio frequency powered multi-hop wireless sensor network," 7th IEEE Conference on Industrial Electronics and Applications (ICIEA), pp. 1721–1726, 2012.

[3]   S. Kim, R. Vyas, J. Bito, K. Niotaki, a Collado, a Georgiadis, and M. M. Tentzeris, "Ambient RF Energy-Harvesting Technologies for Self-Sustainable Standalone Wireless Sensor Platforms," Proceeding of the IEEE, vol. 102, no. 11, pp. 1649–1666, 2014.

[4]   G. Mahan, B. Sales, and J. Sharp, "Thermoelectric Materials: New Approaches to an Old Problem," Physics Today, vol. 50, no. 3, pp. 42-47, 2008.

[5]   Zungeru, Adamu Murtala, Li-Minn Ang, S. Prabaharan, and K.P. Seng "Radio Frequency Energy Harvesting and Management for Wireless Sensor Networks," Green Mobile Devices and Networks: Energy Optimization and Scavenging Techniques, pp. 341–368, 2012.

[6]   J. Zbitou, M. Latrach, and S. Toutain, "Hybrid rectenna and monolithic integrated zero-bias microwave rectifier," IEEE Transactions on Microwave Theory Techniques, vol. 54, no. 1, pp. 147–152, 2006.

[7]   D. Pozar, Microwave Engineering, 4th Edition, Wiley, 2011.

[8]   Valenta, and C. Ryan "Microwave-Energy Harvesting At 5.8 Ghz for Passive Devices," 2014.

[9]   R. Mehta, and V.K. Mehta, Principles of Electronics, S.Chand, 2008.

[10]   Cockcroft, J. D., and E. T. S. Walton. "Experiments with high velocity positive ions." Proceedings of the Royal Society of London. Series A, Containing Papers of a Mathematical and Physical Character pp. 477-489, (1930).

[11]   G. A. Vera, A. Georgiadis, A. Collado, and S. Via, "Design of a 2.45 GHz rectenna for electromagnetic (EM) energy scavenging," IEEE in Radio and Wireless Symposium, pp. 61–64, 2010.

[12] R. Dehbashi, K. Forooraghi, and Z. Atlasbaf, "A harmonic-rejecting inset-fed U-slot antenna for rectenna application," IEEE in Sarnoff Symposium, pp. 1-3, 2006.

[13] M. R. Moorthi and M. E. Technology, "Rectenna Model for 2 . 45GHz Microwave Wireless Power Transmission," International Conference on Energy Efficient Topologies for Sustainability (ICEETS) pp. 1360–1364, 2013.

[14] H. Takhedmit, B. Merabet, L. Cirio, B. Allard, F. Costa, C. Vollaire, and O. Picon, "A 2 . 45-GHz Low Cost and Efficient Rectenna," Proceedings of the Fourth European Conference on Antennas and Propagation (EuCAP), pp. 1–5, 2010.

[15] Yadav, R. Kumar, S. Das, and R.L. Yadav "Performances Analysis of a 5 GHz Rectenna for Indoor Applications," IEEE International Conference on Microwave and Photonics, pp. 1-6, 2013.

[16] Dehbashi, Reza, Keyvan Forooraghi, and Zahra Atlasbaf. "Dual-Fed Antenna for Wireless Power Transmission and Data Communication," Antennas and Propagation Society International Symposium, pp. 2201-2204, 2006.

[17] Hao, Hu, and Kong Li. "A novel 5.8 GHz circularly polarized rectenna for microwave power transmission." 7th International Symposium on Antennas, Propagation & EM Theory, ISAPE'06., pp. 1-4, 2006.

[18] Rahim, R. A., S. I. S. Hassan, F. Malek, M. N. Junita, S. F. W. Anwar, and H. F. Hassan. "A harmonic suppression circularly polarized patch antenna for an RF ambient energy harvesting system." IEEE Conference on Clean Energy and Technology (CEAT), pp. 33-37, 2013.

[19] Olgun, Ugur, Chi-Chih Chen, and John L. Volakis. "Low-profile planar rectenna for batteryless RFID sensors." Antennas and Propagation Society International Symposium (APSURSI), pp. 1-4, 2010.

[20] Zhu, Ning, Kihun Chang, Mingguang Tuo, Peng Jin, Hao Xin, and Richard W. Ziolkowski. "Design of a high-efficiency rectenna for 1.575 GHz wireless low power transmission." Radio and Wireless Symposium (RWS), pp. 90-93, 2011.

[21] Hoang, T. Q. V., A. Douyere, J. L. Dubard, and J. D. Luk. "TLM design of a compact PIFA rectenna." International Conference on Electromagnetics in Advanced Applications (ICEAA), pp. 508-511, 2011.

[22] H. Sun, Y. Guo, and Z. Zhong, "A High-Sentivity 2 . 45 GHz Rectenna for Low Input Power Energy Harvesting," Antennas and Propagation Society International Symposium (APSURSI), pp. 9–10, 2012.

[23] Phongcharoenpanich, Chuwong, Komkris Boonying, and Sompol Kosulvit. "Dual-polarized flat rectenna for 2.45 GHz." Antennas and Propagation in Wireless Communications (APWC), APS Topical Conference on, pp. 1433-1436, 2013.

[24] Sun, Jiang-Tao, Xue-Xia Yang, Toshihiko Yoshimasu, and Xiao-Meng Sun. "Bow-Tie Loop Printed Antenna with High Gain and Broad Beam Width for 5.8 Ghz Rectenna Application." 4th IEEE International Conference on Circuits and Systems for Communications CCSC, pp. 312-314, 2008.

[25] Kazanc, Onur, F. Maloberti, and C. Dehollain. "Simulation oriented rectenna design methodology for remote powering of wireless sensor systems." International Symposium on Circuits and Systems (ISCAS), pp. 2877-2880, 2012.

[26] Rahim, R. A., S. I. S. Hassan, F. Malek, and M. N. Junita. "A 2.45 GHz circular patch antenna with harmonic suppression for wireless power transmission." Colloquium on Humanities, Science and Engineering (CHUSER), pp. 283-287, 2012.

[27] Rahim, R. A., S. I. S. Hassan, F. Malek, M. N. Junita, M. F. Jamlos, and M. N. Azizan. "A 2.45 GHz harmonic suppression rectangular patch antenna." IEEE Symposium on Computer Applications and Industrial Electronics (ISCAIE), pp. 242-246, 2012.

[28] Hosain, Md Kamal, and Abbas Z. Kouzani. "Electromagnetic energy harvesting in a head-mountable DBS device using a circular PIFA." International Conference on Complex Medical Engineering (CME), pp. 541-546, 2013.

[29] R. H. Chen, Y. C. Lee, and J. S. Sun, "Design and experiment of a rectifying antenna for 900 MHz wireless power transmission," Proceedings of Asia Pacific Microwave Conference APMC 2008, pp. 5–8, 2008.

[30] Ren, Y-J., and Kai Chang. "Bow-tie retrodirective rectenna." Electronics Letters vol. 42, no. 4, 191-192, 2006.

[31] C. H. K. Chin, Q. Xue, and C. H. Chan, "Design of a 5.8-GHz rectenna incorporating a new patch antenna," IEEE Antennas and Wireless Propagation Letters, vol. 4, no. 1, pp. 175–178, 2005.

[32] Hiramatsu, Yasuo, Tsunayuki Yamamoto, Kazuhiro Fujimori, Minoru Sanagi, and Shigeji Nogi. "The design of mW-class compact size rectenna using sharp directional antenna." European Microwave Conference EuMC, pp. 1243-1246, 2009.

[33] T. Matsunaga, E. Nishiyama, and I. Toyoda, "5.8-GHz stacked differential mode rectenna suitable for large-scale rectenna arrays," Asia-Pacific Microwave Conferenec Proceedings, APMC, pp. 1200–1202, 2013.

[34] Yang, Xue-Xia, Chao Jiang, Atef Z. Elsherbeni, Fan Yang, and Ye-Qing Wang. "A novel compact printed rectenna for communication systems." Asia-Pacific Power and Energy Engineering Conference (APPEEC), pp. 1-4, 2012.

[35] H. Takhedmit, L. Cirio, S. Bellal, D. Delcroix, and O. Picon, "Compact and efficient 2.45 GHz circularly polarised shorted ring-slot rectenna," Electronic Letters, vol. 48, no. 5, pp. 253-254, 2012.

[36] Yo, Tzong-Chee, Chien-Ming Lee, Chen-Ming Hsu, and Ching-Hsing Luo. "Compact circularly polarized rectenna with unbalanced circular slots." IEEE Transactions on Antennas and Propagation, 56, no. 3, 882-886, 2008.

[37] Huang, Fu-Jhuan, Tzong-Chee Yo, Chien-Ming Lee, and Ching-Hsing Luo. "Design of circular polarization antenna with harmonic suppression for rectenna application." Antennas and Wireless Propagation Letters, pp. 592-595, 2012.

[38] Lin, Ding-Bing, Kuo-Lin Weng, and Hsueh-Jyh Li. "Novel T-shape slot couple feed dual circular polarized rectenna." International Symposium on Antennas and Propagation (ISAP), 2012.

[39] Z. Harouni, L. Cirio, L. Osman, A. Gharsallah, and O. Picon, "A Dual Circularly Polarized 2.45-GHz Rectenna for Wireless Power Transmission," IEEE Antennas Wireless and Propagation Letters, vol. 10, pp. 306–309, 2011.

[40] M. Ali, S. Member, G. Yang, and R. Dougal, "A New Circularly Polarized Rectenna for Wireless Power Transmission and Data Communication," IEEE Antennas Wireless and Propagation Letters, vol. 4, pp. 205–208, 2005.

[41] P. Transmission, J. Heikkinen, and M. Kivikoski, "Low-Profile Circularly Polarized Rectifying Antenna for Wireless Power Transmission at 5.8 GHz," IEEE Microwave and Wireless Components Letters, vol. 14, no. 4, pp. 162–164, 2004.

[42] Pham, Binh, Jia-Chi Samuel Chieh, and Anh-Vu Pham. "A wideband composite right/left hand rectenna for UHF energy harvesting applications." Antennas and Propagation Society International Symposium (APSURSI), pp. 1-2, 2012.

[43] Shinki, Y., Daisuke Kanemoto, Kenta Yoshida, Ramesh K. Pokharel, Kuniaki Yoshitomi, and Haruichi Kanaya. "Wireless power transmission circuit on a small planar wide-band antenna." TENCON Region 10 Conference, pp. 1-4, 2013.

[44] Congedo, Fabrizio, G. Monti, L. Tarricone, and M. Cannarile. "Broadband bowtie antenna for RF energy scavenging applications." Proceedings of the 5th European Conference on Antennas and Propagation (EUCAP), 2011.

[45] Yo, Tzong Chee, Chien-Ming Lee, Ching Hsing Luo, and Chih-Ho Tu. "Stacked implantable rectenna for wireless powering the medical implants." Antennas and Propagation Society International Symposium, pp. 3189-3192, 2007.

[46] H. Sun, Y. X. Guo, M. He, and Z. Zhong, "A dual-band rectenna using broadband yagi antenna array for ambient rf power harvesting," IEEE Antennas and Wireless Propagation Letters, vol. 12, pp. 918–921, 2013.

[47] D. Masotti, a. Costanzo, and S. Adami, "Design and realization of a wearable multi-frequency RF energy harvesting system," Proceedings of the 5th European Conference on Antennas and Propagation (EUCAP), pp. 517–520, 2011.

[48] Costanzo, A., F. Donzelli, D. Masotti, and V. Rizzoli. "Rigorous design of RF multi-resonator power harvesters." Proceedings of the Fourth European Conference on Antennas and Propagation (EuCAP), pp. 1-4, 2010.

[49] Costanzo, Alessandra, and Luca Roselli. "EM-and piezo-scavengers: Two useful solutions in highly humanized scenarios toward a" greener world"." IEEE Microwave Workshop Series on Innovative Wireless Power Transmission: Technologies, Systems, and Applications (IMWS), pp. 15-18, 2012.

[50] Ren, Yu-Jiun, Muhammad F. Farooqui, and Kai Chang. "A compact dual-frequency rectifying antenna with high-orders harmonic-rejection." IEEE Transactions on Antennas and Propagation, 55, no. 7, pp. 2110-2113, 2007.

[51] Rizzoli, Vittorio, Giacomo Bichicchi, Alessandra Costanzo, Francesco Donzelli, and Diego Masotti. "CAD of multi-resonator rectenna for micro-power generation." European Microwave Conference, EuMC., pp. 1684-1687, 2009.

[52] X. L. Bao and M. J. Ammann, "Dual-frequency circularly-polarized patch antenna with compact size and small frequency ratio," IEEE Transactions on Antennas and Propagation, vol. 55, no. 7, pp. 2104–2107, 2007.

[53] F. Huang, C. Lee, C. Chang, L. Chen, T. Yo, and C. Luo, "Rectenna Application of Miniaturized Implantable Antenna Design for Triple-Band Biotelemetry Communication," IEEE Transactions on Antennas and Propagation, vol. 59, no. 7, pp. 2646–2653, 2011.

[54] Horng-Dean Chen, Wen-Shyang Chen, Yuan-Tung Cheng, and Yin-Chang Lin,

"Dualband meander monopole antenna," Antennas and Propagation Society International Symposium , pp. 48–51, 2003.

[55] H.-D. Chen, "Compact CPW-fed dual-frequency monopole antenna," Electronics Letters, vol. 38, no. 25, p. 1622, 2002.

[56] Z. Zakaria, N. A. Zainuddin, M. Z. A. Abd Aziz, M. N. Husain, and M. A. Mutalib, "A parametric study on dual-band meander line monopole antenna for RF energy harvesting," in 2013 IEEE International Conference on RFID-Technologies and Applications (RFID-TA), pp. 1–5, 2013.

[57] N. T. Pham and F. De Flaviis, "Minimized dual-band coupled line meander antenna for system-in-a-package applications," Antennas and Propagation Society Symposium, pp. 1451–1454, 2004.

[58] A. B. Numan and M. S. Sharawi, "A printed dual-band meander-line MIMO antenna system," Antennas and Propagation Society International Symposium (APSURSI), pp. 188–189, 2013.

[59] C.-N. Hu, B. Tai, A. Yang, and D.-C. Chang, "A compact dual-band antenna design for UMTS/HSDAP-based data-card applications," International Workshop on Antenna Technology: Small Antennas and Novel Metamaterials, pp. 370–373, 2008.

[60] W. Yang, K. Ma, K. S. Yeo, W. M. Lim, and Z. H. Kong, "A compact dual-band meander-line antenna for biomedical applications," International Microwave Workshop Series on RF and Wireless Technologies for Biomedical and Healthcare Applications (IMWS-BIO), pp. 1–3, 2013.

[61] A. Khaleghi, A. Azoulay, and J. C. Bolomey, "A Dual Band Back Coupled Meanderline Antenna For Wireless LAN Applications," 61st Vehicular Technology Conference, vol. 1, pp. 226–229, 2005.

[62] A. Khaleghi, "Dual Band Meander Line Antenna for Wireless LAN Communication," IEEE Transactions on Antennas and Propagation, vol. 55, no. 3, pp. 1004–1009, Mar. 2007.

[63] S. Lin, G. Wang, K. Pan, X. Ge, and Y. Yang, "A novel dual-frequency monopole antenna for WCDMA and 2.5 GHz extension band," International Conference on Microwave and Millimeter Wave Technology, pp. 362–365, 2010.

[64] A. K. Panda, R. Suryanarayana, A. Sahoo, J. Nayak, and R. K. Mishra, "A Printed Monopole Antenna with Symmetric Meandered Arms for WLAN, WiMAX

Applications," 2011 International Conference on Communication Systems and Network Technologies, pp. 224–227, 2011.

[65] Li Jian-Ying, Yu Yu Kyi, and Gan Yeow Beng, "Analysis of Dual-Band Meander Line Antenna," Antennas and Propagation Society International Symposium, pp. 2033–2036, 2006.

[66] Sultan, K. S., Haythem H. Abdullah, E. A. Abdallah, and E. A. Hashish. "Low SAR, compact and multiband antenna for mobile and wireless communication." Middle East Conference on Antennas and Propagation (MECAP), pp. 1-5, 2012.

[67] The Nan Chang and Jing-Hae Jiang, "Meandered T-Shaped Monopole Antenna," IEEE Transactions on Antennas and Propagation, vol. 57, no. 12, pp. 3976–3978, Dec. 2009.

[68] H. Hsiao, J. Wu, J. Lu, and Y. Wang, "Multi-Band Dual-Meander-Line Antenna for Mobile Handsets," Antennas and Propagation Society International Symposium, pp. 4705–4708, 2006.

[69] D. Das Krishna, a. R. Chandran, and C. K. Aanandan, "A compact dual frequency antenna with Sierpinski gasket based slots," 2007 European Microwave Conference, pp. 1078–1080, 2007.

[70] M. A. Al-Joumayly, S. M. Aguilar, N. Behdad, and S. C. Hagness, "Dual-Band Miniaturized Patch Antennas for Microwave Breast Imaging.," IEEE Antennas and Wireless Propagation Letters, vol. 9, pp. 268-269, 2010.

[71] Wei, Yuqing, Yingzeng Yin, Yi Yang, Shaohong Jing, and Wei Hu. "Compact dual-band antenna with modified open U-shaped slot for WLAN applications." IEEE International Conference on Microwave Technology & Computational Electromagnetics (ICMTCE), pp. 35-37, 2011.

[72] M. Noghabaei, S. K. A. Rahim, and M. I. Sabran, "Dual band single layer microstrip antenna with circular polarization for WiMAX application," 6th European Conference on Antennas and Propagation (EuCAP), pp. 1996–1999, 2012.

[73] A. Saghir, S. M. Abbas, M. U. Afzal, T. Tauqeer, and M. H. Tariq, "Compact dual band microstrip antenna design using slits," 3rd IEEE International Conference Computer, Control & Communication, pp. 1–4, 2013.

[74] I. W. Application, U. Chakraborty, A. Kundu, S. K. Chowdhury, and a K. Bhattacharjee, "Compact Dual-Band Microstrip Antenna for IEEE 802.11a WLAN

Application," IEEE Antennas and Wireless Propagation Letters, vol. 13, pp. 407–410, 2014.

[75] S. H. S. Esfahlani, a. Tavakoli, and P. Dehkhoda, "A compact single-layer dual-band microstrip antenna for satellite applications," IEEE Antennas and Wireless Propagation Letters, vol. 10, pp. 931–934, 2011.

[76] Liu, Guangdong, D. Wang, F. Jin, and S. Chang. "Compact broad dual-band antenna using a shorted patch with a thick air substrate for wireless body area network application." 4th International Symposium on Microwave, Antenna, Propagation, and EMC Technologies for Wireless Communications (MAPE), pp. 18-21, 2011.

[77] Samsuzzaman, Md, Mohammad Tariqul Islam, Mohammad Rashed Iqbal Faruque, and W. Hueyshin. "Dual wideband n shaped patch antenna loaded with shorting pin for wireless applications." International Conference on Advances in Electrical Engineering (ICAEE), pp. 273-276, 2013.

[78] Meng, Fanji, and Sanjay Kumar Sharma. "A single feed dual-band (2.4 GHz/5.8 GHz) miniaturized patch antenna for wireless local area network (WLAN) Communications." URSI General Assembly and Scientific Symposium (URSI GASS), pp. 1-4, 2014.

[79] W. C. L. and W. R. Chen, "CPW-fed compact meandered patch antenna for dual-band operation," Electronics Letters, vol. 40, no. 2418, pp. 1094–1095, 2004.

[80] K. G. Thomas and M. Sreenivasan, "Compact CPW-fed dual-band antenna," Electronics Letters, vol. 46, no. 1, p. 13, 2010.

[81] W. C. Liu, C. M. Wu, and N. C. Chu, "A compact CPW-Fed slotted patch antenna for dual-band operation," IEEE Antennas and Wireless Propagation Letters, vol. 9, pp. 110–113, 2010.

[82] S. Nagar, U. Nagar, and R. S. Meena, "CPW-Fed Dualband Patch Antenna for Mobile Applications," 5th International Conference on Computer, Intelligence & Communication Networks, pp. 1–5, 2013.

[83] Taouzari, M., J. El Aoufi, A. Mouhsen, H. Nasraoui, and O. El Mrabat. "900 MHz and 2.45 GHz compact dual-band circularly-polarized patch antenna for RFID application." Conference on Microwave Techniques (COMITE) , pp. 1-4, 2015.

[84] P. Consul, K. K. Sharma, C. Engineering, S. Uni, and U. Pradesh, "Dual band Gap Coupled Microstrip Antenna Using L-Slot DGS For Wireless Applications,"

International Confrenece on Computing, Communication and Automation (ICCCA) pp. 1381–1384, 2015.

[85] W. Liao, Q. X. Chu, and S. Du, "A small frequency ratio dual-band circularly polarized microstrip antenna," Asia Pacific Microwave Conference APC, pp. 2798–2801, 2009.

[86] Gupta, Nisha, and Vibha R. Gupta. "Reduced Size, dual frequency band antenna for wireless communication." International Conference on Personal Wireless Communications, ICPWC, pp. 321-323, 2005.

[87] Tizyi, Hafid, Fatima Riouch, Abdelwahed Tribak, Abdellah Najid, and Angel Mediavilla. "Compact dual-band microstrip antenna for handheld RFID reader." Third International Workshop on RFID And Adaptive Wireless Sensor Networks (RAWSN), pp. 68-72, 2015.

[88] B. Zong, G. Wang, C. Zhou, Y. Wang, A. Structure, and T. U. Cell, "Compact Low-Pro fi le Dual-Band Patch Antenna Using Novel TL-MTM Structures," IEEE Antennas and Wireless Propagation Letters, vol. 14, pp. 567–570, 2015.

[89] V. Prabhakar, H.V., Kummuri, U.K., Yadahalli, R.M., Munnappa, "Effect of various meandering slots in rectangular microstrip antenna ground plane for compact broadband operation," Electronics Letters, vol. 43, no. 16, pp. 848–850, 2007.

[90] J.L. Volakis, C.C. Chen, and K. Fujimoto, Small antennas: miniaturization techniques & applications, McGraw Hill, 2010, pp.1– 16.

[91] "P2110-EVAL-01." [Online]. Available: http://www.powercastco.com/PDF/P2110-EVAL-01-manual.pdf. [Accessed: 12-Dec-2014].

[92] "TX91501." [Online]. Available: http://www.powercastco.com/PDF/TX91501-manual.pdf [Accessed: 12-Nov-2015].

[93] "P2110-EVB." [Online]. Available: http://www.powercastco.com/PDF/P2110-EVB-RevA.pdf [Accessed: 12-Nov-2015].

[94] N. Shinohara. "Rectennas for microwave power transmission," Electronics Express (IEICE) Vol. 10, No. 21, pp. 1-13, 2013

VITAE

Name   : Ahmad Abu Elhassan Salih Ibrahim

Nationality   : Sudanese

Date of Birth   : 4/7/1988

Email   : g201304530@kfupm.edu.sa, eng.ahmad054@gmail.com

Address   : H.no. 7, Nisheshiba, Medani Sudan

Academic Background   : MS in Electrical Engineering (Major: Electromagnetics)

                              KFUPM, Dhahran 2015

                              BSc. in Electrical and Electronic Engineering,

                              University of Khartoum 2010

PUBLICATIONS

1. Ahmad A. Salih and Mohammad S. Sharawi, "A miniaturized dual-band meander line antenna for RF energy harvesting application," IEEE Third Applied Electrical Engineering and Computing Technologies (AEECT) conference, Amman, Jordan, pp. 1-4, Nov. 2015.

2. Ahmad A. Salih and Mohammad S. Sharawi, "Highly miniaturized dual band patch antenna," Submitted to EuCAP 2016, under review.

3. Ahmad A. Salih and Mohammad S. Sharawi, "A dual-band highly miniaturized patch antenna," Submitted to AWPL, submitted Oct. 2015, under review.